Smart Siting Guide: Portugal

Balancing energy, conservation, and community priorities in developing ground-mounted solar and onshore wind low conflict sites – Technical Annex v1.0.0.

Girolamo-Neto[1], C. D.; Oakleaf[2], J. R.; Bhattacharjee[3], A.; Sochi[2], K.; Pontonio[1], M.; Gündüzyeli[1], E.; Kiesecker[2], J. M. 2026. Smart Siting Guide: Portugal - Balancing energy, conservation, and community priorities in developing ground-mounted solar and onshore wind on low conflict sites – Technical Annex v1.0.0. The Nature Conservancy. DOI: **10.5281/zenodo.18242153**

[1] The Nature Conservancy, Europe Renewable Energy Programme.
[2] The Nature Conservancy, Global Protect Oceans, Lands and Waters.
[3] The Nature Conservancy, Global Tackle Climate Change.

Contact information

Cesare Di Girolamo-Neto (Renewable Energy Scientist, The Nature Conservancy):
cesare.neto@tnc.org

Elif Gündüzyeli (Renewable Energy Programme Director, The Nature Conservancy):
elif.gunduzyeli@tnc.org

Contents

1. Introduction

This technical annex provides an overview of the spatial modeling methodologies, datasets, and frameworks used to support Smart Siting Guide for Portugal. It is designed to serve as documentation of methods and a technical reference for practitioners, planners, and researchers engaged in renewable energy siting.

The annex is structured to guide users through the modeling pipeline, from the development of probabilistic maps of wind and solar energy potential, to the integration of biodiversity and social value layers for identifying low conflict areas. It details the data sources, spatial analysis techniques, and modeling decisions used for the energy development potential maps (Chapter 2). It also outlines the biodiversity mapping approach using a coarse-filter/fine-filter framework (Chapter 3), and the social values mapping methodology, including viewshed analysis based on social media-derived landscape values and cultural heritage datasets (Chapter 4).

Whether used to replicate the modeling process, adapt it to other geographies, or inform policy and planning decisions, this annex provides the technical foundation for evidence-based, nature-inclusive renewable energy siting. All data used or produced for the Smart Siting analysis are available in open data formats compatible with any GIS software and can be downloaded at www.nature.org/en-us/about-us/where-we-work/europe/stories-in-europe/smart-siting-renewable-energy-portugal. Final outputs from the Smart Siting analysis can be viewed within a web mapping application at https://tnc-ps-web.s3.amazonaws.com/Renewables/PRT/index.html.

2. Energy modeling

Our energy modeling analysis focused on creating Development Potential (DP) maps to predict where future onshore wind turbines and ground-mounted photovoltaic (PV) solar farms are most likely to be built across mainland Portugal. These DP maps rank DP from 0 (highly unlikely) to 1 (highly likely) and help guide decision makers in understanding where potential impacts may occur from development (Oakleaf et al., 2019). When combined with biodiversity and social value layers, these DP maps are a critical component of the smart siting approach (Sochi et al., 2023).

Given Portugal's strong commitment to renewable energy, previous wind and photovoltaic (PV) development has occurred across the country. Due to publicly available and accurately mapped past development locations, a predictive modeling approach was used to produce a DP map for each technology. This process has two main components: spatial data preparation using Geographic Information System (GIS) techniques and spatial statistical modeling.

Due to previous modeling experiences (Copeland et al., 2009; Evans & Kiesecker, 2014; Strager et al., 2015; Kiesecker et al., 2023), we applied a non-parametric, probabilistic Random Forests (RF) algorithm (Breiman, 2001), using a bootstrapped Classification and Regression Tree (CART) approach for modeling both wind and PV DP. This modeling technique required three key data products:

i) a map representing presence and absence of both wind and PV development;
ii) a map of technically suitable lands for future development; and
iii) a set of parameters maps that are known drivers of development.

Specifically, our workflow followed a nine-step process to produce each DP map (Figure 1):

1. **Map Existing Development:** We created validated maps of current wind and PV installations across mainland Portugal.

2. **Identify Technically Suitable Lands:** Mapped areas suitable for future wind and PV development by applying technical exclusion criteria.

3. **Generate Presence/Absence Data**: Derived point locations for existing (present) and non-developed (absent) RE sites to support predictive modeling.

4. **Map Influential Parameters:** Identified and mapped spatial parameters known to influence wind and PV development (e.g., slope, grid proximity, capacity factors).

5. **Build Training Dataset:** Assigned parameter values to all present and absent locations to create a comprehensive training dataset.

6. **Select Key Parameters:** Used the rfUtilities package in R to remove highly correlated variables and select the most significant predictors for the model development (Liaw & Wiener, 2002; Murphy et al., 2010; R Core Team, 2021; Evans, 2025a; 2025b)

7. **Run Random Forest Models:** Applied the ranger package in R to build ensemble Random Forest models for wind and PV development potential (Wright et al., 2024).

8. **Validate Model Performance:** Assessed model accuracy using metrics like log loss, Cohen's Kappa, and AUC/ROC to ensure reliability.

9. **Generate DP Maps:** Applied the final models across technically suitable lands to produce probabilistic maps of future wind and PV development potential.

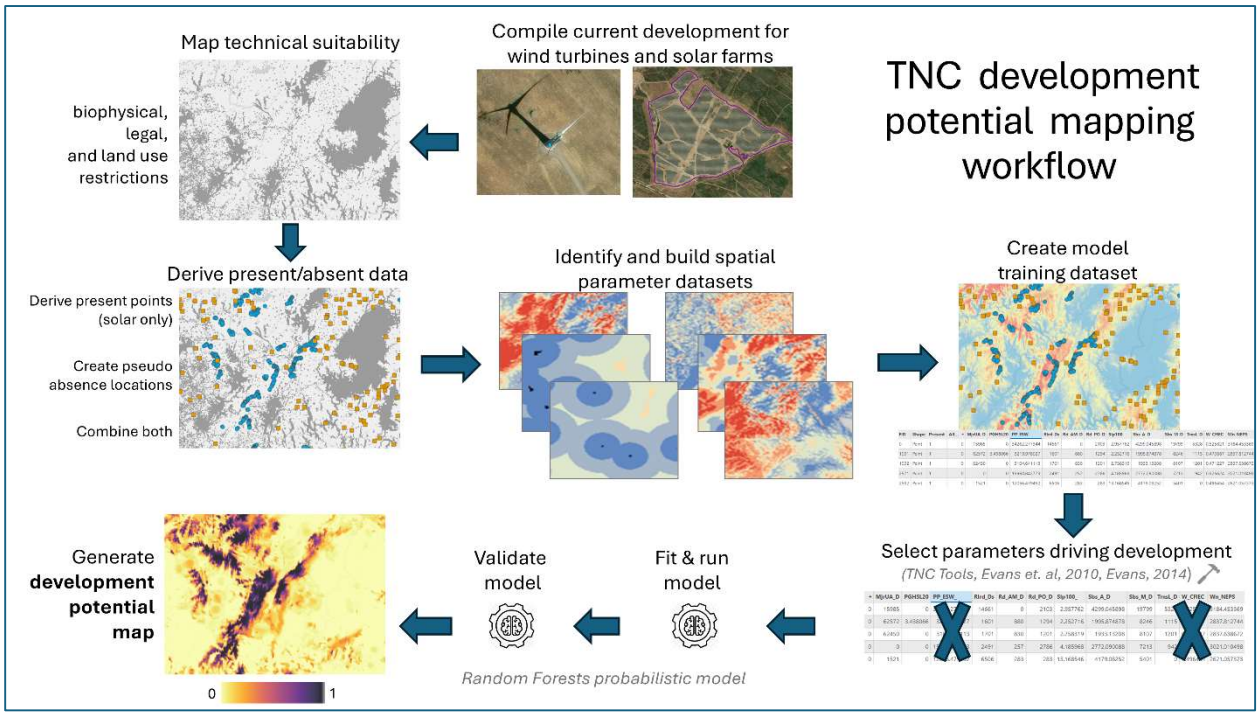

Figure 1: TNC Development Potential (DP) mapping workflow.

Initial draft wind and PV DP maps were presented to an expert working team in September 2024. Based on their feedback, the datasets and modeling inputs were updated, resulting in a second round of DP maps. These revised maps were then shared with LNEG and APREN in December 2024, February 2025 and June 2025. Further input from these meetings led to additional refinements, culminating in a finalized set of parameter datasets presented on the next section (Table 1).

During the modeling process, preliminary results revealed distinct drivers of development when comparing small-scale PV projects (smaller or equal to 10 ha) to large-scale PV projects (greater than 10 ha). Based on this finding, the PV modeling was split into two separate tracks. The 10

hectare threshold was chosen based on the median size of solar farms in the training dataset and aligns closely with the 5 MWac capacity benchmark commonly used to define large-scale solar farms (Bolinger & Bolinger, 2022). This separation not only improved model accuracy but also enabled planners to explore different development scenarios (e.g., several small installations versus fewer large ones) and better support community-level land use planning.

Additionally, due to high grid saturation in Portugal, two additional models were developed: one that excluded substation parameters, and another that excluded all power grid-related parameters. These versions helped to identify development drivers beyond grid infrastructure and offered insights into where grid expansion might be needed to meet long-term renewable energy targets.

In total, our modeling effort produced nine intermediate DP maps (three for wind, three for large-scale PV, and three for small-scale PV). These were used to generate one final wind DP map and two final PV DP maps (split by size). From these, we identified technically suitable areas with high development potential (DP value greater or equal than 0.65) for each technology. These binary maps were then integrated with biodiversity and social value layers as part of TNC's Smart Siting analysis for Portugal.

2.1. Detailed methods for the Development Potential models

2.1.1. Spatial analysis properties and technologies applied

Our analysis focused on mainland Portugal, which was identified using a Portugal boundary map (DGT, 2023) and refined by more accurate coastline representation (OSM, 2024). For all spatial data, we relied on a commonly used Portugal-specific projection of ETRS 1989 Portugal TM06 (EPSG:3763) and projected all data to this coordinate system prior to any derivative spatial analysis, raster conversion, or modeling efforts. All raster datasets used in this analysis were created at 100-m resolution. To ensure common data values and alignment of pixels for all raster datasets, we produced a raster analysis mask by converting the mainland Portugal feature (described above) to a 100-m resolution raster dataset which included all pixels with at least 50% of the pixel within the boundary. All spatial analyses and modeling were conducted using ArcGIS (ESRI, 2024) and QGIS (QGIS Development Team), as well as automated workflows in Python and R, utilizing appropriate modules, packages and libraries.

2.1.2. Current wind and solar development

To map existing renewable energy infrastructure, wind turbines and solar farms locations were gathered from three sources of data:

i) Directorate General for Energy and Geology (DGEG, 2024);
ii) Global Renewables Watch (GREW, 2024);
iii) Endogenous Energies of Portugal (E2P, 2024).

All datasets were visually validated using recent satellite (Planet Labs, 2024) and aerial (OrtoSat, 2023) imagery to confirm that mapped features corresponded to actual installations.

Wind Turbines:

We validated a total of 2,812 wind turbines across Portugal. Of these:

- 2,498 turbines (89%) were mapped by both DGEG and GReW;
- 202 turbines (7%) were uniquely identified by DGEG;
- 112 turbines (4%) were uniquely identified by GReW.

E2P data were excluded from wind modeling because they provided only wind farm locations, not individual turbine points, which are required for spatial modeling.

For the final wind turbine map, we relied first on locations from DGEG and only used GReW locations when data were missing from the DGEG dataset (n=112). We based this decision on visual inspection of the two data sources and found DGEG points were often closer to the true ground location associated with the base of turbine than those points associated with GReW. For modeling efforts, one turbine location was removed due to it being an isolated, demonstration turbine located within a turbine factory.

Solar Farms:

The same three sources (DGEG, GReW, and E2P) were used to map solar farms, with all data validated using Planet (Planet Labs, 2024) and aerial (OrtoSat, 2023) imagery. Before validation, we excluded solar farms smaller than 1 hectare, as these typically represent rooftop installations not relevant to this study.

We validated 268 solar farms, covering a total area of 7,816 hectares, with sizes ranging from 1 ha to 772 ha. From these:

- 118 farms (44%) were identically mapped by both DGEG and GReW;
- 80 farms (30%) were uniquely mapped by DGEG;
- 64 farms (24%) were uniquely mapped by GReW;
- 6 farms (2%) were identified only by E2P.

Since E2P provided only point locations, we screen-digitized the boundaries of these six farms using Planet imagery (Planet Labs, 2024). In a similar process realized for the wind turbines, we prioritized DGEG solar farm boundaries and used GReW and E2P data only when DGEG coverage was missing. For modeling purposes, we focused exclusively on ground-mounted solar farms, reducing the final dataset to 251 installations. This filtering excluded:

- 16 rooftop solar farms on industrial/commercial buildings
- 1 floating solar farm
- 3 mixed installations, which were modified to include only the ground-mounted portion

2.1.3. Technically suitable lands for wind and solar development

To identify where future wind and solar development could technically occur, we applied a series of exclusion criteria. These exclusions were based on three main factors:

- Resource limitations (e.g., low wind speeds);
- Biophysical constraints (e.g., steep slopes);
- Conflicting land uses (e.g., residential areas or artificial surfaces).

The final technical exclusions selected were supported by feedback from exports and ultimately finalized by partner input.

For wind development, we excluded the following areas:

- Locations with average wind speeds below 5 m/s (Feedback from expert group);
- Land with slopes greater than 25% across an entire hectare;
- All areas classified as artificial surfaces (DGT, 2018);
- Lands within 100 meters of residential buildings (GTAER, 2024);
- Areas identified as inland waters (DGT, 2018);
- Areas within 700 meters of existing wind turbines (n = 2,811), with only those 1-ha pixels fully contained within the buffer being removed.

After applying these exclusions, we removed 19,440 km² (or 21.8% of Portugal's mainland area) from consideration, leaving 69,662 km² as technically suitable for wind development.

For ground-mounted PV development, we excluded the following areas:

- Land with slopes greater than 25% across an entire hectare;
- All areas classified as artificial surfaces (DGT, 2018);
- Lands within 100 meters of residential buildings (GTAER, 2024);
- Areas identified as inland waters (DGT, 2018);
- Lands that overlap with existing solar farms.

These exclusions were then combined, removing 18,871 km^2 (or 21.2% Portugal's mainland area) from further solar development, and thus leaving 70,231 km^2 technically suitable for solar development.

2.1.4. Present/absent locational data

Due to applying a presence/absent predictive modeling approach (e.g., using a Random Forest algorithm), it was necessary to produce point data representing not only current wind and PV development (present) but also locations identifying where development has yet to occur (absent). To create a final present/absent dataset, our methodology required several steps:

i) Derive point features to represent development (PV only)
ii) produce random points representing pseudo null locations of development across technically suitable lands, and

iii) combine both the present (current development) and absent (pseudo nulls) locations into one dataset.

Generating development point locations

With all wind turbines already identified by a point location, this task was necessary for PV only. Initial model versions used a single centralized point per PV polygon, but this approach failed to reflect the wide variation in solar farm sizes. To address these size discrepancies, we calculated the median size of all solar farms and then generated random points within each polygon based on a ratio of individual size to this overall median (Eq. 1).

$$\text{Number of points per solar farm} = round\left(\frac{area}{median + 1}\right) \quad (1)$$

We used this method for both the small-scale and large-scale PV with each having a median size of 3.41 and 29.46 ha, respectively. For those PV identified as small-scale, points generated per farm ranged from 1 to 4 and for those identified as large-scale, points generated per farm ranged from 1 to 27.

Pseudo null locations

To produce our pseudo null locations, we applied *pseudo.absence* function within the R spatialEco package (Evans, 2025a). Using the default settings of the function, we generated pseudo-null locations across technically suitable lands at a quantity 1.25 times greater than the number of development point locations (e.g., wind turbine points and the randomly generated points within small- and large-scale solar farms). By default, *pseudo.absence* uses the development point locations to produce an inversed, Isotropic Kernal Density Estimate (KDE) map with the Scott's Rule applied for bandwidth selection. By setting the *ref* parameter of this function to a raster dataset identifying any technically suitable lands regardless of current development (e.g., technical suitable map produced without current development exclusions), an inversed KDE map is produced covering only these lands. The pseudo nulls are then randomly created based on weighted values associated with the KDE map thus increasing null points produced furthest from concentrated development and limiting the number of points closest to development. Additionally, by limiting output to only those technically suitable lands, no pseudo-null locations are generated on sites which have never been an option for development (e.g., steep slopes).

Combining present and absent locations

Once development locations and corresponding pseudo null locations were produced, both datasets were combined into one point dataset. A field identifying developed locations with a value of 1

and those absent of development with a value of 0 was added to distinguish each within the combined dataset.

2.1.5. Identify and create spatial parameter datasets

We created an original set of spatial parameters based on Sochi et al. (2023), which was subsequently refined through expert and partner feedback. The final set includes 14 spatial parameters: 10 common to both wind and PV development, and 2 additional parameters specific to each technology (Table 1). These parameters fall into six main categories:

- capacity factors;
- topographic factors;
- proximity to power grid;
- accessibility for development;
- proximity to demand centers;
- avoidance factors.

Each parameter was derived from an original source dataset and often required multiple processing steps. All source data were reviewed for completeness and accuracy to meet the modeling standards. When available, Portugal-specific datasets were prioritized. Final parameter layers were produced as raster datasets at 100-meter resolution, using the EPSG:3763 coordinate system, and aligned with all other modeling data.

Capacity factors:

All development potential models require a map identifying those areas with the highest resources. For wind and PV, this is typically represented by wind speeds and Global Horizontal Irradiance (GHI), when available. However, spatially explicit capacity factor (CF) maps offer a more accurate predictor of development potential, as they integrate resource availability with biophysical conditions to estimate power output at a given location. For this analysis, we used two CF maps:

- A wind CF map (NPESv2) that estimates, at 100-meter resolution, the number of equivalent operating hours a wind turbine would produce at nominal power across Portugal (LNEG, 2025, Personal communication).
- A PV CF map (PVOUT) that estimates, at 1000-meter resolution, the the daily kilowatt hours per kilowatt capacity (kWh/kWp) of PV solar across Portugal (Solar Atlas V2., 2024).

For the NPESv2, a capacity factor can directly be derived by dividing the hours identified by the dataset by the total hours in a year (8640). NPES values ranged from 1,142 (CF=0.13) to 4,199 (CF=0.49) hours with 95% of values falling between 1,834 (CF=0.21) and 2,826 (CF = 0.33) hours. PVOUT values ranged from 3.36 to 4.84 daily kWh/kWp, with 95% between 3.95 and 4.57 daily kWh/kWp.

Table 1: Final spatial parameter datasets used in mapping development potential for future wind and ground-mounted photovoltaic solar development. Parameters in bold were updated from original effort through expert and partnership feedback.

Parameter Description	Model	Units	Resolution	Data Source
Wind capacity factor (no. of equivalent operation hours at nominal power, NEPS v2)	Wind	hours/year	100 m	LNEG, 2025 (Personal communication)
Solar capacity factor - average daily totals (PVOUT)	Solar	kWh/kWp per day	1 km	Solar Atlas V2. (2024)
Avg multi-scaled topographic position index	Wind	relative index	30 m	Global SRTM mTPI (2024)
Average aspect ranking	Solar	ranking for solar	30 m	NASA, SRTM (2024)
Minimum and average (solar) and (wind) percent slope	Both	%	30 m	NASA, SRTM (2024)
Distance from major substations (size > 2 ha)	Both	meters	~5 m	OSM (2024)
Distance from all substations (size > ¼ ha)	Both	meters	~5 m	OSM (2024)
Distance from transmission lines	Both	meters	~5 m	OSM (2024)
Distance from power plants	Both	meters	~5 m	DGEG (2024) GREW (2024) WRI (2024)
Distance from primary roads	Both	meters	~5 m	OSM (2024)
Distance from all major roads	Both	meters	~5 m	OSM (2024)
Distance from major urban areas	Both	meters	1 km	JRC (2025)
Distance from all cities	Both	meters	1 km	JRC (2025)
Population density	Both	number of people	30 m	META, 2024

Since NPESv2 was already projected to EPSG:3763, we aligned it with other datasets using a nearest-neighbor adjustment to produce the final wind CF parameter (Figure 2a). Alternative wind CF datasets were examined for use (LNEG, 2018; Global Wind Atlas, 2024; New European Wind Atlas, 2024), but expert reviewers and project partners confirmed NPESv2 as the most accurate and reliable dataset available for Portugal.

For PV CF, we were limited to using the only publicly available dataset, PVOUT. This raster dataset required projecting and aligning all 1000 m^2 pixels to our modeling environment using a bilinear approach. We then resampled these data to match our 1 ha pixel size by applying the same PVOUT value across all overlapping pixels resulting in our final *solar CF* parameter (Figure 2b).

Topographic factors:

All topographic parameters were derived from a global 30-meter resolution Digital Elevation Model (DEM) (NASA, SRTM, 2024). The DEM was first projected to EPSG:3763 and aligned with the modeling environment using bilinear interpolation. Then separate analysis and resampling methods were applied to produce four different parameters derived from DEM data: average, multi-scaled topographic position index (mTPI), aspect ranking (de Luis-Ruiz et al., 2024), minimum and average slope.

The mTPI map provides a relative topographic ranking, with higher values representing ridges and peaks, and lower values indicating valley bottoms (Theobald et al., 2015). To calculate this metric, we relied on the mTPI tool within Topography Toolbox Pro software (Dilts, 2023) and maintained the default parameters provided. This tool produced relative values across Portugal at a 30-m resolution which were then averaged across the modeled 100-m resolution to produce our final *mTPI parameter* (Figure 3a). Relative values for mTPI ranged from -3.77 to 3.45, with 95% of the values occurring between -0.951 and 0.918.

To rank aspect values for solar, we followed methods established by de Luis-Ruiz et al. (2024) by deriving aspect values per pixel and then assigning a simple order ranking of these aspect values (Table 2). Again, we aggregated these 30-m pixel data output to our modeling 100-m resolution by averaging the values resulting in our final *aspect ranking* parameter (Figure 3b).

Finally, we derived a percent slope map from DEM data and calculated two slope parameters: *minimum slope* and *average slope*. For the *minimum slope* parameter, we assigned each 1-ha modeling pixel with the minimum 30-meter resolution slope value found across each pixel (Figure 3c). For the *average slope* parameter, we calculated the average of all 30-m slope values located within each modeling pixel (Figure 3d). We applied the minimum slope as a wind parameter due to the ground pads of onshore wind turbines not often exceeding 30 m in diameter (Currie et al., 2015) thus minimizing slope restrictions within a proposed development area.

Table 2: Aspect ranking values

Category	Aspect Values	Assigned Aspect Rank
Flat	-1	5
North	>315 – 360 and 0 - 45	0
Northeast	>45 - 90	1
Southeast	>90 - 135	3
South	>135 - 225	5
Southwest	>225 - 270	4
Northwest	>270 - 315	2

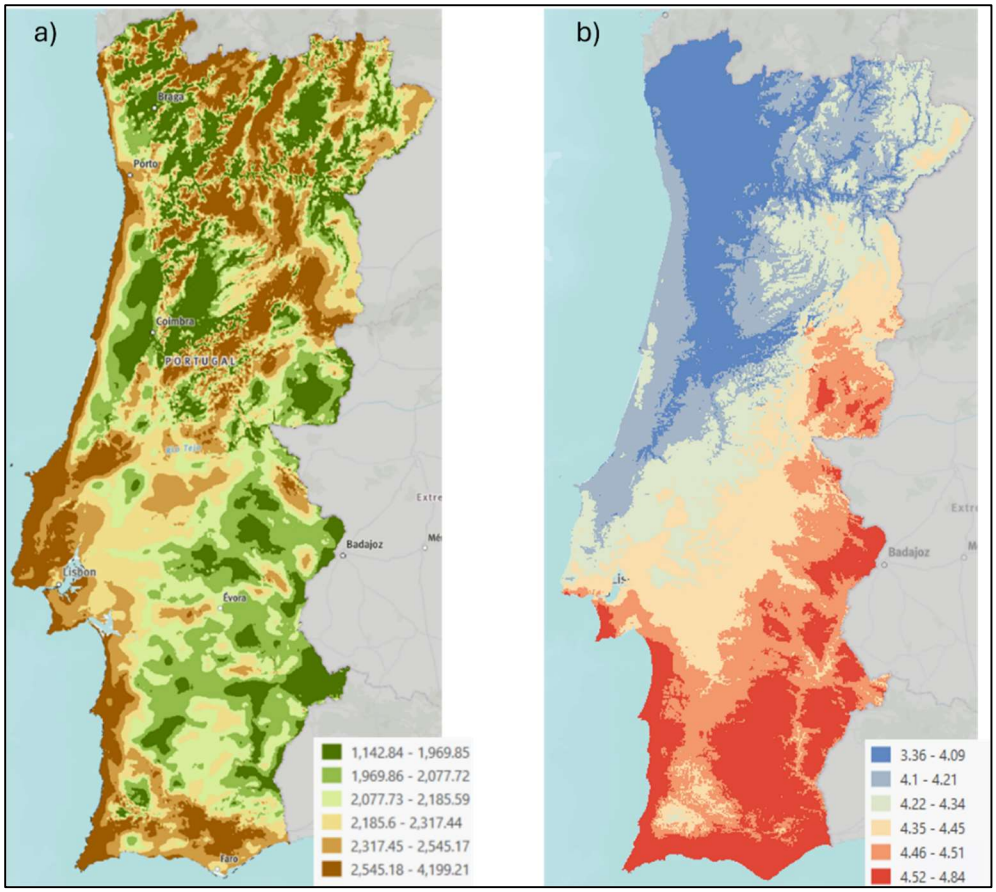

Figure 2: a) Wind and b) solar capacity factor (CF) model parameter maps. Wind CF values measured in hours of equivalent operations at nominal power per year. Solar CF values measured in daily kWh/kWp. All maps have continuous values but are classified for display purposes.

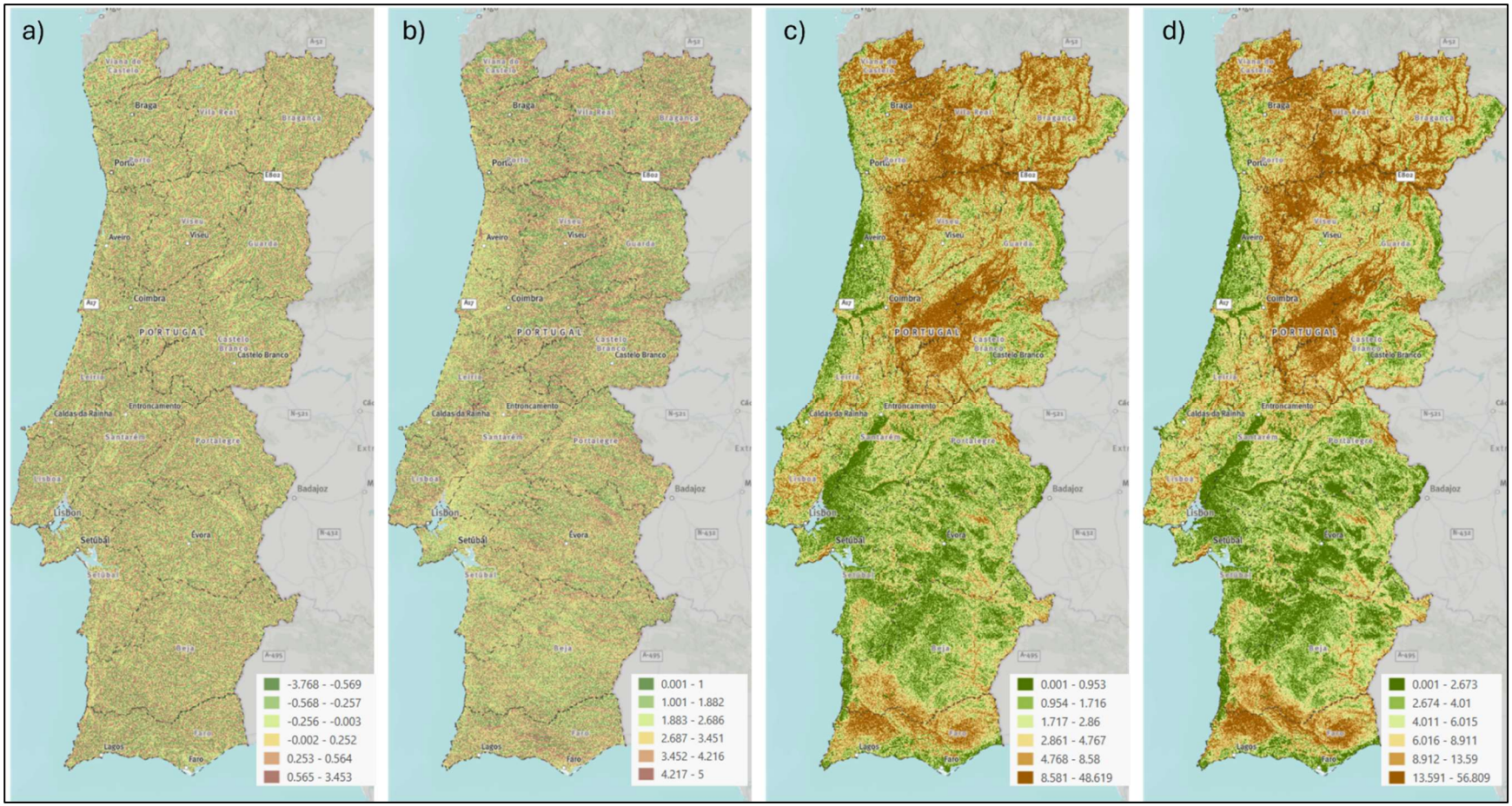

Figure 3: Topographic model parameter maps. Multi-scaled topographic position index (mTPI) map (a) and aspect ranking map (b) have unitless relative values with minimum slope map (c) and average slope map (d) have values described by percent slope. All maps have continuous values but are classified for display purposes.

Proximity to power grid:

We defined proximity to the power grid using three key infrastructure features: substations, transmission lines, and existing power plants. For substations and transmission lines, we used OpenStreetMap (OSM, 2024), selecting features tagged as "power=substation" and "power=line", respectively. For substations, we ensured that all substations were at minimum ¼ hectare in size (n=450) and designated major substations as those mapped 2 hectares or greater in size (n=61) (Shahriar Haque et al., 2022). All features were projected to EPSG:3763, and Euclidean distance was calculated across mainland Portugal to generate three spatial parameters: *distance to major substations* (Figure 4a), *distance to all substations* (Figure 4b), and *distance to transmission lines* (Figure 4c).

To map power plants, we relied on data from DGEG (n=3,017 points and n=591 polygons) (DGEG, 2024) and World Resources Institute (n=469 points) (WRI, 2024), excluding all wind and solar facilities. WRI data were projected to EPSG:3763, and any locations within 1 km of DGEG-identified power plants were removed to avoid duplication. Finally, we combined point data from DGEG locations (n=214) and remaining WRI locations (n=154) and calculated the Euclidian distance from these points across mainland Portugal. Due to DGEG sites mapped also as polygons, we also calculated the Euclidian distance from these features (n=33). We then combined both Euclidian distance maps by maintaining the lowest distance value found within each pixel to produce the *distance to power plants* parameter (Figure 4d).

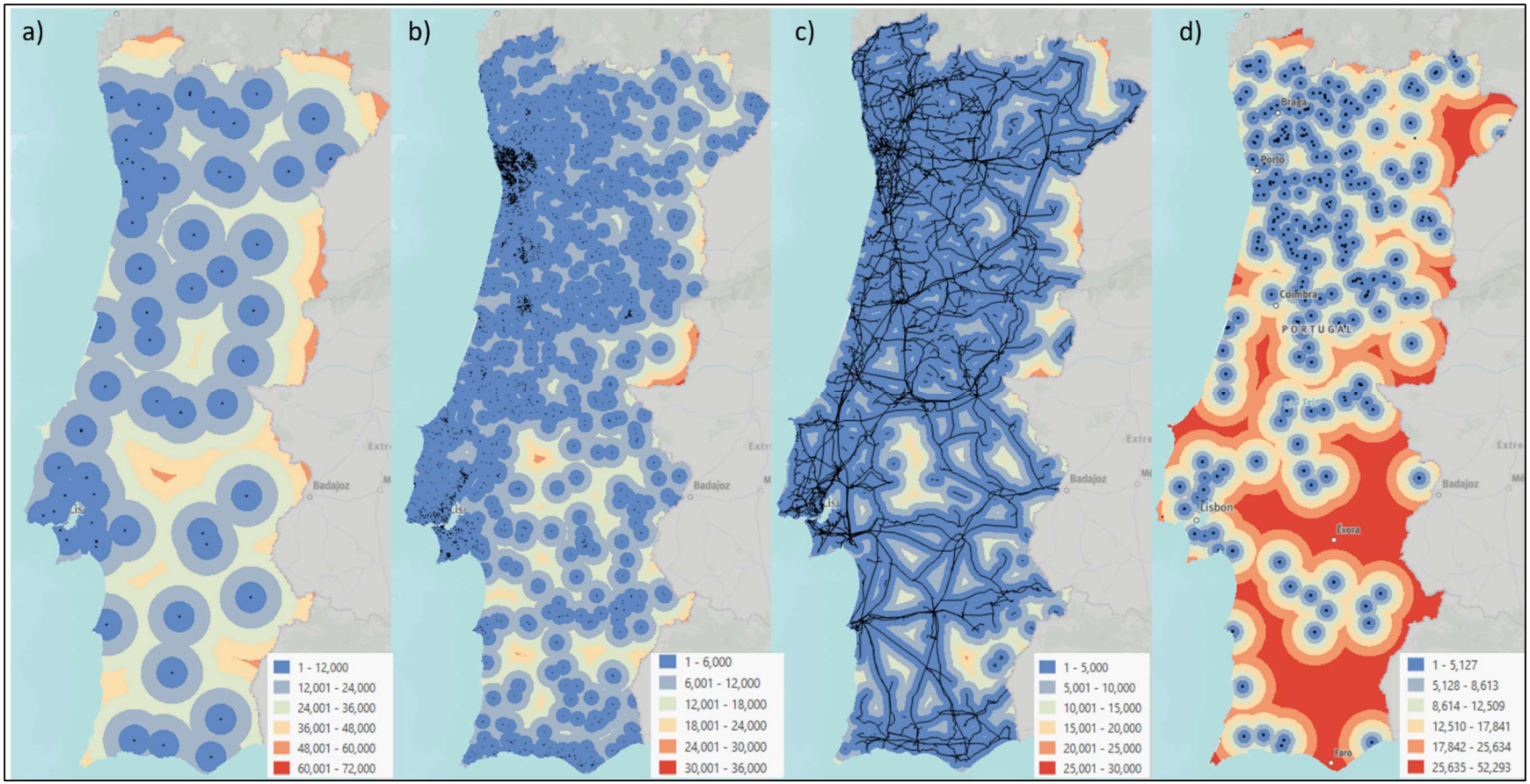

Figure 4: All model parameter maps associated with Portugal power grid. Maps show distance from major substations (a), distance from all substations (b), distance from transmission lines (c), and distance from power plants (d). All distances are measured in meters from features shown in black. All maps have continuous values but are classified for display purposes.

Accessibility for development

We used distance to roads as the main proxy for development accessibility, relying once again on OSM data (OSM, 2024) to identify these features. Euclidean distance was calculated for two road categories: "primary" roads and "all major" roads. For primary roads, we selected all linear features with the "fclass" attribute values of either "motorway", "trunk", or "primary", while for all major roads, added to the previous selection by including "fclass" attribute values of "secondary" and "teritiary". For both selections the associate "link" features were also included (e.g., "motorway link"). After projecting these features to EPSG:3763, we calculated the Euclidian distance from each road dataset to produce our final parameter maps; *distance from primary roads* (Figure 5a) and *distance from all major roads* (Figure 5b). Originally, an often-used parameter in RE siting, "*distance from railroads*" was created and used in the modeling process but later removed due to partner feedback indicating a lack railroads in Portugal being used for transporting development materials (e.g., wind turbine blades).

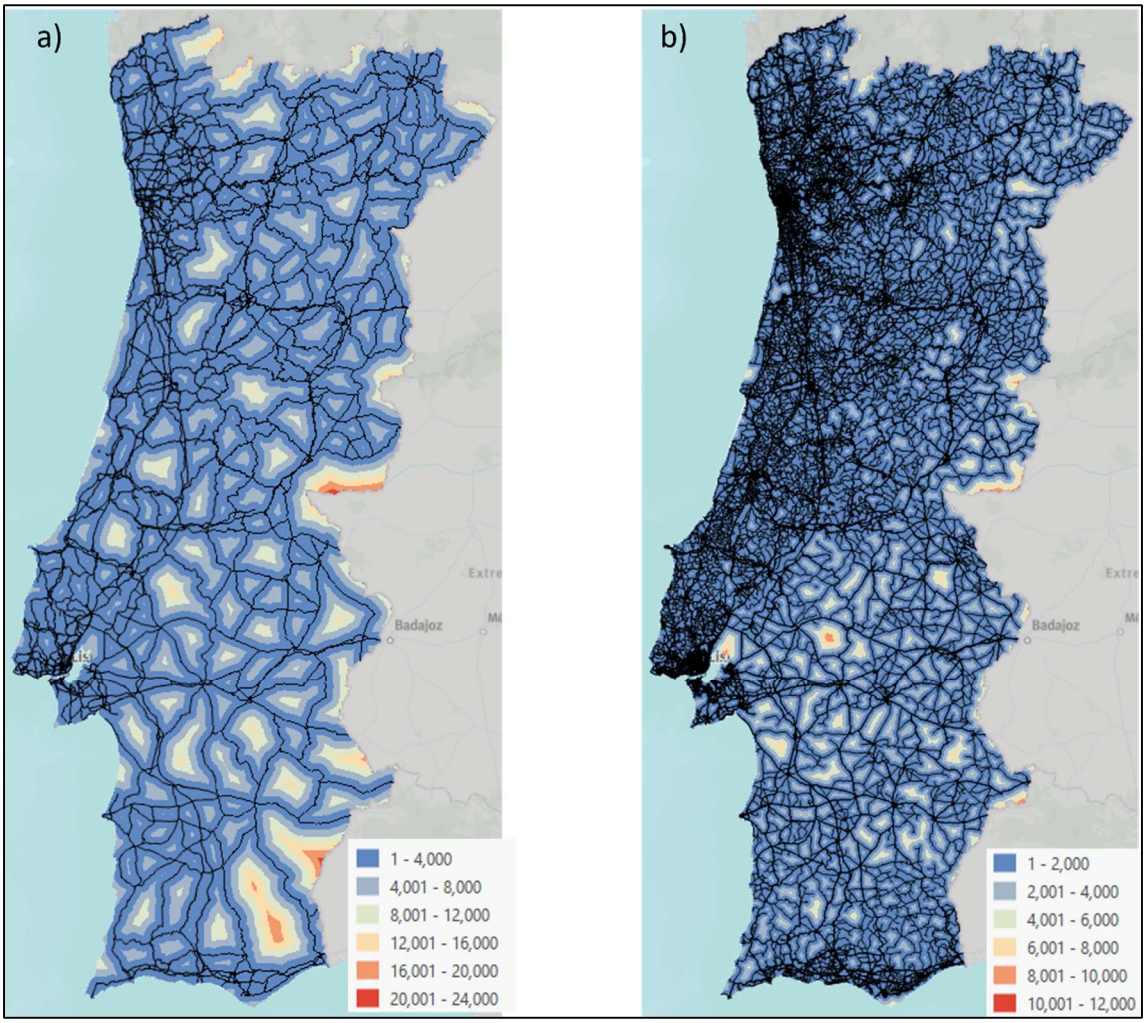

Figure 5: All model parameter maps associated with accessibility for development. Maps show distance from primary roads (a) and distance from all major roads (b). All distances are measured in meters from features shown in black. All maps have continuous values but are classified for display purposes.

Proximity to demand centers

To assess proximity to demand centers, we focused on population centers by mapping the boundaries of major urban areas and cities across Portugal and then calculated the distance from these centers. To identify them, we used the Global Human Settlement Layer (GHSL), Degree Urban 2025, 1-km resolution raster dataset (JRC, 2025). After projecting and aligning this dataset to our modeling environment using a "nearest neighbor" interpolation, we created boundaries for just major urban areas by selecting pixels with a value of 30 indicating "urban centers" and then grouped contiguous pixels (diagonals included) into major urban areas. This method identified five major urban centers: Lisbon, Porto, Coimbra, Braga, and Portimão. To produce boundaries for all cities, we followed the same procedure, but this time included pixel values of 23- "dense urban cluster", 22- "semi-dense urban cluster", and 21- "suburban or per-urban". Euclidian distances were calculated from each set of boundaries to create our final two parameters: *distance from major urban areas* (Figure 6a) and *distance from all cities* (Figure 6b).

Avoidance factors

While RE projects supply power to mainly population centers, these types of power plants, especially wind, are often built in areas with low or no population. To represent this phenomenon spatially within our model parameters, we relied on a 2020 estimated population density map (Meta, 2024). This map estimates the number of people located within a per 30 m^2 pixel across the world. After selecting only data specific to Portugal, we then projected and aligned these data with our modeling environment. We then summed the number of people within each 1-ha pixel to produce the *population density* parameter (Figure 6c).

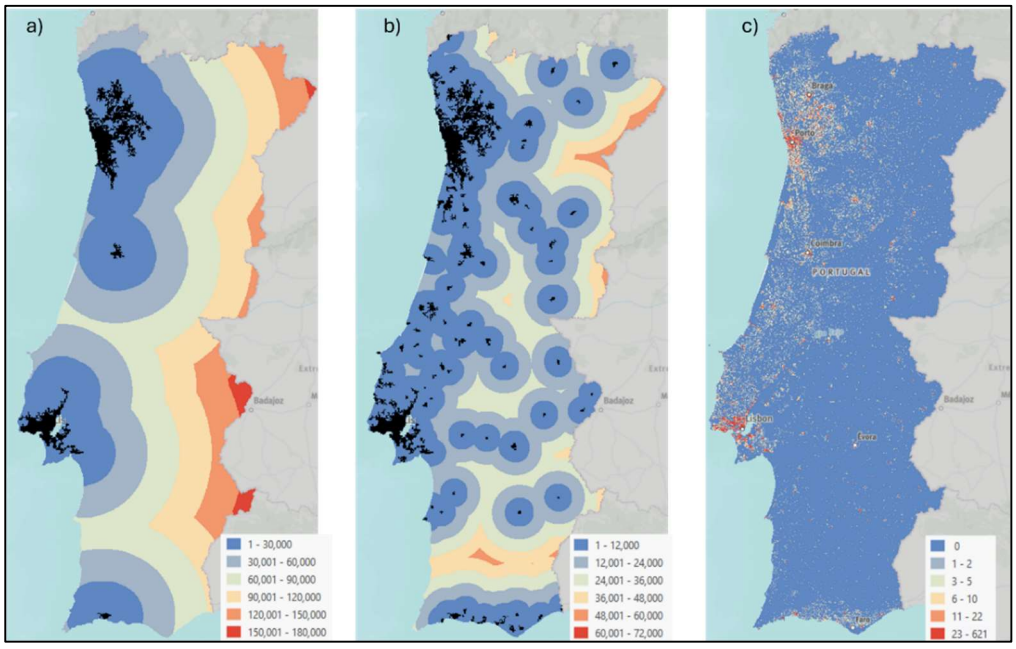

Figure 6: All model parameter maps associated with proximity to demand and avoidance. Maps show distance from major urban areas (a), distance from all cities (b), and population density (c). All distances are measured in meters from features shown in black. Population density value is measured by people count per pixel. All maps have continuous values but are classified for display purposes.

2.1.6. Training Dataset

Once all parameter datasets were developed, we then assigned the overlapping parameter pixel value for all present and absent locations (sections 2.1.4 and 2.1.5). For both wind and solar, this produced twelve parameter values across all locations and provided the foundation for all additional model work.

2.1.7. Selecting Modeling Parameters

With the training dataset, we followed Murphy et al. (2010) by applying the R (Liaw & Wiener, 2002; R Core Team, 2021) package *rfUtilities* (Evans, 2025a; 2025b) to select significant parameters. Parameter sets for each final model were selected based on those which produced the lowest out-of-bag (OOB) error and lowest class error, as identified by *modelSel* command within *rfUtilities*. From these selected parameters, we then checked for multi-collinearity and if needed removed the collinear variable with the lowest importance value from all parameters before rerunning our model selection.

2.1.8. Random forest probabilistic modeling

After identifying a parameter set, we then fit each RF probabilistic model by running the *ranger* command within the R package *ranger* (Wright et al., 2024). Specific to *ranger*, we set a maximum of trees to 501, used all training data with the selected parameter values, and included the importance measure of permutation. We then assessed this model fit by first calculating the log loss value, ensuring a value below 0.5. We further assess the model fit by transforming the model probabilities to a binary outcome using a threshold probability value greater or equal to 0.65 as present and less than 0.65 as absent and then compare these derived values with our original present/absent RE locations. Using the *accuracy* command within *rfUtilities*, we then examined several confusion-based metrics such as percent correctly classified (PCC), Cohen's Kappa, and area under the receiver operating curve (AUC/ROC). To assess model performance, we performed a Bootstrap approach where the full model is evaluated against numerous Bootstrapped models representing different realizations of probabilities. Specifically, we applied the *crossValidation* command within *rfUtilities* and set this command to have 99 replicated predictions withholding 10% of data from each replicate. We then quantified error based on average Kappa and OOB error metrics associated with these withheld data of each iteration. For all models produced, we used these values to overall validate each model and provide comparisons across models.

2.1.9. Development potential maps

We produced final development potential (DP) maps by applying the trained Random Forest (RF) models to all raster datasets associated with the selected parameters. Each pixel was assigned a predicted probability value representing the likelihood of future wind or solar development, ranging from 0 (highly unlikely) to 1 (extremely likely). To focus only on areas that are technically feasible for development, we excluded all regions identified as unsuitable in the technical criteria (Section 2.1.3). Areas with a DP value greater or equal to 0.65 were classified as having high

development potential, following a commonly used threshold in probabilistic modeling (Evans & Kiesecker, 2014).

Initial PV modeling showed varying importance in parameters when modeling small-scale PV development (smaller or equal to 10 ha) vs large-scale PV development (greater than 10 ha). The 10-hectare breakpoint was based on the median size of solar farms in the dataset and coincides with the approximate area required for a 5 MWac utility-scale solar installation (Bolinger & Bolinger, 2022). As a result, separate DP maps were created for small- and large-scale PV development.

Additionally, due to high grid saturation within Portugal, two extra models were developed, one which removed all substation parameters and a second one that removed all parameters associated with the power grid. These alternative models aimed to expand the scope of predicted development opportunities, identify drivers of development independent of grid infrastructure and provide insights regarding grid expansion to support long-term RE targets. This request resulted in three intermediate DP maps which differed only by the initial parameter inputs to derive the model:

1) all available parameters (All),
2) exclusion of substation parameters (Substation Dropped), and
3) exclusion of all parameters referencing the power grid (Power Grid Dropped).

In total, 9 intermediatory DP maps were produced (3 wind, 3 large-scale PV, and 3 small-scale PV), which ultimately led to the development of one wind and two size-dependent PV DP maps. The final wind and two size-dependent PV DP maps were created by combing the intermediary DP maps from the "All" and "Substations Dropped" models via selecting the highest probability per pixel of either DP map. This decision to combine outputs from these two intermediate DP maps was based on several factors. First, there was a lack of knowledge in our model parameters regarding capacity, and expansion opportunities with any substation. Second, substations are often built at, or near, the same time as the wind or solar power plants that are being developed (Ong et al., 2013; Cerveira et al., 2021). Third, while opportunities exist to expand capacity of current transmission lines (e.g., reconductoring), the timing on developing new transmission lines to support unserved areas can be upwards of 10 years (IEA, 2023) and thus not suitable for inclusion in a current DP map. Finally, by not also including the "Power Grid Dropped" DP maps, we maintained a potential comparison necessary to identify future grid expansion.

2.2. Development Potential Results

2.2.1. Wind Development Potential Models

For wind DP models, we discovered that two parameters consistently had the strongest influence across all models: *Average mTPI* and *Wind capacity factor* (Table 3). Average *mTPI* values greater than 0.75 showed the highest level of influence for wind DP and was supported by the vast number of wind turbines currently found on ridgetops. Conversely negative *mTPI* values consistently

produced low overall DP. *Wind CF* values higher than approximately 0.29 (e.g., NPES > 2,500 hours) showed highest influence on wind DP. Like mTPI, low *wind CF* values (e.g., NPES < 2,200 hours) were common in areas associated with low wind DP values.

Besides having various degrees of importance to the models, the parameters of *Distance from All Substations*, *Distance from Transmission Lines, Distance from Major Urban Areas*, and *Distance from Power Plants,* had similar effects, with DP values generally decreasing as distance from these features increased. For both *Distance from All Substations* and *Distance from Transmission Lines* parameters*,* distances up to 5 km and 2 km, respectively, showed strong influences on Wind DP values. This influenced decreased rapidly after these distances and continued until each provided little influence on Wind DP values past distances of 10 km and 6 km, respectively. The *Distance from Major Urban Areas* parameter influenced Wind DP values consistently up to distance of 60 km after which the influence decreased greatly until seeing little to no influence past 100 km. The *Distance from Power Plants* showed only a slight influence on DP values to a maximum distance of 25 km.

The remaining selected parameters had low individual influence, with all three showing slight increases in DP values as distance increased. All selected parameters showed high variability in the level of influence indicating no single parameter alone produced high wind DP values (DP >= 0.65) but more combinations of parameters. For example, high Wind CF values (NPES > 2500 hours) and high mTPI values (mTPI > 0.75) almost always resulted in high Wind DP values with the remainder of parameters providing further but less dramatic increases in DP values.

By dropping both substation parameters, the *Distance to transmission lines* parameter increased in predictive power, but remained only one-third as influential as mTPI or wind CF. When dropping all power grid parameters, the *Distance from major urban areas* parameter became a slightly stronger predictor, though still over four times less influential than mTPI or wind CF. We also discovered that two model parameters (*Distance from all major roads* and *Population density*) were not selected by any DP models and the parameter *Minimum percent slope* only slightly influenced the model that excluded all power grid parameters.

All wind DP maps indicated moderate to high development potential in northern and central mountainous regions, a large area northeast of Lisbon, and mountainous zones in far southern Portugal. Little difference in DP maps was shown across Portugal when running the model with or without the substation parameters, although dropping substations resulted in an increase of approximately 392 km² in high DP areas. The most notable change occurred when all power grid parameters were removed, revealing increased high DP along coastlines and ridgelines lacking grid access. The final combined wind DP map (Figure 7a) identifies nearly 2,223 km^2 (2.5% or PRT) of technically suitable, high wind development potential (DP values >= 0.65; Figure 7b).

Table 3: Parameter set included for wind development potential (DP) modeling with associated parameter importance values used in final models. Importance values are listed for three final models; model derived from using all parameters as input (All), model derived when two substation parameters are removed (Substations Dropped), and model derived when all power grid parameters are removed (Power Grid Dropped). Parameters ordered from highest to lowest importance values associated with final all parameter model. Importance values of -1 indicate parameter was not selected to be used in final model. Importance values tagged with "---" indicate parameter was removed from original parameter list prior to the parameter selection process included in the modeling workflow.

Parameter Description	***Importance Values for Wind DP Models***		
	All	**Substations Dropped**	**Power Grid Dropped**
Average multi-scaled topographic position index (mTPI)	0.144	0.159	0.174
Wind capacity factor (CF) - NEPSv2	0.126	0.145	0.167
Distance from all substations	0.081	---	---
Distance from transmission lines	0.034	0.054	---
Distance from major urban areas	0.020	0.033	0.038
Distance from power plants	0.012	0.021	---
Distance from all cities	0.009	0.017	0.019
Distance from primary roads	0.007	0.011	0.008
Distance from major substations	0.007	---	---
Minimum percent slope	-1	-1	0.012
Distance from all major roads	-1	-1	-1
Population density	-1	-1	-1

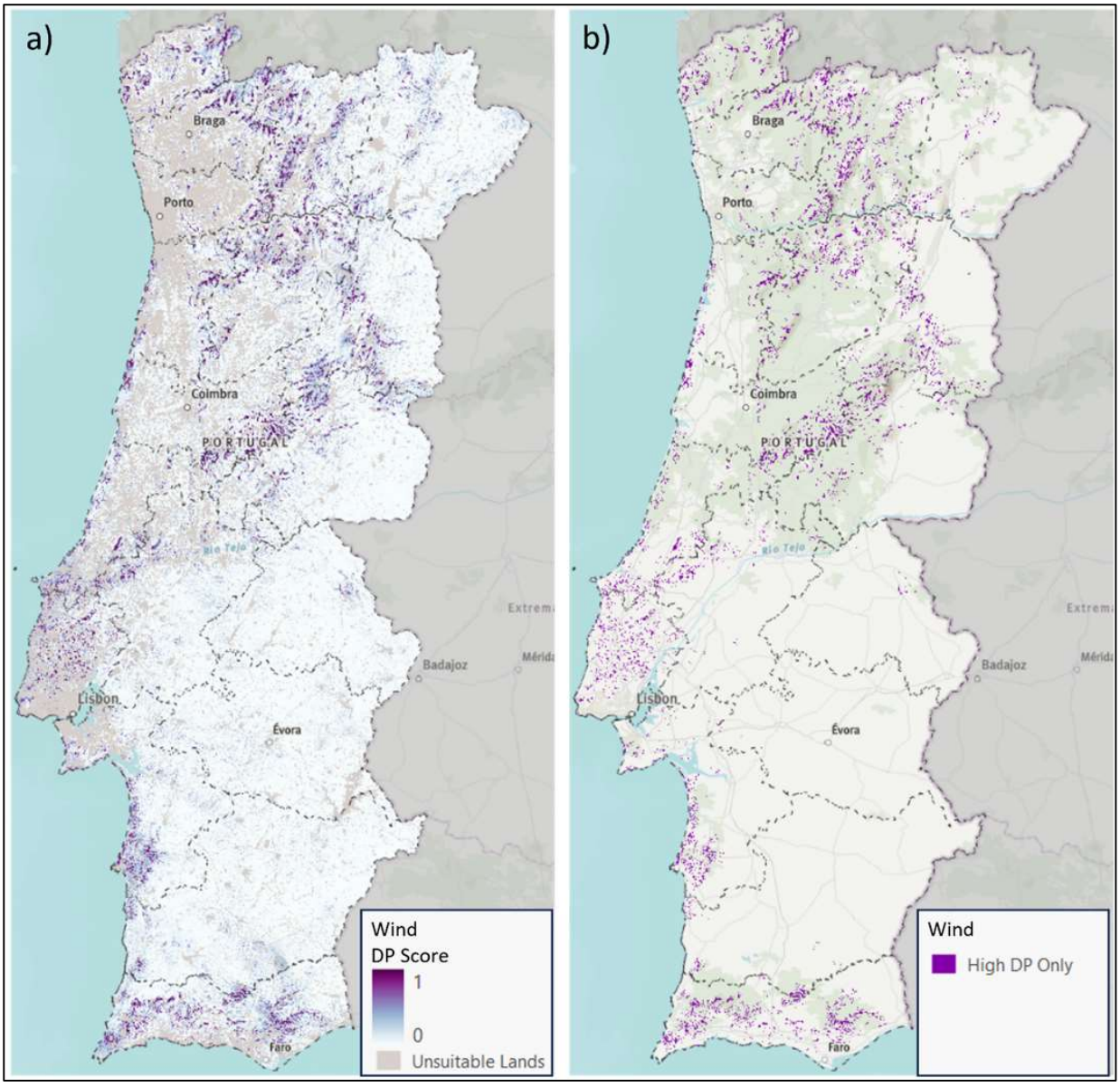

Figure 7: Final development potential (DP) maps for wind energy in Portugal: a) DP values are shown for technically suitable lands, ranging from 0 (lowest potential) to 1 (highest potential). A min/max rendering stretch is applied to display the full range of values. Technically unsuitable lands are depicted in a reddish light grey, while areas outside Portugal are blurred with semi-transparent grey. (b) High DP areas (DP ≥ 0.65) highlighted on technically suitable lands only. This threshold identifies regions most favorable for future wind energy development.

2.2.2. Large-scale PV Development Potential Models

To produce the most accurate large-scale PV DP models, only six parameters were selected out of all thirteen (Table 4). Of these six, only two parameters (*Solar capacity factor* and *Distance from major urban areas)* were not associated with the power grid. In the "All" model, the *Distance from all substations* parameter was the most important one, but only slightly more than *Solar capacity factor* (*CF*). The highest influence in DP values were found in areas within 2.5 km of any substation with a gradual decrease in this influence up to 5 km and becoming negligible beyond

that distance. *Solar CF* showed a rapid increase in influence going from 4.1 to 4.3 UNITS, with a gradual and steady increase thereafter which plateaued at a very high influence from 4.5 and higher. There was a clear gap in model influence between these two top parameters and the remaining four, although all contributed substantial predictive power.

DP values were extremely high within 25 km of major urban areas, decreasing slightly out to 50 km, and providing little additional value beyond that. Interestingly, *Distance from power plants* provided a stronger influence on DP values the further lands were from this feature. Moderate influence still occurred close to power plants, but rose sharply in influence up to a distance of 15 km where a slight but gradual influence continued to occur past this distance. Influence by transmission lines held relatively high up to maximum distance of 2.5 km and then fell sharply to 4 km and had little influence after. Finally, major substations showed strong influence to 10km and then more moderate influences decreasing up to roughly 15 km away from which these features provided little or no influence.

By removing both substation parameters, the *Distance to transmission lines* parameter increased in predictive power slightly. However, it had relatively more influence in the model due to it being second behind *Solar CF.* Also noticeable was an increase in the overall number of selected parameters for the model to eight, even with two parameters being removed. When removing all power grid parameters, *Solar CF* remained consistent as the most important parameter with *Distance from major urban areas* being a close second, followed by *Distance from all cities* with both showing increases in predictive power as moving closer to these areas. We also discovered that two model parameters (*Population density* and *Average aspect ranking*) were not selected by any large-scale PV DP models and the parameter, *Distance from all major roads*, only had very minimally influencing the model that excluded all power grid parameters.

All large-scale solar PV DP maps indicated moderate to high development potential across the southern third of Portugal and portions of east-central Portugal, where solar CF values are the highest. Some differences appeared between models with and without substation parameters, with high development potential shifting away from substations and toward transmission lines in the south. The most notable change when removing all power grid parameters was the expansion of high development areas away from transmission lines and increased focus on areas near roads. The final combined large-scale PV DP map (Figure 8a) identifies nearly 13,840 km^2 (15.5% or PRT) of high development potential (DP values >= 0.65) on technically suitable lands (Figure 8b).

Table 4: Parameter set included for large-scale photovoltaic (PV) solar development potential (DP) modeling with associated parameter importance values used in final models. Importance values are listed for three final models; model derived from using all parameters as input (All), model derived when two substation parameters are removed (Substations Dropped), and model derived when all power grid parameters are removed (Power Grid Dropped). Parameters ordered from highest to lowest importance values associated with final all parameter model. Importance values of -1 indicate parameter was not selected to be used in final model. Importance values with "---" indicate parameter was removed from original parameter list prior to the parameter selection process included in the modeling workflow.

Parameter Description	***Importance Values for Large-scale PV DP Models***		
	All	**Substations Dropped**	**Power Grid Dropped**
Distance from all substations	0.107	---	---
Solar capacity factor (CF) - PVOUT	0.103	0.090	0.094
Distance from major urban areas	0.073	0.060	0.078
Distance from power plants	0.061	0.046	---
Distance from transmission lines	0.059	0.073	---
Distance from major substations	0.047	---	---
Distance from all cities	-1	0.045	0.049
Average percent slope	-1	0.038	0.044
Distance from primary roads	-1	0.030	0.048
Distance from all major roads	-1	-1	0.020
Population density	-1	-1	-1
Average aspect ranking	-1	-1	-1

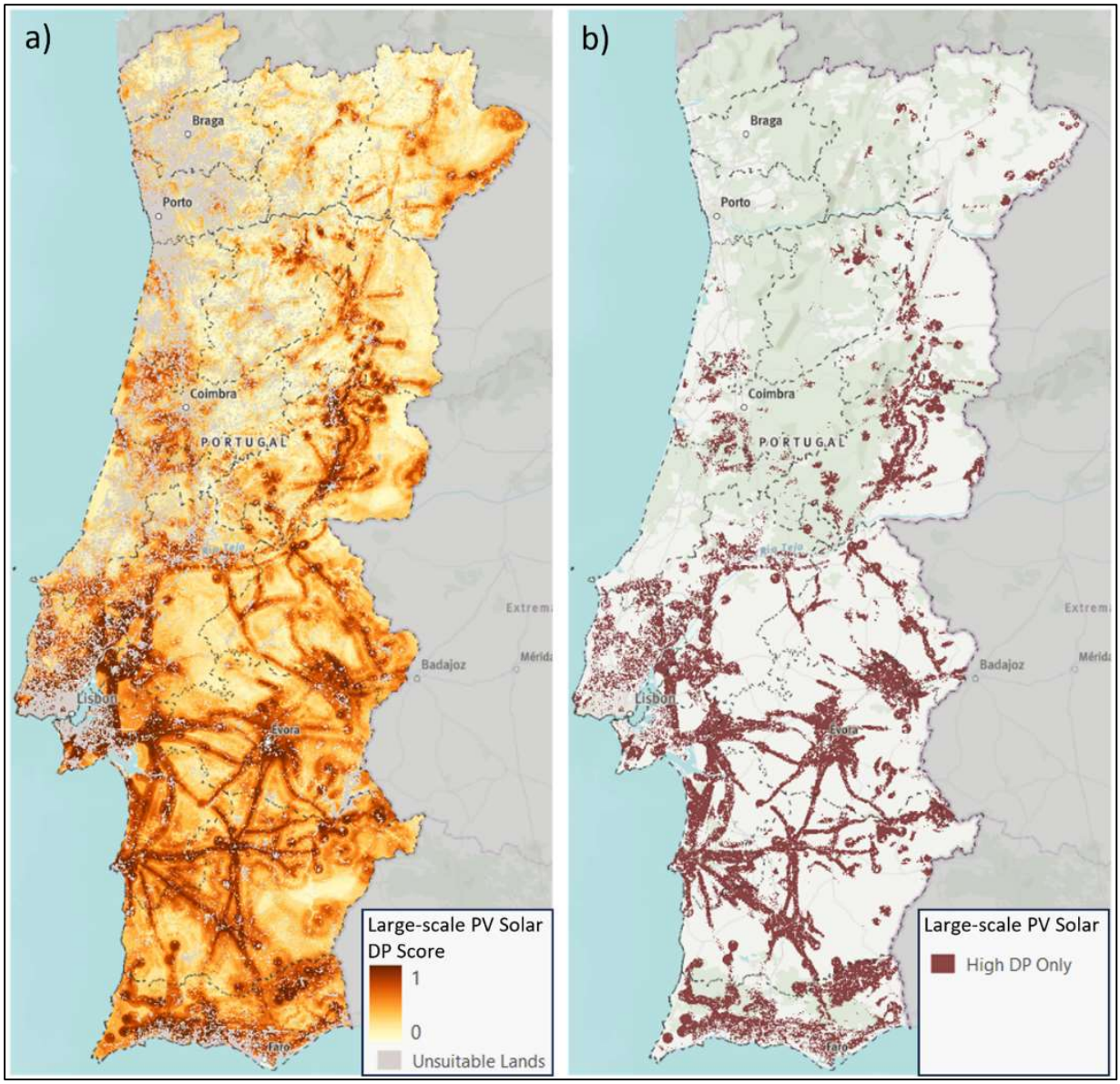

Figure 8: Final development potential (DP) maps for large scale PV solar in Portugal: a) DP values are shown for technically suitable lands, ranging from 0 (lowest potential) to 1 (highest potential). A min/max rendering stretch is applied to display the full range of values. Technically unsuitable lands are depicted in a reddish light grey, while areas outside Portugal are blurred with semi-transparent grey. (b) High DP areas (DP ≥ 0.65) highlighted on technically suitable lands only. This threshold identifies regions most favorable for future wind energy development.

2.2.3. Small-scale Solar Development Potential Models

For small-scale solar DP, eleven parameters out of all thirteen were selected to create the best model (Table 5). In addition to the number of parameters, the drivers of development for small-scale solar differed notably from those in the large-scale PV model. For the small-scale solar model, the *Distance from all substations* was the most important parameter and had nearly double the predictive power of the next three, which were relatively similar in importance. Besides

Distance from all cities, the power grid parameters related to substations and transmission lines comprised the top four drivers. All four parameters strongly influenced development potential when sites were close to these features.

The highest influence in DP values was found in areas within 1 km of any substation, with a rapid decrease in this influence moving to 2.5 km away and followed by little or no influence after this threshold. Proximity within 2 km of cities also displayed strong influences on the model values, with a substantial decrease in influence occurring up to 15 km, from which little to no influence. Those areas within 10 km of major substations showed high influence, which decreased rapidly approaching 20 km. or transmission lines, only lands within 1 km showed high influence, with a sharp decline up to 4 km and negligible effect beyond that.

Flat lands (up to 4 percent slope) were highly favored for development, but influence dropped rapidly as slope increased to 8 percent, with little effect beyond that. Interestingly, among the four least influential parameters, two were also selected by the large-scale PV model displaying similar trends of influence (*Distance from power plants* and *Distance from major urban areas*) with differing thresholds: power plants influenced development at distances greater than 25 km, while urban area influence peaked within 2 km. Additionally, both accessibility parameters (*Distance to primary roads* and *Distance to all major roads*), were selected with influences mainly seen within 1,500 m and 500 m, respectively. Finally and most surprisingly, the small-scale PV solar model did not select solar CF as a model input, which was the second highest parameter for large-scale PV solar.

By removing both substation parameters, *Distance to transmission lines* became more influential, ranking second behind Distance from all cities, which also increased in importance. When removing all power grid parameters, *Distance from all cities* remained the most important parameter, but now had nearly double the influence on the model than the next closest parameter (*Average percent slope*). Similar to the large-scale solar models, two model parameters (*Population density* and *Average aspect ranking*) were not selected by any small-scale PV DP models, while the *Solar CF* parameter only very minimally influencing models that excluded substations and all power grid parameters.

All small-scale solar PV DP maps displayed high development potential across Portugal near cities. Only slight country-wide changes of high DP were visible across models. High DP values initially near cities and substations in the "All" model, transition to lands near cities and transmission lines, and finally flatter lands near cities and roads. The final combined small-scale PV DP map (Figure 9a) identified 4,843 km^2 (5.4% of PRT) of land as having high development potential (DP values >= 0.65) across Portugal (Figure 9b).

Table 5: Parameter set included for small-scale photovoltaic (PV) solar development potential (DP) modeling with associated parameter importance values used in final models. Importance values are listed for three final models; model derived from using all parameters as input (All), model derived when two substation parameters are removed (Substations Dropped), and model derived when all power grid parameters are removed (Power Grid Dropped). Parameters ordered from highest to lowest importance values associated with final all parameter model. Importance values of -1 indicate parameter was not selected to be used in final model. Importance values with "---" indicate parameter was removed from original parameter list prior to the parameter selection process included in the modeling workflow.

Parameter Description	***Importance Values for Small-scale PV DP Models***		
	All	**Substations Dropped**	**Power Grid Dropped**
Distance from all substations	0.098	---	---
Distance from all cities	0.062	0.084	0.103
Distance from major substations	0.055	---	---
Distance from transmission lines	0.053	0.073	---
Average percent slope	0.039	0.048	0.060
Distance from primary roads	0.034	0.039	0.045
Distance from power plants	0.027	-1	---
Distance from major urban areas	0.026	0.034	0.047
Distance from all major roads	0.023	0.032	0.042
Solar capacity factor (CF) – PVOUT	-1	0.033	0.036
Average aspect ranking	-1	-1	-1
Population density	-1	-1	-1

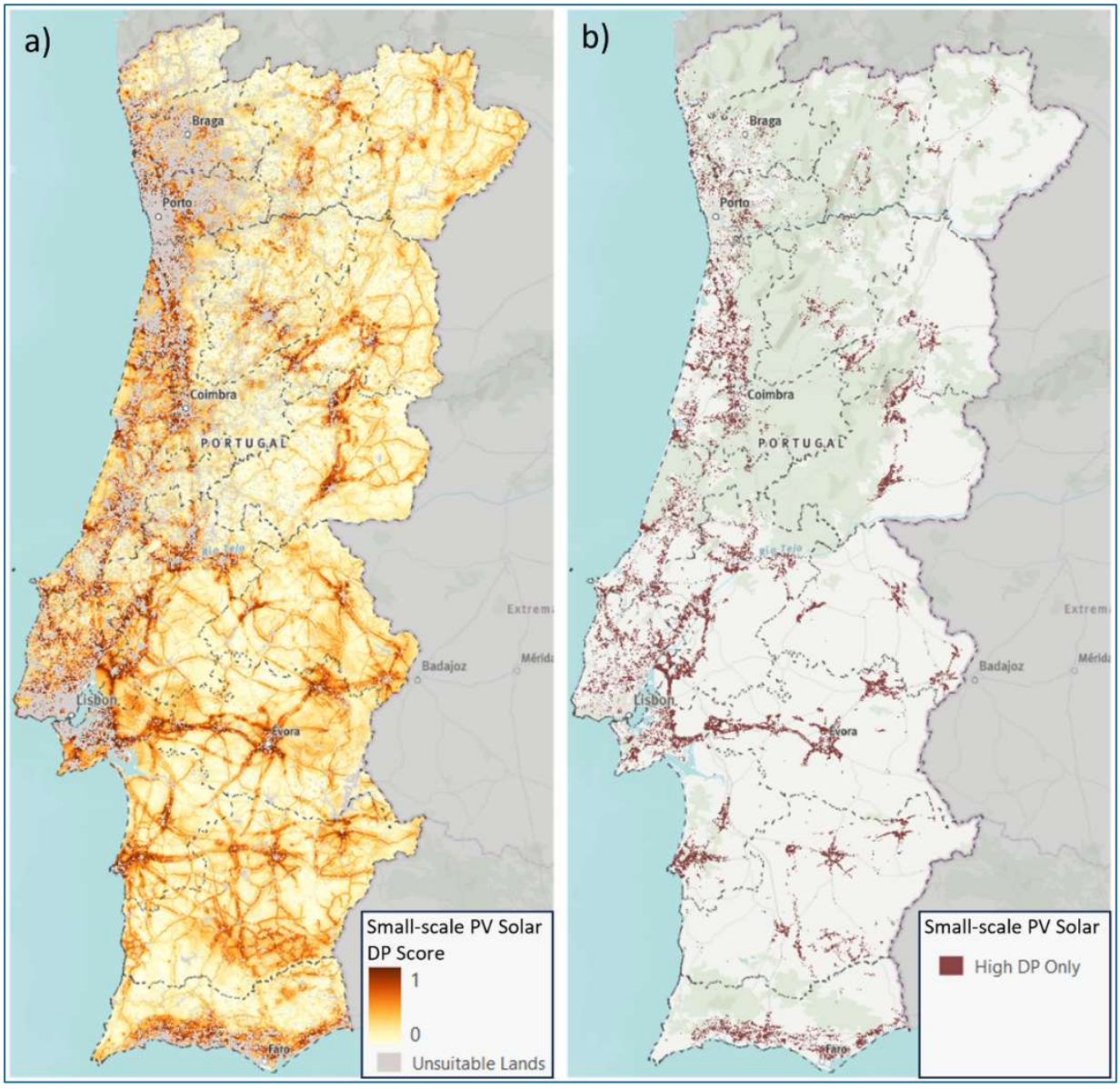

Figure 9: Final development potential (DP) maps for small scale PV solar in Portugal: a) DP values are shown for technically suitable lands, ranging from 0 (lowest potential) to 1 (highest potential). A min/max rendering stretch is applied to display the full range of values. Technically unsuitable lands are depicted in a reddish light grey, while areas outside Portugal are blurred with semi-transparent grey. (b) High DP areas (DP ≥ 0.65) highlighted on technically suitable lands only. This threshold identifies regions most favorable for future wind energy development.

2.2.4. Combining High Development Potential for Solar in Portugal

To accommodate further TNC Smart-siting analysis, a final solar high development potential map was derived by combining both the large-scale and small-scale high DP maps (Figure 8b and Figure 9b). Any pixel identified as having high development potential from either DP map was maintained in the final high DP map. This identified 15,594 km^2 (17.5% of PRT) of land as having high development potential for new ground-based PV solar across Portugal (Figure 10).

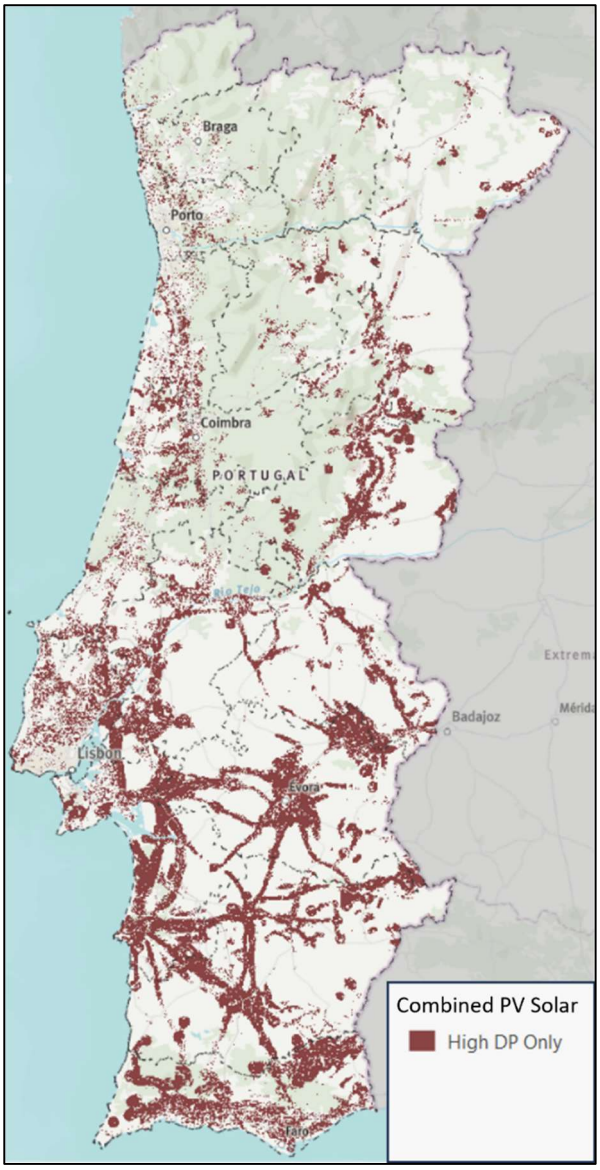

Figure 10: Final high development potential map for PV solar.

2.2.5. Model Validation

Overall, all models demonstrated acceptable validation metrics with wind models consistently outperforming the solar models (Table 6). Across all models, performance generally decreased as parameters were removed from the original set. However, wind models were least affected by these removals, since the two most important parameters (mTPI and Wind CF) remained constant regardless of the parameter set used by the models. Interestingly, previous PV solar models using all parameters that did not model the size classes differently (large-scale and small-scale) showed lower overall validation measures than those produced in this final effort which were separated.

Table 6: Validation measures for all 3 models developed (i.e., 1-model development from all parameters, 2-model developed with substation parameters removed, 3-model developed with all power grid parameters removed) per technology modeled (i.e., wind, large-scale PV solar, and small-scale PV solar). Measures listed: log loss, percent correctly classified (PCC), Cohen's Kappa, area under the receiver operating curve (AUC/ROC), cross-validation (CV) Kappa, and cross-validation (CV) out-of-the-bag (OOB) error.

Measure	Wind Models			Large-scale PV Solar Models			Small-scale PV Solar Models		
	1	2	3	1	2	3	1	2	3
Log loss	0.0406	0.0497	0.0576	0.1241	0.1454	0.1671	0.1313	0.1605	0.1663
PPC	99.25	99.02	98.83	98.31	98.68	99.06	97.05	96.01	96.01
Kappa	0.9849	0.9801	0.9762	0.9601	0.9689	0.9777	0.9400	0.9186	0.9186
AUC/ROC	0.9916	0.9890	0.9868	0.9880	0.9906	0.9933	0.9669	0.9552	0.9553
CV Kappa	0.9368	0.9237	0.9013	0.7610	0.6729	0.5823	0.8052	0.7704	0.7360
CV OOB	0.0315	0.0378	0.0491	0.0910	0.1192	0.1485	0.0983	0.1156	0.1329

2.3. Discussion and Recommendations

A total of nine intermediatory DP maps were produced (3 wind, 3 large-scale PV, and 3 small-scale PV), which were ultimately combined to create one wind and two size-dependent PV DP maps. We recommend using the final wind and two-size dependent PV DP maps when planning for future impact from either development. These DP maps met both validation and accuracy requirements necessary to provide valuable insights on future wind and solar development in Portugal. Even though our final maps have a spatial resolution of 100 m, they are mostly recommended to support general land use planning at multiple governmental levels and therefore should not be used for site specific planning. Also, while DP values range from 0 (unlikely) to 1 (highly likely), small differences in values will not differentiate where development may occur. Additionally, our high DP threshold of 0.65, while supported by other DP models (Evans & Kiesecker, 2014), could be scaled up or down depending on use and extent of an analysis. For example, using a selected percentile of high values may be more appropriate within a planning region.

For simplicity with our Smart Siting approach and due to a lack of knowledge regarding the size of future solar PV development, we produced one high DP map for PV solar. However, we still see value in providing DP maps for both small and large-scale development. For example, municipalities can use both small-scale and large-scale PV DP maps to plan for several small sites, a few large sites, or a combination, depending on their capacity goals.

While valid wind and solar models were produced without power grid parameters, careful consideration should be applied when using any of these models. The wind DP map produced does provide some pointed insights on where to plan for future grid expansion by identifying lands highly suitable for development once provided with transmission line access. The solar models on the other had do not provide this level of insight more because of the abundance of solar resource across Portugal making it more difficult to target certain areas.

Our analysis revealed key drivers for wind and PV solar development. For wind, ridgetops and plateaus landscapes (modeled by mTPI and high wind CFs) are the primary drivers of wind development in Portugal. Power grid parameters influence both wind and solar development, but solar, especially small-scale, is much more dependent on grid accessibility due to economic factors. Interestingly, both solar models showed stronger influence in development potential further away from power plants, likely because most power plants are hydro dams located in steeper terrain, which is less suitable for ground-based solar. At a certain distance, however, crops relying on reservoir water may provide ample opportunities for solar.

All models tended to favor proximity to substations, with large substations consistently influencing DP values at a lower rate. This suggests that smaller, distributed substations are being built to connect wind and solar projects to the grid. This may also indicate that substations are often built simultaneously with wind and large-scale solar installations, rather than being established beforehand to direct where development occurs. Recognizing this potential timing of development, was one of the justifications for combing our DP maps produced from all parameters and the one created by dropping the substation parameters. Finally, current development shows a tendency of large-scale solar to be found in regions with higher solar CF, whereas small-scale solar is more distributed across all of Portugal near all cities.

Population density was the only parameter not selected by any model, likely due to low variability across Portugal, where most areas have very low population density. Additionally, the *Aspect ranking* parameter was not selected by any solar model. Likely the spatial resolution of our analysis limited this parameter and would be better suited for more fine-scale and/or site-level siting analysis. Lastly, the parameter *Distance from all major roads* was rarely selected, and the parameter *Distance from primary roads* only marginally influenced models, indicating that land accessibility is generally not a limiting factor for development in Portugal.

Finally, and most importantly, these DP maps should be used in conjunction with mapped biodiversity and social values to fully identify those potential win-win scenarios where high development potential and low conflict occurs. By showing these areas exist and have potential to reach wind and solar targets, planners and regulators can guide developers to these areas for further research on potential development. Additionally, developers are likely to encounter less resistance in these zones, which can reduce project delays and costs, while focusing efforts on areas with proven lower development costs. While our modeling did not account for grid capacity, it is a key driver of project costs. Conducting grid capacity assessments in selected win-win areas will further support developers in choosing the most economically viable sites.

3. Mapping Environmental and Biodiversity Values

The coarse-filter/fine-filter approach is a framework in conservation planning and widely adopted by TNC and the scientific community in biodiversity assessments across terrestrial and aquatic ecosystems (Noss, 1987; Grooves et al., 2003; TNC, 2007; Tingley et al., 2014; Davidson et al., 2021). The coarse filter targets the conservation of entire ecosystems or habitat types, operating under the assumption that by protecting representative examples of these broader ecological systems, the majority of species and ecological processes they support will also be conserved (Lemelin & Darveau, 2006; TNC, 2007). This includes mapping and prioritizing ecological systems such as forests, wetlands, or grasslands using remote sensing, Land Use and Land Cover (LULC) data, and ecological classifications.

In contrast, the fine filter is applied to address the needs of species or ecological features that may not be adequately protected through coarse-scale ecosystem representation. These include rare, endemic, threatened, or keystone species, as well as critical habitats like breeding sites or migratory corridors (Geselbracht et al., 2005; Lemelin & Darveau, 2006). Fine-filter assessments often rely on species distribution models, occurrence records, and expert input to ensure that conservation strategies are inclusive of biodiversity elements that are spatially restricted or ecologically unique.

Together, these filters form a complementary system: the coarse filter ensures broad ecological representation and resilience, while the fine filter provides precision and safeguards for irreplaceable biodiversity components. This dual approach enhances the robustness of spatial planning and is particularly effective in identifying low-conflict zones for renewable energy development, as demonstrated in TNC's smart siting work across Europe (Sochi et al., 2023; Kiesecker et al., 2024).

3.1. Biodiversity Coarse Filter for Portugal

The coarse-filter biodiversity map was constructed by integrating three spatially explicit ecological parameters (Extent, Connectedness, and Rarity) in order to capture broad-scale patterns of biodiversity values across Portugal.

Extent quantifies the distribution and composition of the LULC types that support biodiversity by maintaining essential ecological processes. This layer was primarily derived from the most updated LULC map from Portugal (COS2018) (DGT, 2018). However, based on recommendations from the expert consultation meetings, the dataset was selectively complemented with CORINE 2018 LULC map (Copernicus, 2018) to address a specific limitation: the aggregation of "Temporary rainfed crops" and "Temporary irrigated crops" into a single class. Experts emphasized that these two agricultural systems differ significantly in their ecological characteristics and biodiversity value. As a result, this class was disaggregated into two distinct categories to better reflect their respective contributions to biodiversity (Figure 11).

Each LULC class was assigned a biodiversity favorability score of 1.0 (favorable), 0.5 (partially favorable), or 0.0 (not favorable), based on its capacity to sustain ecological functions. These values were gathered and validated during an in person event with experts realized in September 2024, where we had 35 participants. The entire list of classes from the LULC map and the biodiversity values can be found in the supplementary materials.

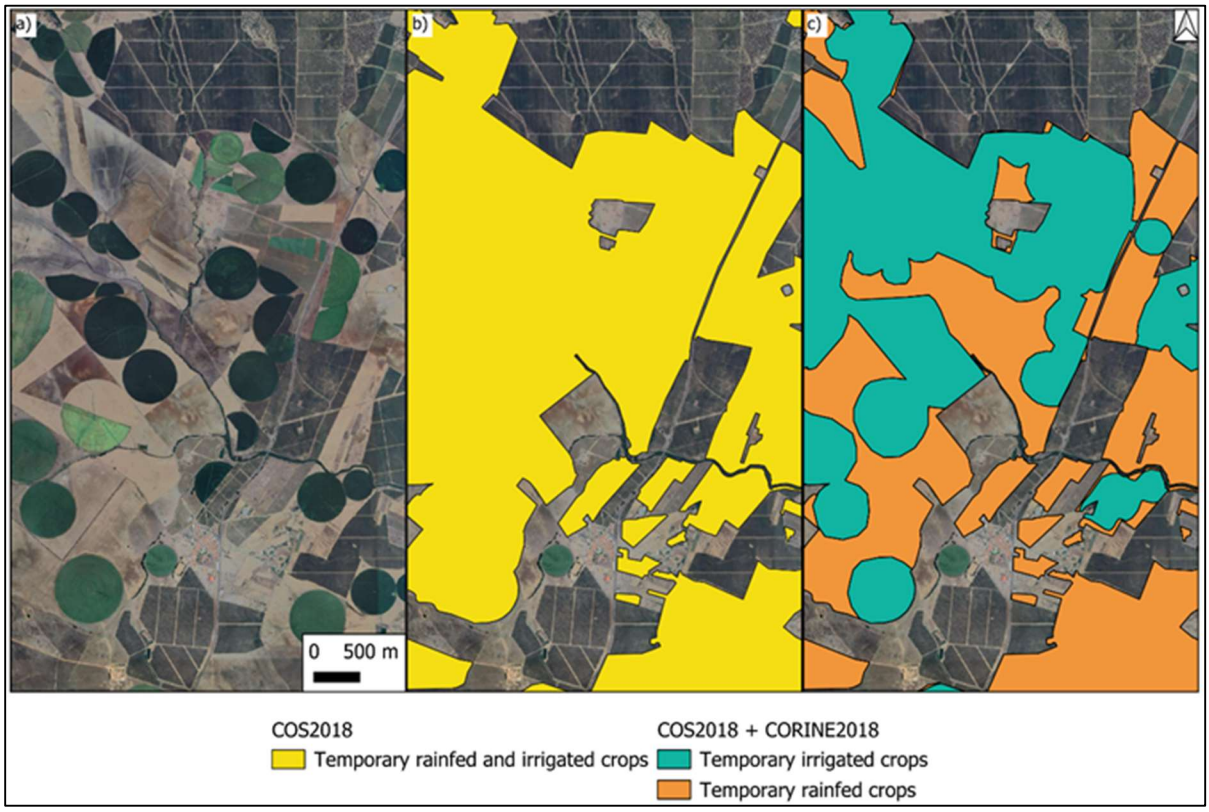

Figure 11: a) Imagery from google maps for a sample region in Portugal; b) COS2018 map with a single class of "Temporary rainfed and irrigated crops"; c) Combination from COS2018 and CORINE2018 with two different classes for temporary crops.

Connectedness is a landscape-scale measure of how linked natural land cover types are across the territory. A formal definition would be: "Connectedness refers to structural links between elements of the spatial structure of a landscape and can be described from mappable elements" (Baudry & Merriam, 1988). It reflects the degree to which favorable habitats are spatially arranged to support ecological processes (e.g., species movement and connectivity). There are several factors that influenced on the decision of using connectedness rather than other fragmentation metrics, such as: i) aligns with the coarse-filter objective of capturing broad ecological patterns without focusing on specific species; ii) it is scale-appropriate for national-level planning, avoiding the scale-dependence and species-specific assumptions of many fragmentation indices; iii) it emphasizes ecological function, particularly movement and connectivity, which are essential for maintaining biodiversity and ecosystem services such as pollination and climate adaptation (Brennan et al., 2021).

In this assessment, connectedness was derived from the Extent layer using a series of moving windows to generate a continuous surface (Ritters et al., 1997; 2000). Each pixel was assigned a value between 0.0 and 1.0, where 1.0 represents areas embedded within large, uninterrupted patches of favorable habitat, and 0.0 indicates isolated areas.

Rarity identifies areas of high conservation value based on expert consultation. This layer includes data on protected areas in Portugal, such as Natura 2000 sites (ICNF, 2024a), which cover both Sites of Community Importance and Special Protection Areas. It also incorporates Ramsar sites (ICNF, 2024b; RSIS, 2024), the National Network of Protected Areas (RNAP) (ICNF, 2024c), and UNESCO Biosphere Reserves (UNESCO, 2024; Palliwoda et al., 2021), including both core and buffer zones. Although Important Bird Areas do not have legal status by default (SPEA, 2024), they are included due to their recognized ecological relevance. Beyond these layers we also added two layers available on the Institute for Nature Conservation and Forests (ICNF) database: i) Areas under forestry regime, both total and partial regimes (REFLOA) and ii) Bioenergetic reserves (ICNF, 2024c).

In addition to these areas, two expert recommendations were also adopted. First, a buffer of 500 meters was applied around all water and wetland classes from the LULC map, based on the understanding that these zones are typically covered by riparian vegetation, which plays a key role in supporting key biodiversity services for species (e.g., habitat, food, movement corridors). Second, a buffer of 500 meters was applied around *geosites*, which are geologically significant areas recognized for their scientific value. These *geosites* contribute to conservation and land-use planning through their ecological importance and integration into national nature protection strategies (LNEG, 2025).

Another suggestion from expert consultation was the development of a Rarity Index (RI) to identify which LULC types could be considered rare habitats for species at the national scale (Eq. 2). The index is based on the relative abundance of each LULC class, excluding artificial surfaces. It is calculated as:

$$RI\ (\%) = \left(\frac{Class\ area}{Total\ area}\right) * 100 \qquad (2)$$

Rare habitats were selected statistically, using the median RI as a threshold. All habitats that had RIs under the median value were selected as rare habitats, with the exception of some agricultural classes that were excluded from the rare category (temporary crops and pastures associated with vineyards, orchards, olive groves, agricultural nurseries, and rice fields). Similar habitat types were grouped together to support interpretation and application (Table 7).

Table 7: List of groups and respective classes that were considered rare habitats for Portugal, including the total group area (ha) and the Rarity Index (RI) (%)

Group	Class	Area (ha)	RI (%)
Forests I		**36978**	**0.437**
	Other coniferous forests		
Forests II		**18499**	**0.219**
	Chestnut forests		
Agroforestry		**44677**	**0.528**
	Mixed cork and holm oak		
	Stone pine		
	Mixed classes		
	Other oaks		
	Other species		
Dunes		**9711**	**0.115**
	Interior beaches, dunes and sands		
	Coastal beaches, dunes and sands		
Wetlands		**26414**	**0.312**
	Intertidal zones		
	Saltwater marshes		
	Freshwater marshes		
Bare rock		**6172**	**0.073**
	Bare rock		

After all these layers were developed, they were merged into a single conservation dataset to avoid double counting, as several overlaps were identified. The rarity layer was assessed for its condition based on the degree of land modification from human activities, using the Human Modification Index (HMI) (Kennedy et al., 2018; Theobald et al., 2025). The rule used to assign the biodiversity values to the Rarity layer was based on the HMI values of each pixel (Figure 12):

- If the HMI was between 0.0 and 0.1 (inclusive), the biodiversity value is **1.0**.
- If the HMI was greater than 0.1 and up to 0.4, the biodiversity value is **0.85**.
- If the HMI was greater than 0.4 and up to 0.7, the biodiversity value is **0.65**.
- If the HMI was greater than 0.7 and up to 1.0 (inclusive), the biodiversity value is **0.5**.

Areas that didn’t belong to the layers mentioned before, were classified with a biodiversity value of 0.0.

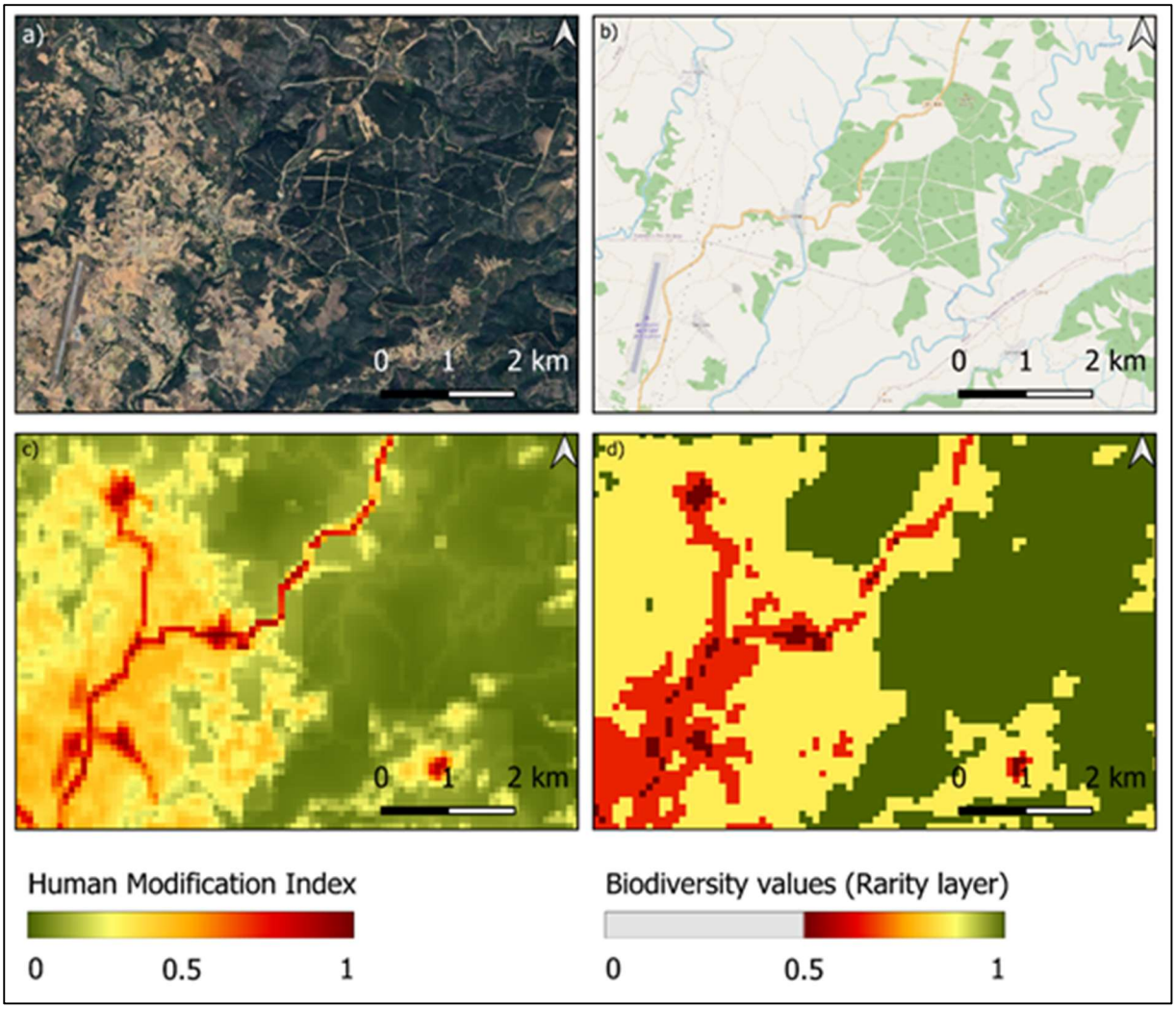

Figure 12: a) Imagery from google satellite for a region inside the Natura 2000 Montesinho/Nogueira area; b) Imagery from google open street maps for the same region, highlighting the Bragança regional airport; c) The entire region covered with the Human Modification Index from Theobald et al. (2025), where 0 represents habitats with a low modification index and 1 habitats with very high modification index; d) The biodiversity values for the rarity layer after reclassifying the Human Modification Index, where 1 represents habitats with high biodiversity value and 0.5 habitats with low biodiversity value. Pixels with the value of 0 are observed only outside of the layers used to create the rarity layer.

3.1.1. Combining the layers from the coarse filter

The final coarse-filter map was generated by summing the three previously developed layers into a composite biodiversity index. This index produces a continuous scale from 0, indicating low biodiversity value, to 3, indicating high biodiversity value. To ensure strong representation of formally protected areas, important bird areas and other rare LULC classes, all areas from the rarity layer were assigned the maximum biodiversity value (3). The resulting map integrates all coarse-filter components into a unified index, offering a spatially consistent representation of biodiversity importance across the Portuguese landscape at a national level (Figure 13). All the datasets used are on Table 8.

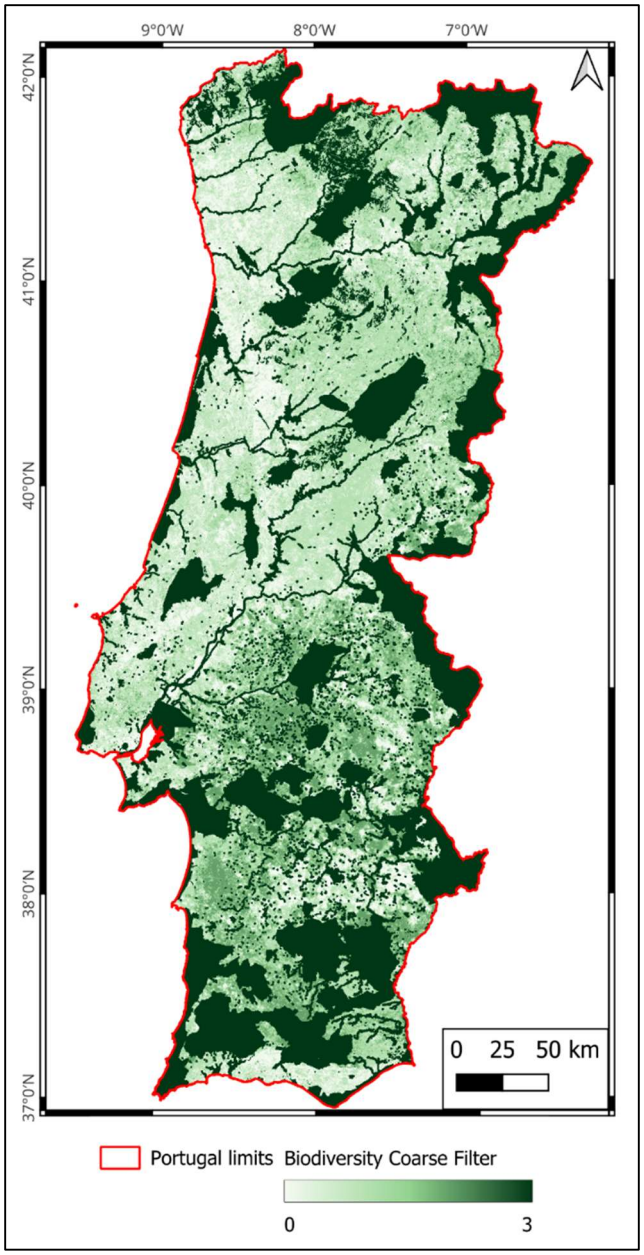

Figure 13: Map that presents a composite biodiversity index derived from three coarse-filter layers (Extent, Connectedness and Rarity). The index is a continuous value and ranges from 0 (low biodiversity value) to 3 (high biodiversity value)

Table 8: All datasets used for the Coarse Filter maps in Portugal

Spatial Dataset	Description	Original Resolution	Type	Original Source
COS2018	LULC map for Portugal	1ha	Vector	DGT (2018)
CORINE2018	LULC map for Pan-European region	-	Vector	Copernicus (2018)
Natura 2000	Protected areas from the Natura 2000 network	-	Vector	ICNF (2024a)
Ramsar Sites	Important wetlands from the Ramsar convention	-	Vector	ICNF (2024b)
RNAP	*Rede Nacional de Areas Protegidas* from Portugal	-	Vector	ICNF (2024c)
UNESCO Biosphere reserves	UNESCO Biosphere reserves with zones	-	Vector	UNESCO (2024)
IBAs	Important Bird Areas for Portugal	-	Vector	SPEA (2024)
Geossítios	Geosites from Portugal with a 500m buffer	-	Vector	LNEG (2025)
Bioenergetic Zones	Bioenergetic Zones for Portugal	-	Vector	ICNF (2024c)
Areas under forestry regime	Areas under forestry regime (REFLOA)	-	Vector	ICNF (2024c)
HMI	Human Modification Index	300m	Raster	Theobald et al. (2025)

3.2. Biodiversity Fine Filter for Portugal

The fine-filter biodiversity map was developed aiming to capture the information of 3 major animal groups: Birds, Bats and Other Mammals (which we will refer only as Mammals in this report). Two major datasets were used for each group to derive sensitivity maps used in the fine filter, the first one we are naming Atlas data and the second one is the Area of Habitats.

The Atlas data is based on national research done by institutions from the environmental protection area. The Portuguese Society for the Study of Birds (SPEA, BirdLife's partner in Portugal) provided the dataset related to the III Atlas of Breeding Birds from Portugal (SPEA, 2025) and the Red Book of Birds from Portugal (Almeida et al., 2022). The first represents the current distribution and abundance of breeding bird species across mainland Portugal and the autonomous regions. It also tracks changes over the past 15 years and has a resolution of 10x10km. This dataset was provided under a non-disclosure agreement, so we will not be able to share specific data for certain bird species. The second represents the extinction risk of bird species in mainland Portugal using IUCN criteria. It goes beyond listing threatened species by providing detailed information on their distribution, population size, ecological needs, and the pressures they face. The goal is to support informed decision-making for bird conservation and management.

The Atlas data for Bats and Mammals was obtained directly via the Red Book of Mammals for Portugal (Mathias et al., 2023), which is a comprehensive assessment of the extinction risk facing both terrestrial and marine mammal species in mainland Portugal. It evaluates 82 species using the criteria of the IUCN criteria and has also a resolution of 10x10km. For this project, we just considered distribution and occurrence records from 2005-2021, since this publication also brings information on records before 2005.

In addition to the two Atlas datasets, several complementary sources were incorporated into the analysis (Table 9**Error! Reference source not found.**). These datasets served as supplementary information, enhancing the species occurrence records derived from the Atlas data (Figure 14). Importantly, only species classified as Vulnerable, Endangered, or Critically Endangered were included in the analysis (All the species and the IUCN status considered are in the supplementary material of this document). However, two exceptions were made:

- The bird *Bubo bubo* (Eurasian Eagle-Owl), although listed as Near Threatened, was highlighted by SPEA as a species of national conservation concern due to its high sensitivity to various types of energy infrastructure (Rubolini et al., 2001; Sergio et al., 2004; Torre et al., 2025).
- The mammal *Ursus arctos* (Brown Bear), categorized as Regionally Extinct in Portugal for nearly two centuries, was recently observed in northern Portugal. This sighting is likely linked to population growth and habitat expansion in neighboring Spain (Gregório et al., 2020). For the purposes of this analysis, the species was treated as Critically Endangered.

Table 9: All datasets used for the Fine Filter maps in Portugal

Spatial Dataset	Description	Original Resolution	Type	Original Source
Red Book of Birds for Portugal	IUCN status for birds in Portugal	-	.pdf	Almeida et al. (2022)
III Atlas of Breeding Birds of Portugal	Occurrence data for birds in Portugal	10x10 Km	Vector	SPEA (2025)
Red Book of Mammals for Portugal	IUCN status for Mammals in Portugal	-	.pdf	Mathias et al. (2023)
Eurasian eagle-owl additional information	Nesting sites and complementary occurrence data	10x10 Km 2x2 Km	Vector	SPEA, 2024 (Personal communication)
Black Vulture additional information	Complementary occurrence data	10x10 Km	Vector	LIFE Aegypius Return (2024)
Bonelli Eagle additional information	Complementary occurrence data	10x10 Km	Vector	SPEA, 2024 (Personal communication)
Montagu's harrier additional information	Complementary occurrence data	10x10 Km	.pdf	Gameiro et al. (2023)
National wolf census (2019-2021)	Complementary occurrence data	10x10 Km	.pdf	Pimenta et al. (2023)
Conservation of Key Underground sites: the database	Bat shelters for Portugal	Points	.pdf	Eurobats (2025)
Area of Habitats	Occurrence data for all groups in Portugal	100m	Raster	Lumbierres et al. (2022)

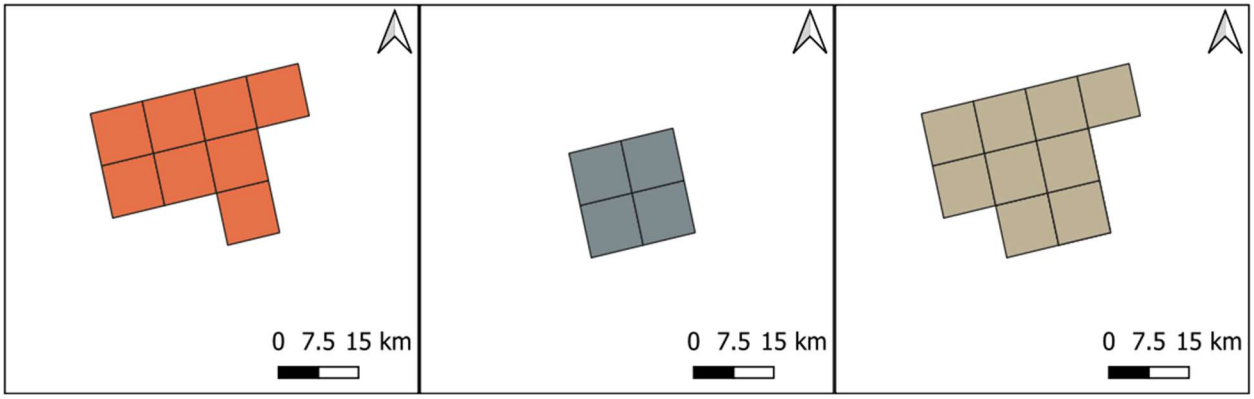

Figure 14: a) Dataset for the Bird X obtained with SPEA; b) Dataset obtained with a partner for the Bird X; c) Combined datasets used in our fine filter approach

While the Atlas data provided valuable insights, its relatively coarse resolution introduced a risk of overgeneralizing the actual areas where species may occur. To address this limitation and achieve a more precise representation of species distributions and habitat suitability, we incorporated the Area of Habitat (AOH) dataset into our analysis (Lumbierres et al., 2022). AOH represents the portion of a species' geographic range that contains suitable habitat conditions for its survival. Unlike traditional range maps, which often overestimate species presence, AOH maps refine these estimates by excluding areas deemed unsuitable based on habitat type and elevation preferences.

The AOH dataset offers a high spatial resolution of 100 meters and includes over 15,000 terrestrial bird and mammal species. In our analysis, all species listed in the supplementary materials were covered by AOH data, with the exception of two bird that were considered marine species (*Gulosus aristotelis* and *Uria aalge*). Within this project, AOH serves as a valuable complement to the Atlas data, providing a finer-scale, habitat-specific perspective that enhances the accuracy sensitivity maps. In this project, we are considering a total of 85 species (62 birds, 7 bats and 16 other mammals).

To integrate the AOH data with the Atlas datasets, we followed the methodology recommended in the AVISTEP Guide, developed by BirdLife International (Serratosa and Allinson, 2022). This approach involved spatially intersecting the high-resolution AOH maps with the coarser-resolution Atlas data to refine species distribution layers and improve ecological relevance. For each species, we generated a composite raster with values ranging from 0 to 3, representing different levels of spatial agreement between the two datasets:

0: Areas with neither national-level observations (Atlas) nor modeled suitable habitat (AOH).

1: Areas modeled as suitable habitat by AOH but lacking Atlas observations.

2: Areas with Atlas observations but not modeled as suitable habitat by AOH.

3: Areas where both Atlas observations and AOH-modeled habitat overlap.

This classification allowed us to prioritize areas with the strongest evidence of species presence (value 3), while still incorporating areas supported by only one dataset (values 1 and 2) at a lower confidence level (Figure 15).

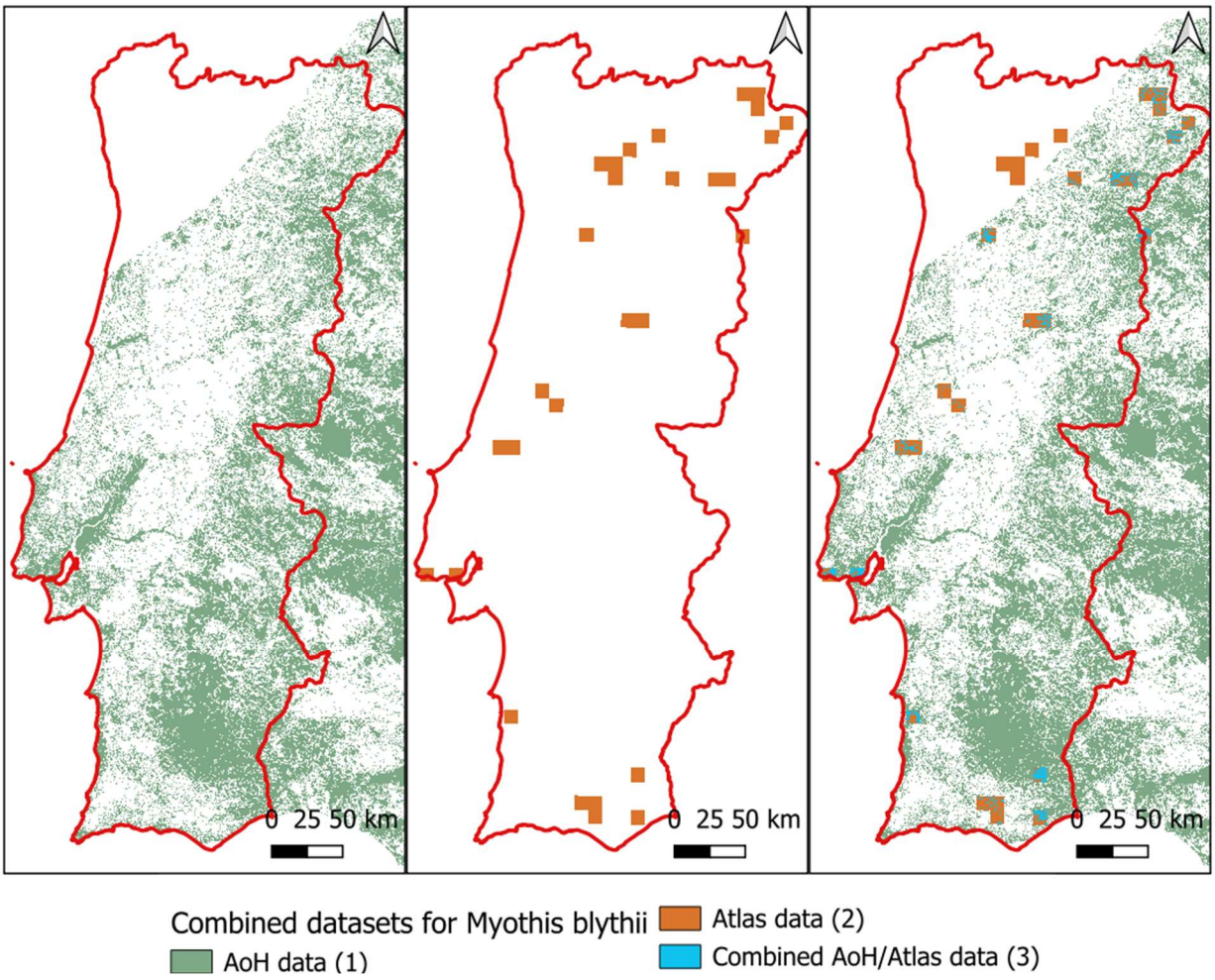

Figure 15: a) Area of Habitats data only; b) Atlas data only; c) Overlap between Area of Habitats and At-las data for one specie and the values assigned to each combination

At this stage, we had a combined spatial dataset for each species, integrating both Atlas observations and AOH-modeled habitat suitability. To generate the final sensitivity maps, we applied a weighting system based on each species' conservation status. Following the IUCN Red List categories, we assigned numerical values to each status (Table 10), allowing us to reflect the relative conservation importance of each species in the analysis (Serratosa & Allinson, 2022; Guilherme et al., 2023). These weights were then multiplied by the combined raster values derived from the previous step (ranging from 0 to 3), which represented the spatial agreement between Atlas and AOH data. This process was repeated for all species individually. Finally, the resulting weighted rasters were summed and normalized within each taxonomic group (birds, bats, and mammals), producing group-specific sensitivity maps that emphasize areas of high conservation concern while accounting for both habitat suitability and national occurrence records.

Table 10: IUCN Conservation status and the respective numerical values associated with each one of them.

Conservation Status	Assigned Value
LC (Least Concern)	0.2
NT (Near Threatened)	0.4
VU (Vulnerable)	0.6
EN (Endangered)	0.8
CR (Critically Endangered)	1.0

To produce a unified biodiversity sensitivity map, we combined the group-specific sensitivity layers (birds, bats, and mammals) using a maximum value approach. This method, based on the precautionary principle, ensures that the final map reflects the highest level of sensitivity observed across any of the three taxonomic groups at each spatial location. By applying a pixel-wise maximum operation, we prioritized the most restrictive conservation signal, thereby capturing the worst-case scenario for biodiversity impact. For example, if a given location had sensitivity scores of 0.6 for birds, 0.4 for bats, and 0.5 for mammals, the final sensitivity value assigned to that location would be 0.6.

The resulting sensitivity map ranges from 0 to 1, where 0 represents areas of low biodiversity conflict (e.g., locations with minimal overlap between species of conservation concern and suitable habitats) and 1 represents areas of high biodiversity conflict (e.g., where multiple species with elevated conservation status are likely to occur in suitable habitats) (Figure 16).

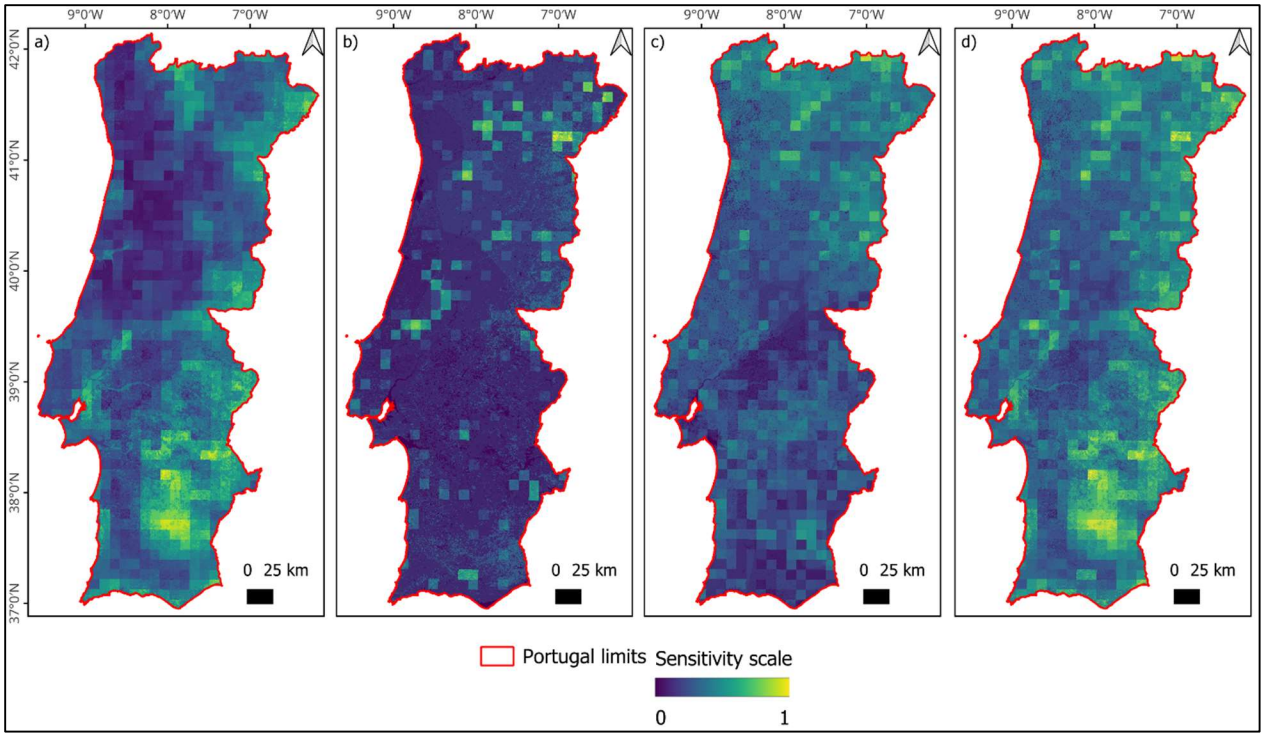

Figure 16: Sensitivity maps and scale ranging from 0 (low biodiversity conflict) to 1 (high biodiversity conflict) for a) Birds; b) Bats; c) Other Mammals and d) Combined species.

3.3. Defining low conflict sites based on the coarse filter/fine filter combination

To identify areas of low biodiversity conflict suitable for renewable energy development, we combined the outputs of the coarse and fine filters using a structured, threshold-based method. Each filter was first analysed separately using statistical tools such as boxplots, distribution curves, quantiles, means, and medians. These helped us understand how the data was distributed and allowed us to build a continuous conflict scale. We then interpreted these statistical patterns through an ecological lens to ensure that the resulting classifications reflected real-world biodiversity priorities and supported practical spatial planning.

As a next step, we focused on the quantiles and median values to define initial thresholds (all the statistical values and distributions are presented in the supplementary material). We then assessed what these statistical ranges meant in ecological terms (e.g., such as rare species presence, habitat quality, LULC classes and presence of protected areas). Our goal was to create conflict classes that not only made sense statistically but also grouped the territory into ecologically meaningful and spatially coherent regions.

For the coarse filter, we analysed the distribution of the final raster values both with and without the inclusion of areas assigned that had a biodiversity value of 3. These values were manually

attributed to protected areas and other rare habitats on the rarity layer in order to reflect their elevated conservation importance. However, their inclusion skewed the distribution toward the upper end, causing the third quantile to align with the maximum value. To address this, we excluded the value-3 areas (representing approximately 38% of Portugal's territory) and treated the classification as a two-part problem. We then used the median value (rounded up) to define the first threshold, which corresponded to a value of 1 on the coarse filter map and is aligned with ecologically meaningful criteria described in Table 11. The second threshold was defined similarly, with values equal to or greater than 2 also supported by strong ecological justification. This approach allowed us to create conflict classes that were both statistically grounded and ecologically relevant.

Table 11: Conflict categorization of coarse filter areas in Portugal based on Biodiversity and Statistical considerations

Conflict Category for the Coarse Filter	Description
Low Conflict ($0 \leq x < 1$) **Total area: 34748 Km^2** **Approximately 39.0% of Portugal**	Areas where the LULC is not favourable or only partially favourable to biodiversity, with poor connectedness, no rare habitats, and outside protected areas.
Moderate Conflict ($1 \leq x < 2$) **Total area: 20200 Km^2** **Approximately 22.6% of Portugal**	Areas with mixed characteristics: Favourable to biodiversity values with low connectedness and no Rare habitats; Partially favourable to biodiversity with medium connectedness and no Rare habitats; Not favourable to biodiversity with medium or low connectedness and the possibility of degraded rare habitats. All cases are outside of protected areas.
High Conflict ($2 \leq x \leq 3$) **Total area: 34153 Km^2** **Approximately 38.4% of Portugal**	Areas with favourable or partially favourable LULC for biodiversity, high values of connectedness, and/or with the presence of rare habitats and/or close to water resources. All values of 3's fall within areas from the rarity layer (which includes all protected areas), regardless of other factors.

The approach for the fine filter was more straightforward, as species were already weighted according to their IUCN conservation status. This meant that species of higher concern (e.g., Critically Endangered) had a greater influence on the final sensitivity values. As a result, these species were less likely to appear in the lower end of the fine filter distribution, since their higher

weights naturally elevated the values of the areas where they occurred. Based on this, we used the rounded-up quantile values to define the conflict categories. We also examined the presence of modelled and observed habitats for these species within each class, ensuring that the classification reflected the goal of prioritizing protection for the most threatened species. Despite the coarse resolution of the Atlas data, we observed only minimal overlap between critically endangered species and areas classified as low conflict, which supports the reliability of the classification in identifying zones of lower ecological risk (Table 12).

Table 12: Conflict categorization of fine filter areas in Portugal based on Biodiversity and Statistical considerations

Conflict Category for the fine filter	Description
Low Conflict ($0 \leq x < 0.3$) **Total area: 24732 Km^2** **Approximately 27.8% of Portugal**	These areas show a low likelihood of occurrence for species of highest conservation concern (IUCN status = CR), with minimum overlap (1%) between confirmed and modelled habitats of critically endangered birds, bats, or mammals.
Moderate Conflict ($0.3 \leq x < 0.5$) **Total area: 42207 Km^2** **Approximately 47.3% of Portugal**	These areas show a moderate likelihood of occurrence for species of highest conservation concern (IUCN status = CR), with moderate overlap (19%) between confirmed and modelled habitats of critically endangered birds, bats, or mammals.
High Conflict ($0.5 \leq x \leq 1.0$) **Total area: 22161 Km^2** **Approximately 24.9% of Portugal**	These areas show a high likelihood of occurrence for species of highest conservation concern (IUCN status = CR), with high overlap (80%) between confirmed and modelled habitats of critically endangered birds, bats, or mammals.

Once the thresholds for both the coarse and fine filters were defined, we merged them to produce a combined biodiversity conflict classification. This was done by combining the categorical values of each filter by creating a matrix of all possible combinations, resulting in nine distinct classes. Each combination was assigned a unique raster ID and grouped into five final conflict categories: Low, Mod-Low, Moderate, Mod-High, and High (Table 13 and Table 14).

Table 13: Combined biodiversity conflict categories in Portugal using the coarse and fine filter categories with area estimates

Conflict category	Coarse Filter (Ecosystem filter)	Fine Filter (Species filter)	Area (Km^2)
Low	Low	Low	12073
Mod-low	Mod	Low	5672
Mod	Low	Mod	17136
Mod	Mod	Mod	10171
Mod-High	Low	High	5538
Mod-High	Mod	High	4356
High	High	Low	6987
High	High	Mod	14899
High	High	High	12676

The spatial distribution of these combined conflict categories can be visualized (Figure 17), which overlays the coarse filter, fine filter, and the resulting integrated classification. This visualization allows for a clear comparison between ecosystem-level and species-level sensitivities, and highlights areas of alignment and divergence between the two approaches.

This integrated classification provides a robust framework for spatial planning, balancing statistical rigor with ecological relevance. It supports transparent decision-making by clearly identifying areas of low conflict while acknowledging zones that require caution or further ecological review. The map and classification system are designed to be adaptable, allowing for future refinement as new data becomes available or as planning priorities evolve.

While the current biodiversity conflict maps do not differentiate between specific renewable energy technologies (e.g., wind vs. solar), this was a decision based on the scope, available data, and timeline of the project. The team did not have access to species-specific interaction data that would allow the development of separate biodiversity layers tailored to individual technologies, particularly within the Portuguese context. Additionally, the datasets provided lacked parameters linking species to specific types of infrastructure impacts, such as turbine collision risk, habitat avoidance due to turbine noise or electrocution on transmission lines.

Table 14: Combined biodiversity conflict categories descriptions and summed area estimates

Conflict Category for the combined filter	Description
Low Conflict **Total area: 12073 Km²** **Approximately 13.5% of Portugal**	Areas where both filters agree on minimal biodiversity sensitivity, making them strong candidates for renewable energy development with reduced ecological risk. These areas are typically characterized by low species presence, poor habitat connectivity, and absence of rare or protected habitats.
Moderate-Low Conflict **Total area: 5672 Km²** **Approximately 6.4% of Portugal**	Areas where ecosystem-level sensitivity is moderate, but species-level sensitivity remains low. These landscapes may support broader ecological functions but do not host species of high conservation concern. These areas are primarily located in Alentejo, particularly in the western part of *Alto Alentejo* and *Alentejo Litoral*, and may be suitable for development with minimal ecological risk, provided that appropriate safeguards are in place.
Moderate Conflict **Total area: 27308 Km²** **Approximately 30.6% of Portugal**	Areas where species of conservation interest are moderately present, and ecosystem-level sensitivity is also evident but not dominant. While not classified as critical, they warrant careful planning and ecological review.
Moderate-High Conflict **Total area: 9894 Km²** **Approximately 11.1% of Portugal**	Areas with high species-level sensitivity that are not flagged as ecologically critical by the coarse filter. These zones often lie adjacent to protected areas and may serve as important corridors or buffer habitats, supporting species movement and ecological connectivity. Their elevated fine-filter values indicate the presence of sensitive or threatened species, making them ecologically significant despite moderate or low ecosystem-level indicators. These areas require careful consideration in planning to avoid unintended impacts on biodiversity.
High Conflict **Total area: 34153 Km²** **Approximately 38.4% of Portugal**	Areas with elevated conservation value as identified by the coarse filter, regardless of species-level sensitivity. These zones include protected areas, rare habitats, and landscapes with high ecological connectivity, all of which are essential for maintaining ecosystem integrity. Due to their critical role in biodiversity conservation, development in these areas is strongly discouraged.

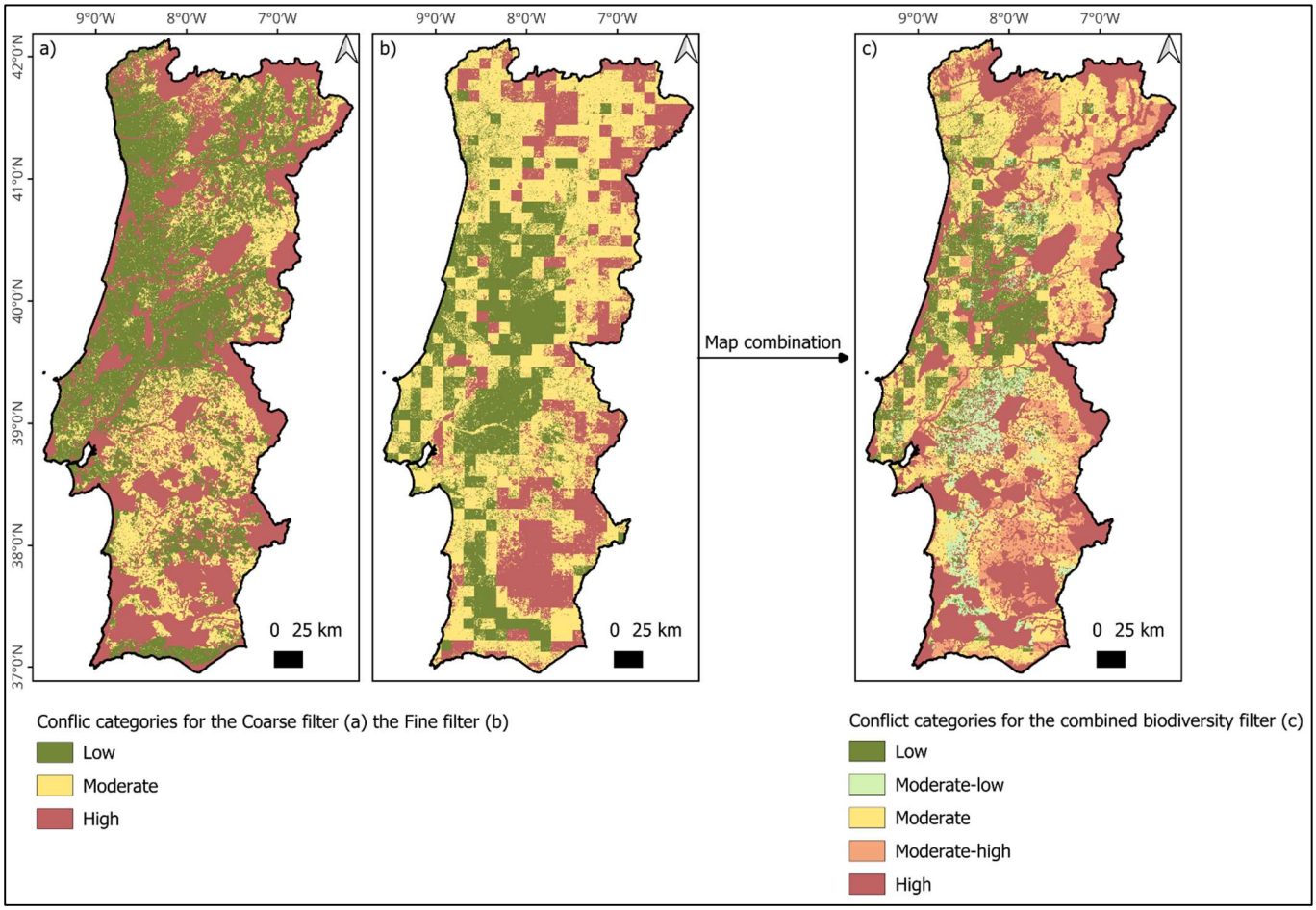

Figure 17: Biodiversity conflict classification maps for Renewable Energy siting in Portugal, considering a) Conflict categories derived from the Coarse Filter (ecosystem-level assessment); b) Conflict categories derived from the Fine Filter (species-level assessment) and c) Combined conflict classification integrating both filters to identify zones of ecological sensitivity

Instead, the biodiversity layers were designed to reflect general ecological sensitivity, capturing potential impacts across multiple phases of renewable energy development, including habitat loss, land use change, and fragmentation. This approach ensures broad applicability while maintaining ecological relevance. That said, the development of technology-specific biodiversity layers remains a promising direction for future refinement. Should more detailed ecological data become available, especially regarding species' behavioural or spatial responses to different technologies, this framework could be expanded to support more targeted siting decisions. However, such refinements fall outside the scope of the current study and would require additional data collection and modelling efforts.

4. Social Values Mapping Approach

Within the social values mapping component of TNC's "smart siting" project for Portugal, three primary data layers are used:

I. Viewsheds: A visibility analysis based on landscape values derived from social media;
II. Social-cultural values: A merged binary layer of important cultural and archaeological sites identified by national experts.
III. Coastal sensitive areas: A buffer zone extending 2 km inland from the shoreline, including all nearby islands, to represent areas sensitive to landscape and coastal dynamics.

All three layers serve as the coarse-filter for social values. However, we encourage decision-makers and practitioners to use this information strategically to identify areas with concentrated social value, landscape sensitivity, and potential conflict, and to effectively target community engagement and public consultations at the local scale. All analyses conducted in this chapter used R version 4.4.1 (R Core Team, 2021).

4.1. Viewsheds

We conducted a visibility analysis based on viewpoints defined by social-media derived Landscape Values (LV). Mapping LV is one method for integrating nature's contributions to people into spatial planning and identifying sensitive areas where land-use change may affect socially meaningful places (Gobster et al., 2007). These values are often linked to the landscape's aesthetic appeal, its importance for recreation or tourism, and its contribution to well-being (Brown & Raymond, 2007). Traditional methods to assessing these values include in-person surveys, focus group discussions, participatory mapping, or valuation studies. However, these are typically limited to local scales and can be resource-intensive, which restricts their scalability and broader relevance. Recent studies have leveraged georeferenced social media content as proxies for in situ aesthetic and recreational landscape values (Dunkel 2015, Zhang et al., 2022). This information can provide insights into landscapes where people attribute a relatively higher social importance, and how intensively they are visited or perceived as meaningful (Casalegno et al., 2013). Specifically, photo-sharing platforms like Flickr provide spatially explicit data across a large scale that reflect individual engagement with landscapes (Wood et al., 2013; Kim et al. 2019), including additional information such as captions or hashtags that convey personal meaning, emotional connection, or recreational use.

In geography and landscape planning, a viewshed refers to the set of locations within the line of sight from a specific vantage point, constrained by landform and other potential visual barriers. The viewshed analysis involves interpolating a straight line between an observer point and every other cell in a Digital Elevation Model (DEM) or in a Digital Surface Model (DSM), then

comparing the elevation of intervening cells to determine whether they obstruct the line of sight. Each cell is classified as visible or not based on this test, producing a binary raster surface (commonly referred as a visibility map), where visible cells are coded as one and non-visible cells as zero (Wheatley, 2022). Accordingly, we produced binary rasters of visibility for each observation point considered in our analysis. Unlike conventional viewshed analyses anchored to physical infrastructure or fixed observation sites, our approach derives viewpoints directly from the spatial distribution of socially perceived landscape value. This enables the visibility analysis to focus on locations of touristic, cultural, and aesthetic significance rather than arbitrary or purely physical features.

The use of social media data for mapping cultural ecosystem services and landscape value has gained increasing traction in recent years (Sonter et al., 2016; Richards et al., 2018; Kim et al. 2019). Across diverse disciplines, several studies have also used visibility modelling and viewshed analyses for assessments of the impact of visibility and visual quality on potential land use change and development (Poudyal et al., 2010; Swetnam et al., 2017; Inglis et al., 2022; Dai et al., 2023; Lehto et al. 2024). While our work contributes to this emerging field, a growing number of studies have begun integrating social media data with viewshed analysis or other spatial distribution methods (Van Berkel et al., 2018; Wilson et al., 2019; Fox et al., 2022; Zhang et al., 2022). However, our contribution is distinct in that it applies to this integration within the context of renewable energy, specifically wind energy development, where it addresses a critical social conflict (i.e., landscape aesthetics and visual impacts) that continues to shape discourse and decision-making in the field.

4.1.1. Landscape value raster

First, we created a LV dataset Portugal that captures patterns of perceived value and benefits for a range of characteristics (e.g., scenic, cultural, recreational, tourism) throughout the country. The acquisition of geotagged social media content from Flickr was undertaken to construct a spatial proxy for LV across mainland Portugal, closely following and adapting the methodological framework of (van Zanten et al. 2016). Concentrations of filtered social media content serve as a quantitative, spatial indicator of the aesthetic and recreational value that people attribute to different landscape. We assume LV increases as more people post, photograph, and share information about a given area. This dataset was then used to identify key viewpoints (medium and high LV) for running viewshed analyses. As a relatively novel approach, we paired open access social media data (LV dataset) with a viewshed analysis, thereby helping to evaluate the potential visual impact of renewable energy development on socially valued landscapes.

Our analysis focused on mainland Portugal, which was identified using a Portugal boundary map (DGT, 2023) and refined by more accurate coastline representation (OSM, 2024). To ensure systematic coverage and minimize radial overlap, a diamond pattern sampling grid was generated, providing evenly distributed centroid locations (Figure 18a). We used a bounding box search radius and post-query filtering with a 5 km buffer to restrict photos to the relevant area and maximize area coverage (Figure 18b). These centroids were used as input for programmatic queries to

Flickr's REST API via the 'FlickrAPI' R package. For each grid point, the API was queried for up to ten paginated result sets within a 5 km radius, retrieving comprehensive metadata including upload and capture dates, user ID, geographic coordinates, free text tags, titles, and thumbnail URLs. Returned coordinates were subject to post query spatial filtering to guarantee that all points lay within their intended radial buffers.

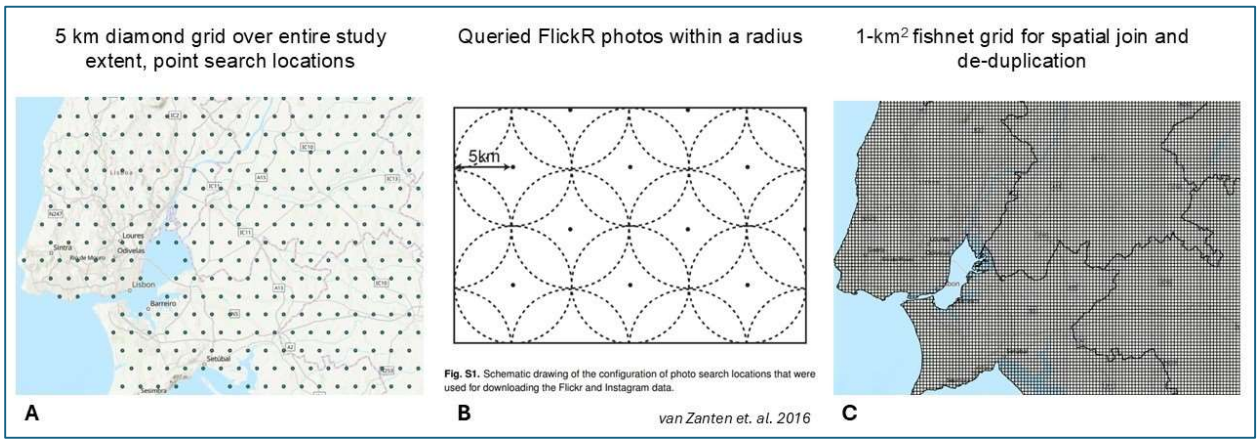

Figure 18: Spatial grids used for maximizing coverage, querying the FlickR data, and rasterizing filtered landscape value: a) 5 km diamond grid covering the entire study area, showing the point locations used for searching Flickr data. b) Example of queried Flickr photos within a 5 km radius around each grid point, illustrating how geotagged images are collected for landscape value analysis. c) 1-km² fishnet grid used for spatial joining and de-duplication of Flickr uploads, enabling the creation of a raster layer representing landscape value density.

Content filtering was performed to retain photographs indicative of recreation and visual-aesthetic dimensions of cultural ecosystem services. The multilingual keyword filtering system included a lexicon of five languages (Portuguese, English, Spanish, German and Italian). This system was organized into three tiers: first, retaining uploads with tags categorized as "unambiguous cultural services"; second, selecting uploads containing keywords identified as "ambiguous cultural services"; and third, retaining these second-tier uploads only if their tags also included terms classified as "generic landscape features" (Figure 19). In other words, the filtering logic retained any photograph whose metadata matched at least one "unambiguous" term, or a combination of one "generic" and one "ambiguous" term.

In addition to sub setting the matched terms, the filtering process preserved the original language of each match for subsequent analysis of linguistic contributions to coverage (Figure 20). The tiered system of keywords considered in this analysis can be found on the supplementary materials. Filtered datasets from each language were then merged and de-duplicated to mitigate oversampling by prolific users; specifically, only one upload per unique user per 1 km² cell was retained.

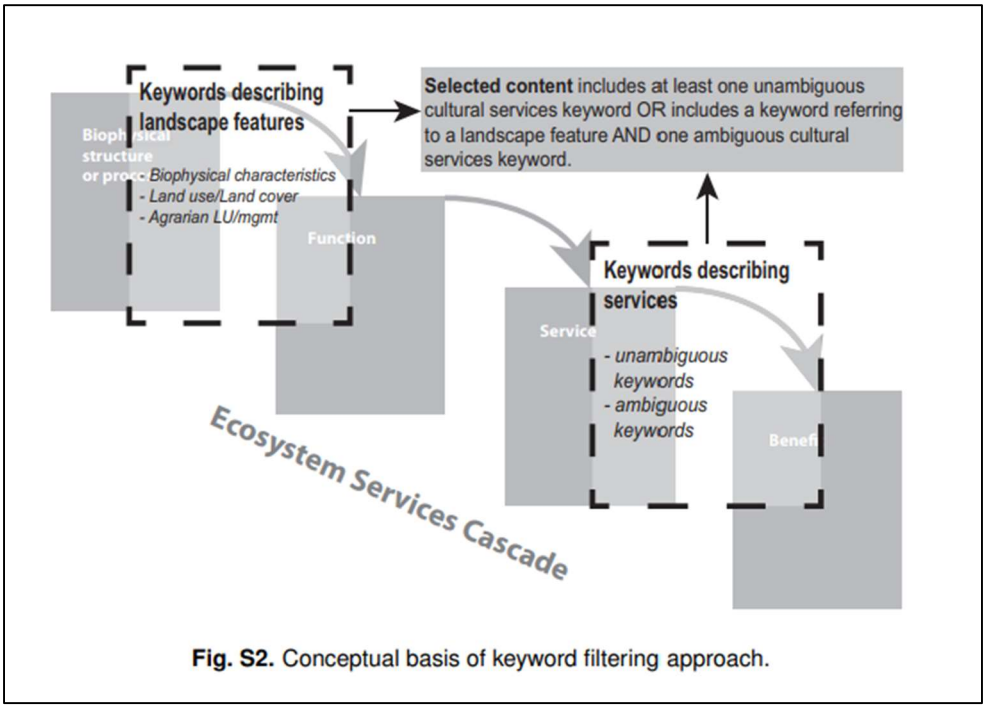

Fig. S2. Conceptual basis of keyword filtering approach.

Figure 19: Schematic diagram from van Zanten et al. 2016 representing the keyword filtering approach for FlickR data.

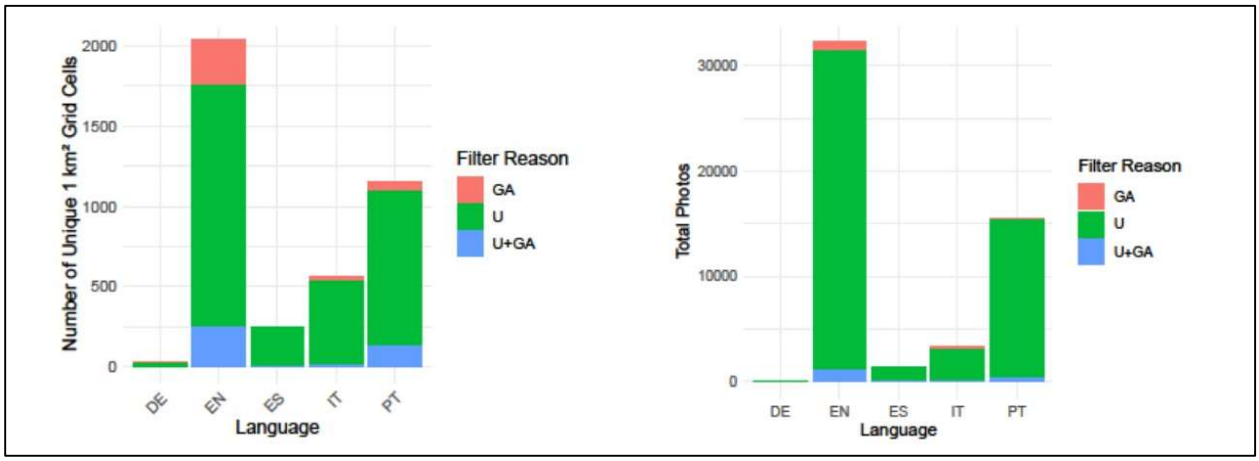

Figure 20: Contribution of each language (Portuguese, English, Spanish, German and Italian) considered in the keyword filtering system. Bar plot on the left represents the frequency of unique cells per language that were filtered and retained per the given rule (content retained whose metadata matched at least one "unambiguous" term – "U", a combination of one "generic" and one "ambiguous" term – "GA", and those that met both rules – "U+GA").

All retained points were snapped to a national 1 km² grid to harmonize spatial resolution (Figure 18c) before being rasterized to count the number of unique uploads per cell. This produced a national map of Flickr upload density, which serves as a proxy for perceived "landscape value" (Figure 21). This process yielded two principal datasets: one filtered using only English and Portuguese keywords, and another using the full set of five languages. Our final layer represents the analysis that incorporates all five languages.

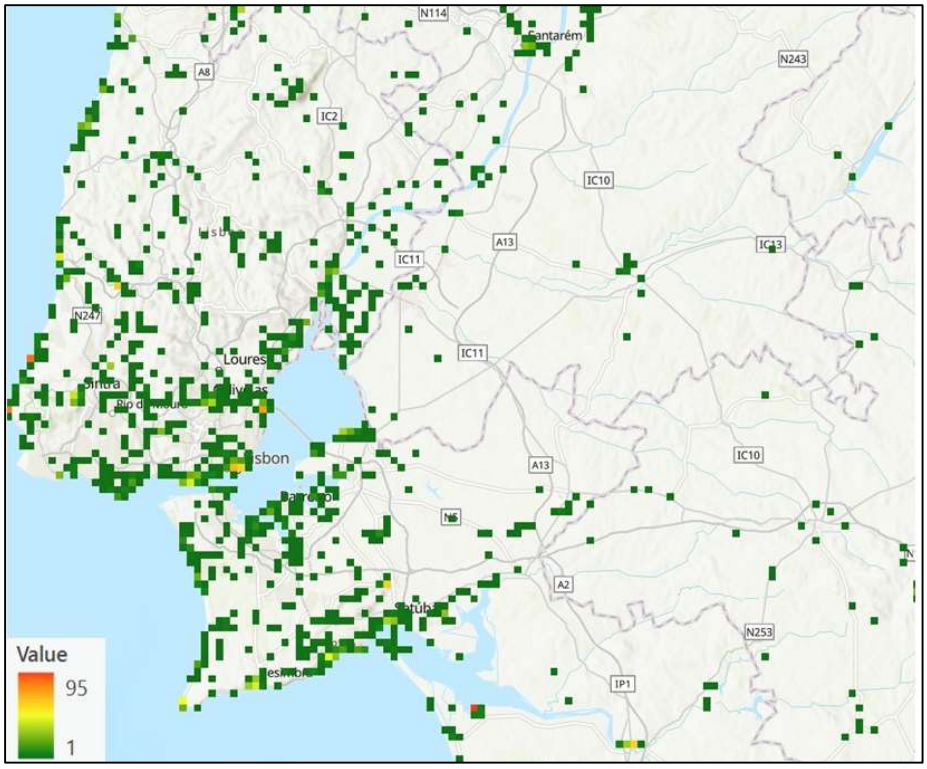

Figure 21: Illustrative example (zoomed in area in Portugal) of the "landscape value" raster layer generated from filtered FlickR data, representing a national map of Flickr upload density i.e., the number of unique uploads per cell.

Results for the Landscape Value raster:

The querying procedure returned metadata for 3,564 grid centroids, with nonresponse occurring at fewer than 4 % of points. Using the -two language filter, 47,857 photographs were retained- after keyword screening, while applying the five language filter increased this total to 52,495. These photographs collectively covered approximately 6 % of Portugal's 1 km² cells. The linguistic composition of retained social media content was dominated by English and Portuguese, while Spanish, German, and Italian contributed additional- but geographically complementary coverage. Deduplication reduced the two language dataset by ~76 % to 11,084 unique uploads, and the -five language- dataset to 12,135 unique uploads concentrated within 5,655 cells (Figure 22).

In the final raster dataset, the most intensively represented cell contained 95 unique uploads, while the mean and median across occupied cells were approximately 2.1 and 1 photo, respectively. This raster serves as the foundation for mapping and quantifying the spatial distribution of social media-derived landscape values in our analysis, providing a robust proxy for public perception of landscape value across Portugal.

The final raster was cropped and masked to match the extent of mainland Portugal. Cells were then classified using the head/tail breaks method, a recommended approach for data with a heavy-tailed distribution (Jiang, 2013), which is common in human activity and social media datasets (Ross & Jones, 2015). This classification resulted in three bins (Figure 23): low (1 to 6 uploads), medium (7 to 13 uploads), and high (greater or equal than 14 uploads).

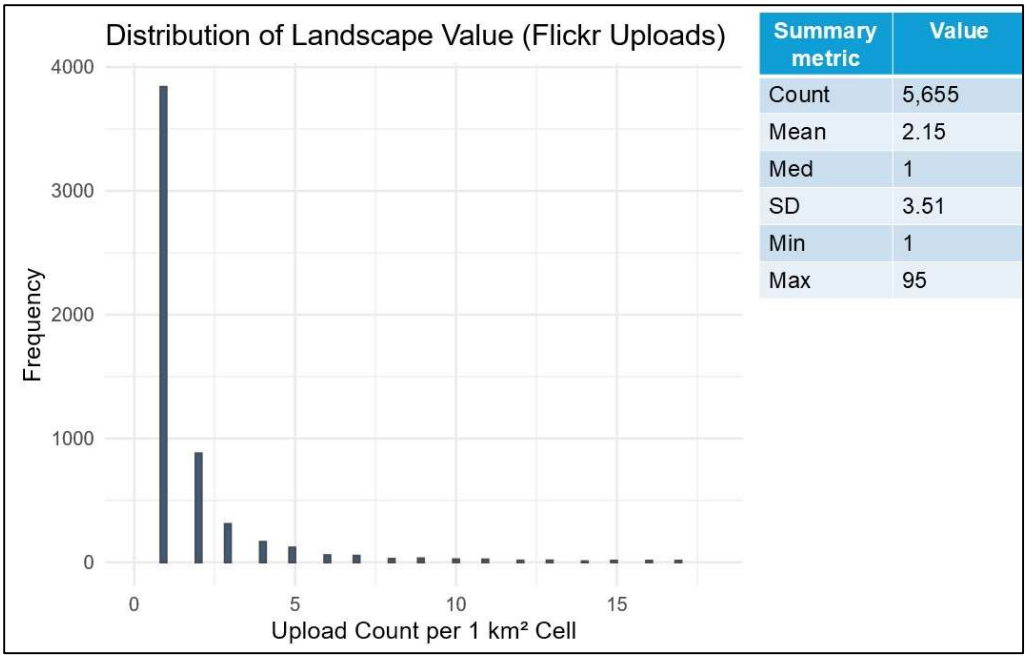

Figure 22: Frequency distribution of the count of FlickR uploads per cell, with a range between 0-95.

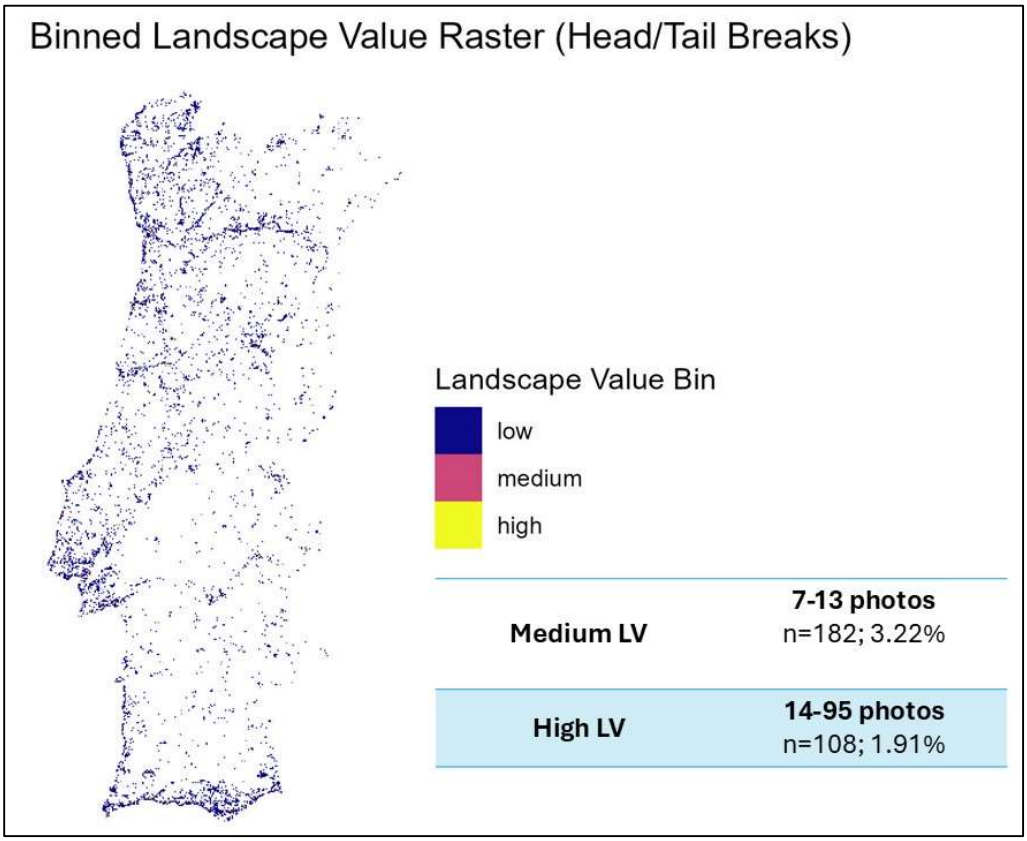

Figure 23: Landscape value raster with 1km2 cells binned into low, medium, and high value, using a head/tail breaks method of classification. Only cells with medium or high landscape value were considered in our viewshed analysis.

4.1.2. Viewshed analysis

We used viewshed analysis to identify areas of visual exposure from landscapes valued for their cultural, touristic, and aesthetic significance across mainland Portugal. This was based on a national-scale raster of LV derived from geotagged Flickr uploads. Specifically, we examined where renewable energy development, particularly in the context of wind energy, may be most visible and potentially contentious. This involved the combination of our LV layer with a viewshed analysis using the viewscape R package (Yang et al., 2024) (Figure 24). All spatial datasets. including the AW3D30 DSM, the LV raster, and administrative boundaries were reprojected to EPSG:3763 to ensure consistency.

From the LV raster, we selected cells with medium (7–13 photos) and high (14–95 photos) landscape value, representing 3.2% and 1.9% of the raster area, or 182 and 108 cells, respectively. These cells were converted to point features to serve as observer locations for viewshed modeling (Figure 25). Our sets of cumulative viewsheds were stratified by LV bin and assigned buffer distances corresponding to different sensitivity scenarios. Following the 'viewscape' package requirements for computing viewsheds, we also included the DSM and an observer height offset of 1.6 meters to simulate human eye level.

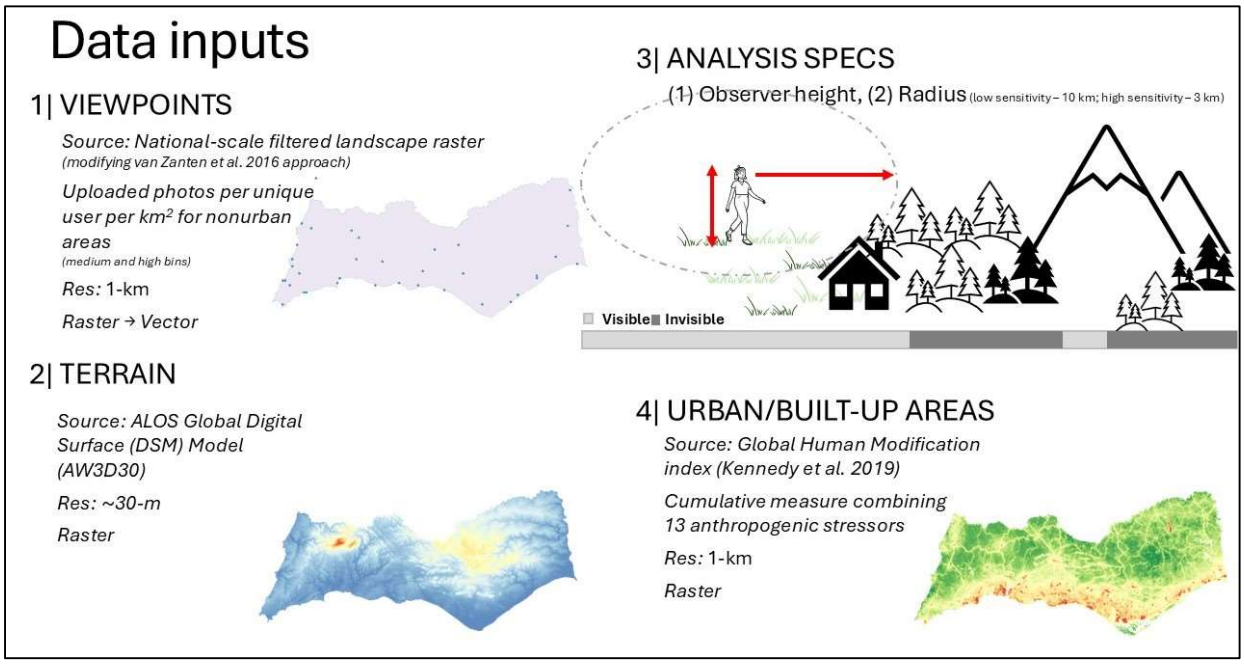

Figure 24: Workflow, specifying data inputs, for the viewshed analysis considering medium and high view-points (n=182, 108) at a national scale.

We considered visibility zones or maximum viewing distance typologies from existing literature on visual impact assessments and viewsheds (Palmer, 2022a). For each set (medium and high LV) of viewpoints, we generated binary viewshed rasters using a DSM under two visibility buffer scenarios (Takaku et al., 2021). These buffers were applied uniformly across terrain, while

recognizing that actual visibility is influenced by topography, land cover, and atmospheric conditions.

The rationale for selecting buffer distances for our viewshed modeling primarily relied on wind energy literature, due to the limited availability of standardized methods for solar development. The decision to use wind-based literature was made due to the absence of standardized solar visibility zones and the analogous vertical prominence of wind infrastructure in open landscapes. Moreover, while solar visibility assessments often focus on reflectance and a hyper-local landscape context (Florio et al., 2016; Sullivan et al., 2016), wind energy visual impact assessments offer robust frameworks for spatial visibility zones (Fischer & Roth, 2021).

A comprehensive review on distance zones and visibility exposure for visual impact assessments outlines five concentric distance zones based on visual prominence and perceptual thresholds for wind turbines, particularly considering the GE 5.3–158 model (Palmer, 2022a). These zones range from:

(1) Immediate Foreground (0.0 to 0.8 km), where turbines dominate the view and auditory presence is notable,
(2) Foreground (0.8 to 3.2 km), where turbines remain visually prominent and attract attention,
(3) Near-Midground (3.2 to 8.1 km), where multiple turbines are perceived as a cohesive visual unit,
(4) Far-Midground (8.1 to 16.1 km), where turbines become subordinate to the overall project footprint, and
(5) Background (16.1 to 32.2 km), where turbines are generally minimally perceptible within the broader landscape.

For this study, following methodology on uniform distance decay effect (Fischer & Roth, 2021), we adopted two buffer distances aligned with the Near-Midground and Far-Midground zones (Table 15):

- 3 km buffer: reflects “high-sensitivity” zones, where turbine movement and form retain strong visual prominence (Breuer, 2001)
- 10 km buffer: a “low sensitivity” radius that captures broader landscape visibility and the collective perception of turbine arrays, consistent with Fischer & Roth (2020)

While our buffer thresholds reflect general distance-based typologies, it is important to note that visual impact is also shaped by factors such as turbine exposure, model type, landscape context, and the number of visible turbines (Palmer et al., 2022b). As such, we recommend that practitioners refine viewshed parameters when downscaling the analysis to specific sites, particularly where visual impact is a key concern or where utility-scale turbine siting may substantially amplify perceptual effects.

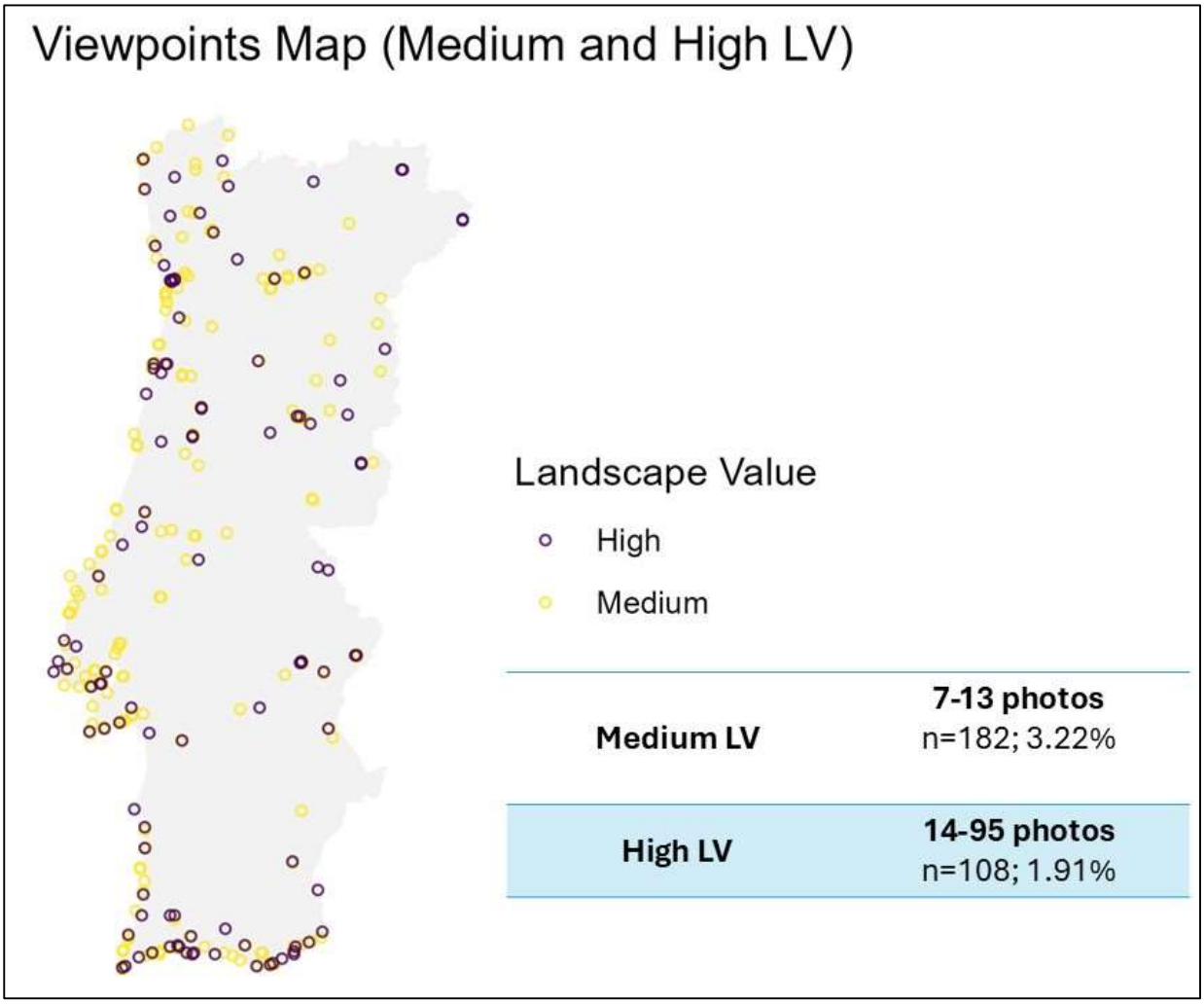

Figure 25: Viewpoints derived from the centroids of medium and high landscape value raster cells for Por-tugal.

Table 15: Buffer distance considered in viewshed analysis alongside rationale for selection.

Buffer Distance	Sensitivity Level	Corresponding Distance Zone	Source	Rationale
3,000m	High	Near-Midground (3.2–8.1 km)	Breuer, 2001	Captures dominant visual presence and blade movement; used for high-sensitivity impact from viewpoints
10,000m	Low	Far-Midground (8.1–16.1 km)	Fischer & Roth, 2020	Represents broader visibility of turbine clusters; used for medium-sensitivity impact from viewpoints

Results of the Viewsheds:

Viewshed calculations were run in parallel across four workers, and the output rasters were merged using union and resampling functions. The results were individual, cumulative viewsheds representing national-scale composite rasters of visibility from multiple viewpoints:

1. Medium LV viewpoints with a low sensitivity distance buffer (10 km)
2. High LV viewpoints with a low sensitivity distance buffer (10 km)
3. Medium LV viewpoints with a high sensitivity distance buffer (3 km)
4. High LV viewpoints with a high sensitivity distance buffer (3 km)

To exclude highly urbanized or disturbed areas, we filtered out cells likely to be in a degraded or modified condition based on the Human Modification Index (HMc) (Kennedy et al., 2019; Theobald et al., 2025). Areas with an HMc value greater than 0.4 were excluded to focus the analysis on relatively intact, nature-oriented landscapes. The final viewshed rasters were resampled to match the resolution of a common template applied to all layers in this project and clipped to the land extent of mainland Portugal, producing visibility layers suitable for integration into renewable acceleration area siting assessments. Our final viewshed layer merges the above rasters 1 and 2, combining both medium and high LV viewpoints with a low sensitivity buffer (10 km), representing a more conservative approach to visual impact assessment.

The viewsheds provided a quantification of distinct areas of visual exposure from landscapes and locations valued for a range of cultural, touristic and aesthetic assets, as defined by user uploaded FlickR content. After filtering with the HMI, approximately 606 km² of land was visible from high landscape value viewpoints under the low sensitivity (10 km) scenario, while 755 km² was visible from medium LV viewpoints. Ultimately, this layer represents zones where visual impacts from renewable energy infrastructure may intersect with viewscapes that hold significant landscape and visual aesthetic value to both residents and visitors.

Overall, the two maps generated in this analysis (i.e., landscape value raster and cumulative viewsheds) serve two core functions within the broader spatial planning framework. First, they identify highly visible landscapes of social value where new renewable energy infrastructure, particularly wind, may generate significant social concern or opposition. Second, they integrate social values into a broader siting process that considers energy yield, technical feasibility, and conservation priorities. The methodology is fully reproducible and adaptable to other geographies, using open-source tools and publicly accessible data.

4.2. Social-cultural value

In complement with our viewshed layer, we developed a unified national-scale dataset representing areas of high social-cultural significance within the study area. This approach follows GTAER's methodology and is based on five vector datasets provided by LNEG via *Património Cultural, I.P.* (PCIP, 2024; GTAER, 2024). Additionally, we added a dataset of Public Interested Trees in Portugal, a dataset identifies individual trees or groups of trees in Portugal that are considered to

be of significant public interest due to their representativeness, rarity, size, age, historical importance, cultural significance, or landscape value (ICNF, 2024c). The datasets used for the Social-cultural value layer are displayed on Table 16.

These national datasets of known cultural and archaeological sites across mainland Portugal capture distinct aspects of cultural heritage and archaeological protection. These layers are integrated into a single "social-cultural" dataset, combining multiple authoritative sources selected in consultation with domain experts to ensure comprehensive coverage of zones with cultural sensitivity, heritage value, and long-standing societal importance.

Table 16: Recommended datasets for the "social-cultural" raster.

Spatial Dataset	Description
Classified cultural heritage sites	Classified or under classification cultural heritage sites (e.g., monuments, historical sites).
Restriction zones	Restriction zones associated with classified or under classification cultural heritage sites.
Special Protection Zones	Special Protection Zones (*Zona de Proteção Especial)* associated with classified or under classification cultural heritage sites.
General Protection Zones	General Protection Zones (*Zona de Proteção Geral)* associated with classified or under classification cultural heritage sites.
Documented archaeological sites	Documented archaeological sites with recommended 150m buffers.
Public Interest Trees	Public interest individual trees or groups of trees in Portugal with 150m buffer.

The selected shapefiles were harmonized to the standard coordinate reference system (EPSG:3763) and merged into a single vector layer using the 'sf' package. The merged layer was then rasterized using a cell-based rule: each cell is assigned a value of 1 if at least 50% of its area overlaps with any cultural feature. For practitioners seeking a more conservative approach, this threshold can be replaced with the *'touch=TRUE'* logic (see 'terra' package), which assigns a value of 1 to any cell touched by a feature, regardless of coverage. This method helps reduce overestimation in fringe areas and improves alignment with other spatial layers in the assessment.

Results for the Socio-Cultural values:

The final output is a binary raster layer at 100 m resolution, indicating the spatial presence (value = 1) or absence (value = NA) of cultural or archaeological features. This dataset highlights zones of concentrated cultural or archaeological heritage, including areas under protected status that signify potential cultural sensitivity. The mapped footprint covers approximately 4556 km² of mainland Portugal. Final layers were clipped to the study area and masked to exclude non-land zones.

4.3. Coastal Sensitive Areas

In addition to the viewsheds and social-cultural values layer, we developed a dedicated national-scale dataset to identify coastal areas with heightened sensitivity for renewable energy siting. This layer was created based on the recommendation from the project partners and incorporates a 2 km buffer zone along the entire Portuguese coastline. This dataset also includes small islands adjacent to the mainland coast, ensuring more comprehensive spatial coverage. The resulting coastal protection layer was rasterized at 100 m resolution, with each cell assigned a value of 1 if it falls within the buffered coastal zone or on an included island, and NA otherwise.

Results for the Coastal Sensitive Areas:

The final coastal protection raster identifies approximately 1846 km² of mainland Portugal and adjacent islands as sensitive coastal zones. These areas are flagged for special consideration in renewable energy planning, particularly where development may intersect with dynamic coastal processes, habitats, or valued landscapes. As with other layers, the final output was clipped to the study area extent and masked to exclude non-land zones.

4.4. Results for the Social value mapping

To provide a comprehensive and precautionary screening tool for social conflict in renewable energy siting, we integrated three independently developed spatial layers: viewsheds representing landscape and aesthetic value, socio-cultural features encompassing cultural and archaeological sites, and coastal sensitivity zones.

All three layers were harmonized and prepared for integration in previous sections, rasterized at 100 m spatial resolution and clipped to the study area extent. This ensured direct comparability and eliminated spatial misalignment. The integration followed a logical union approach: for each cell in the study area, the presence of a conflict in any one of the three layers resulted in that cell being classified as a social conflict zone in the final combined raster. In other words, if a cell was flagged as sensitive in at least one layer, whether due to visual prominence, cultural heritage, or coastal protection, it was included in the final social conflict map. This method captures all potential sources of social sensitivity, prioritizing a precautionary approach in the early stages of spatial planning.

The final social values layer identified 7,269 km² of mainland Portugal as high-conflict sites in terms of social conflict (*Figure 26*).

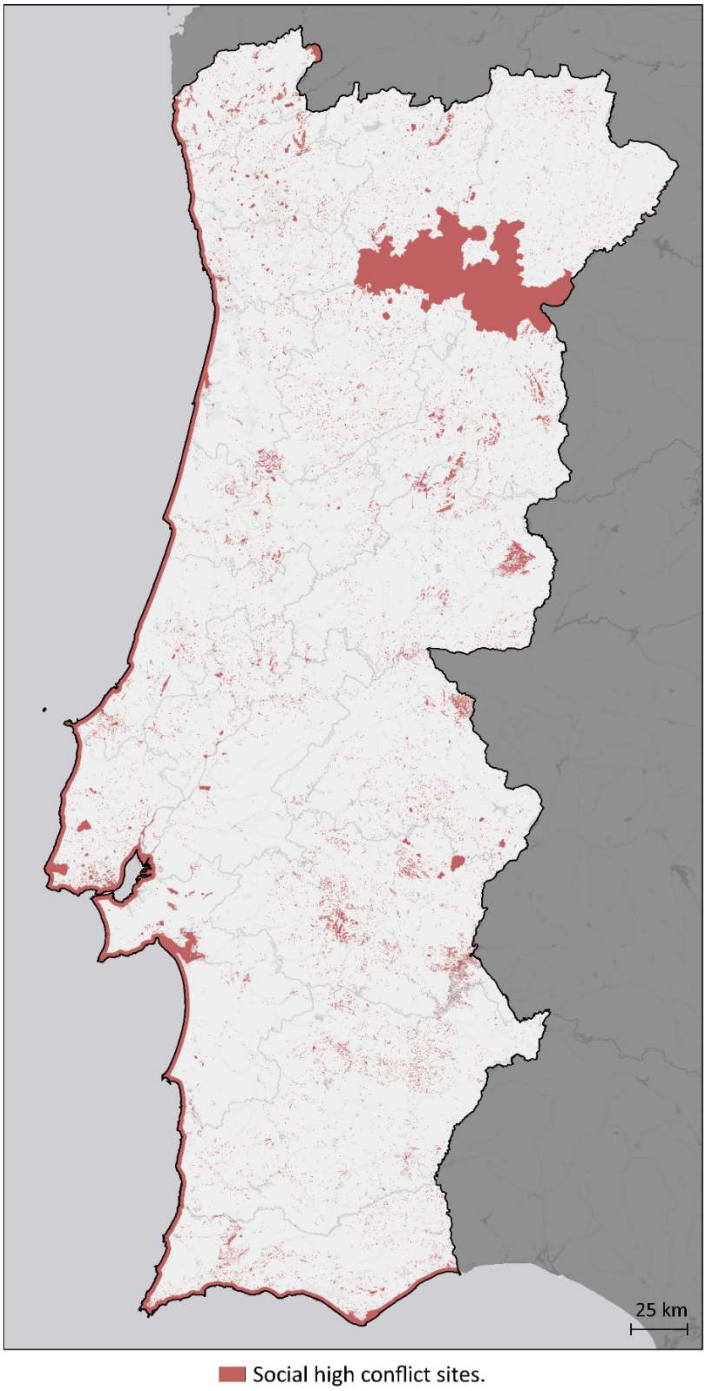

Figure 26: Conflict mapping for social values.

The combined social value layers in our work are intended to support informed decision-making by practitioners and policy makers. While these datasets primarily function as a screening tool, highlighting locations of landscape, aesthetic, cultural, or archaeological significance, they also serve to flag areas where potential conflict may arise in the context of renewable energy

development. Importantly, if a given location is deemed suitable based on development potential and compatibility with biodiversity value, this information can guide the strategic allocation of resources toward more localized engagement when social-cultural features are prominent. In such cases, practitioners are encouraged to complement this national-scale mapping with site-specific data collection and participatory methods, including participatory mapping, public consultation, and the design of benefit-sharing schemes that center local residents, their experiences, and priorities.

4.5. A pilot participatory mapping exercise in Silves municipality

We conducted a pilot participatory mapping (PPGIS) exercise in the Silves municipality, Portugal, to 1) explore how local scale community values align with coarse-filter spatial datasets used in renewable energy siting, and 2) engage communities in co-creating spatial knowledge on valued landscapes and the overall RE decision-making and siting process in their area. A total of 18 participants and 160 mapped points were collected across five social value categories (agricultural, biodiversity, cultural, economic/tourism, and landscape/visual aesthetics).

All spatial analyses were performed in the ETRS89 / Portugal TM06 projection (EPSG:3763), ensuring alignment with our study's national-scale datasets. The analysis window was defined as the Silves municipal boundary (source: geoBoundaries), supplemented with a small (300 m) buffer around any mapped points that fell outside of the administrative polygon that still displayed on the PPGIS application. This "practical boundary" ensured that all community-mapped values were retained within a valid analysis domain, while remaining geographically realistic for the analysis.

We applied a kernel density estimation (KDE) approach to generate continuous spatial surfaces representing the relative intensity of mapped social value points across the study area. We used an automatic bandwidth selection method, the likelihood cross-validation method (bw.ppl), from the R package 'spatstat.explore', an approach well-suited for tight clustered point distributions (Baddeley et al., 2016). For visualization and interpretability, the selected bandwidth was scaled by a factor of 1.25 ($\sigma \times 1.25$). KDE surfaces were computed at a 100 m resolution, aligned with the resolution of our national-scale coarse-filter conflict raster, and a minimum patch size of 16 grid cells (~0.16 km²) that filtered out spurious small clusters.

Hotspot extraction was performed by retaining ~70% of mapped points within the highest-density KDE cells (the "retention threshold"). This threshold is somewhat lower than the 80% used in Pocewicz et al. (2013), but was selected to balance inclusivity with interpretability given the pilot nature of our dataset (n = 160). Sensitivity checks at 65% and 75% retention confirmed that the main clusters were stable across thresholds. Through this analysis, we produced polygons representing social value hotspots suitable for visualization, comparison with our coarse-filter outputs, and planning insights.

We analyzed both pooled hotspots (all values combined) and per-category hotspots (n=5). Our report primarily presents patterns from the pooled hotspots. In addition, we tested sensitivity to the hotspot retention threshold (65%, 70%, 75%). Finally, we compared the identified local-scale

hotspots with our study's national combined conflict raster to assess how community-mapped values aligned or diverged from a pre-screening approach of coarse-filter siting.

4.5.1. Results from the participatory mapping exercise

As part of this exercise, citizens in Silves municipality mapped 160 points of social value across 5 categories: Cultural value (40), Landscape/visual aesthetics (38), Biodiversity importance (34), Agricultural value (31), and Economic or tourism value (23). Across all our results, in line with The Nature Conservancy'ss Human Subject Research guidelines, we present figures with aggregated data on important social value areas (i.e., hotspot polygons) and withheld individual participant mapped points to protect their exact locations. Contact the project team to inquire about accessing figures with participant points, which may be made available upon reasonable request and with appropriate measures taken to ensure participant anonymity.

For all the public participatory mapped points, pooled across the social value categories, our KDE identified 11 hotspot clusters that cover about 13% of Silves (~85 km²), while capturing ~70% of all mapped points (*Figure 27*). These patch sizes ranged from 0.3 km² to nearly 35 km², with a median of 0.57 km² (*Table 17*). This indicates that participants mapped several values in a concentrated manner, suggesting some key value areas, but at least some valued areas were spread across the municipality.

Table 17: Summary metrics for hotspots at a 70% retention thres (pooled across all mapped points).

Metric	***Value***
# Patches	11
Area (km²)	84.5
% of Window Area	13.1
% Points Inside	70
Median Patch Size (km²)	0.57
Mean Patch Size (km²)	7.68
IQR Patch Size (km²)	8.84
Min Patch Size (km²)	0.28
Max Patch Size (km²)	35.4

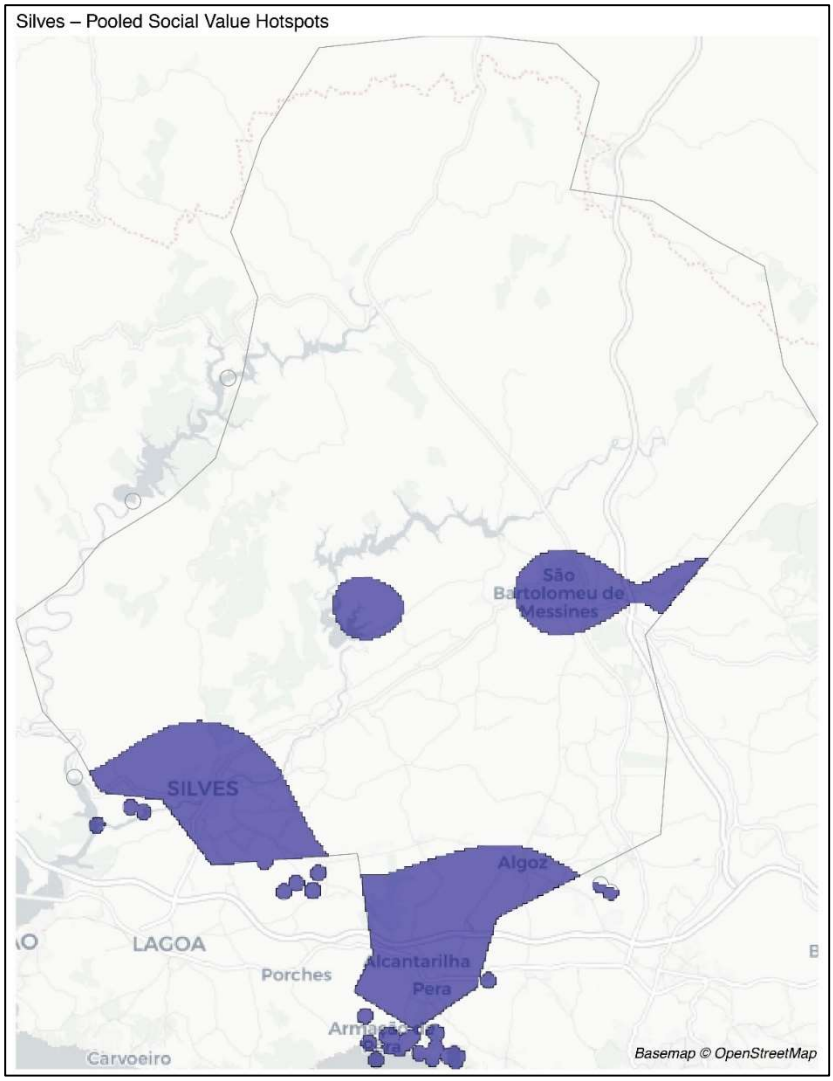

Figure 27: Pooled social value hotspots in Silves (blue). Participant points are masked to protect exact locations. Our analysis considered a minimum density threshold (hereafter, retention threshold) that captured ~70% of the points. Projection EPSG:3763.

A central purpose of this public participatory mapping exercise was to understand how local-scale, community values attributed to the landscape may differ or correspond with the spatial conflict data our study has developed through a pre-screening, coarse-filter approach.

When we compared our identified clusters (for the pooled participant data) with the national conflict raster (combining both social and environmental layers), more than 90% of our hotspot area overlapped with land classified as having potential conflict (*Figure 28*). This pattern generally aligned with was expected from the coarse-filter layer, which indicated large portions of the municipality as high conflict, when combining all the conflict layers. Only 8% of the pooled hotspots fell in "non-conflict" zones, and in most cases those areas were located adjacent to areas of potential conflict. If we consider value-specific hotspots, clusters pertaining to biodiversity and economic/tourism values were almost entirely within areas we had identified as conflict (>97%).

Hotspots for landscape value and visual aesthetics had the greatest representation, with nearly 13% falling outside of known, pre-screened conflict areas. These patterns indicate that in this population sample of public participatory mapping, the local data was well-aligned with the coarse-filter datasets but also provided insight to the relative priorities (social value types) within a blanket "conflict" designation.

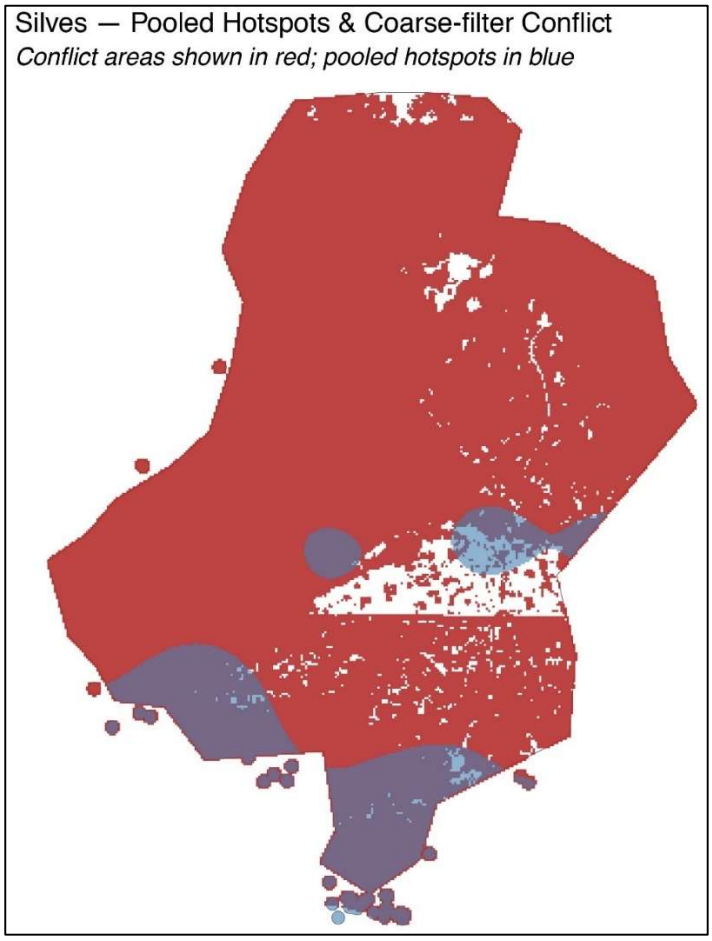

Figure 28: Hotspot polygons for pooled social value points (blue) overlaid with lands classified as "conflict" per coarse-filter environmental and social data (red). Individual social value points have been masked to protect exact locations. Projection EPSG:3763.

Despite the limited geographic and temporal scope of this participatory component of the project, we tested for the degree of clustering using the Clark-Evans nearest-neighbor test and confirmed significant clustering present across value attributes in our sample.

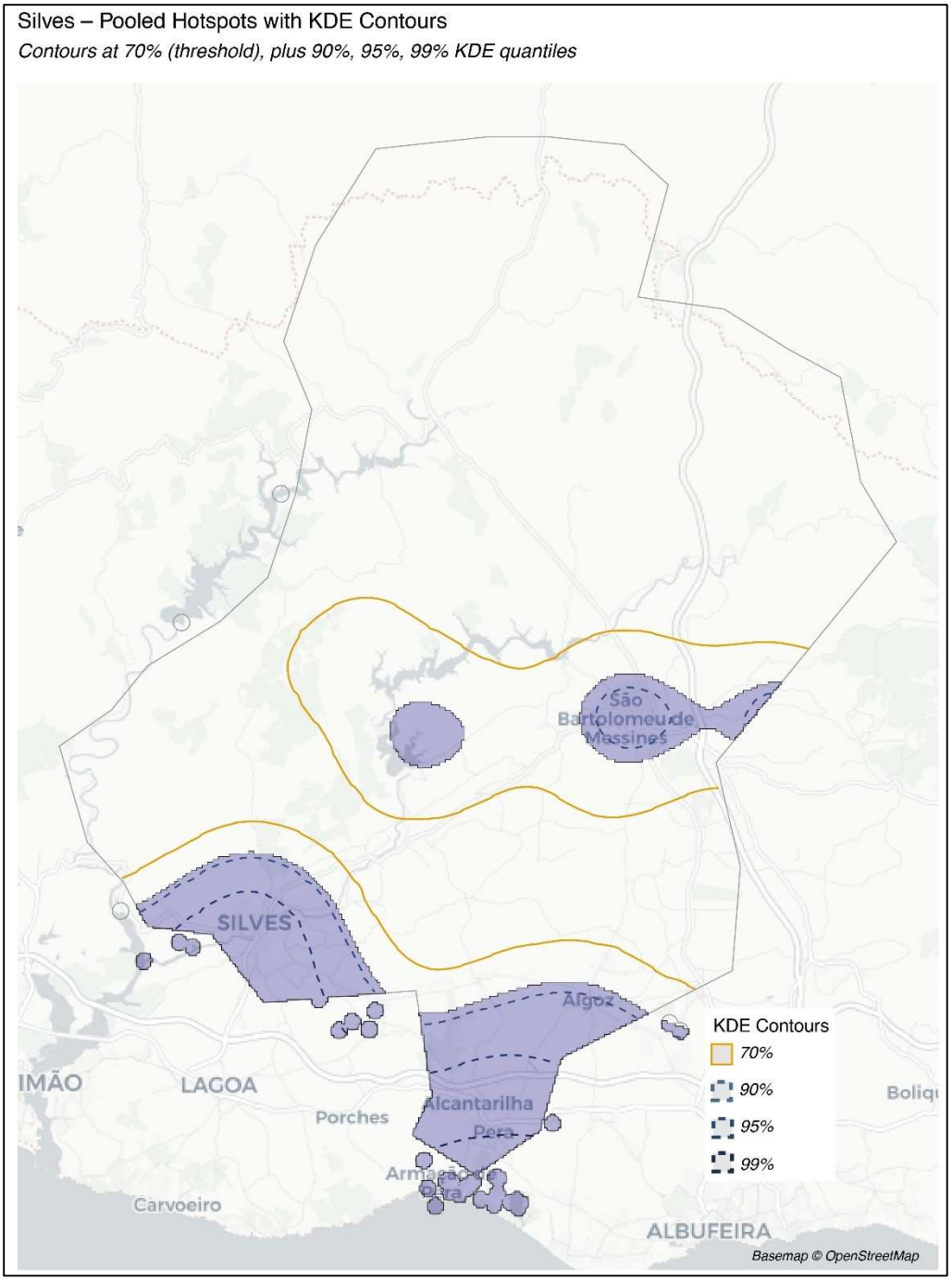

Figure 29: Hotspot polygons identified in our analysis for pooled social value data, with KDE contour lines representing successive quantiles that highlight progressively higher-density clusters of participant input. Our analysis retained areas enclosing ~70% of mapped points (i.e., the top 30% of KDE density values), shown here by the amber contour line.

4.5.1.1. Identified hotspots categorized by social value type

While our main analysis focused on pooled hotspots across all values (n=160), for exploratory purposes, we also generated per-category clusters to examine any differences in spatial expression of social values (*Table 18*). As a caveat, these results should be treated as preliminary insights due to the relatively small sample sizes of mapped points for each category. Nonetheless, we can highlight distinct patterns within this constrained sample (*Figure 30*).

Table 18: Summary of hotspot metrics by social value categories in Silves.

Category	**# Patches**	**Area (km²)**	**% of Window Area**	**% Points Inside**	**Median Patch Size (km²)**	**Mean Patch Size (km²)**	**IQR Patch Size (km²)**	**Min Patch Size (km²)**	**Max Patch Size (km²)**
Agricultural Value	9	194.9	30.2	71.0	0.5	21.7	0.3	0.3	191.3
Biodiversity Importance	9	23.2	3.6	70.6	0.5	2.6	1.6	0.2	11.1
Cultural Value	8	55.0	8.5	74.4	0.6	6.9	2.5	0.2	42.7
Economic/Tourism Value	10	112.9	17.5	68.2	0.4	11.3	0.5	0.3	86.1
Landscape/Visual Aesthetics	9	201.5	31.2	70.6	0.5	22.4	0.6	0.3	107.3

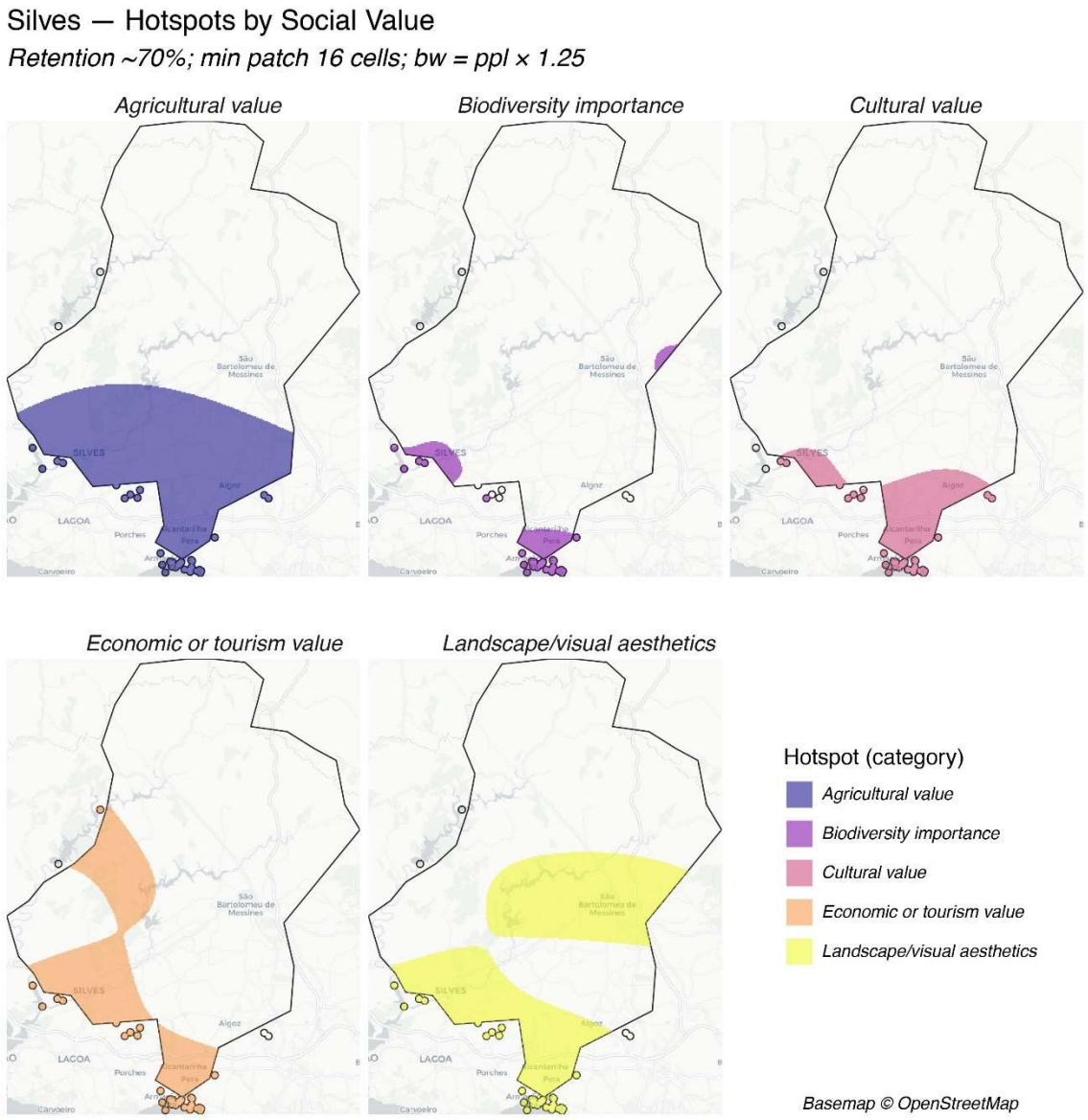

Figure 30: Hotspot polygons shown separately for each social value category.

We find the largest footprints of a social value hotspot for agricultural and landscape/visual aesthetic values, covering approximately 195 km² (30% of the analysis boundary, i.e., Silves municipality) and 201 km² (31%), respectively. In both cases, the large area was driven by one or two dominant patches (maximum sizes of 191 km² and 107 km²), alongside several much smaller fragments. This indicates that agricultural and aesthetic values were mapped broadly across the landscape, consistent with expectations from coarse-filter consultations.

In contrast, we found more compact clusters for biodiversity importance, covering only 23 km² (3.6% of Silves), with a maximum patch size of 11 km². These clusters reflect more localized values attributed to the landscape, suggesting that participants reported locations of biodiversity importance with highly specific areas in mind rather than spanning broader swaths of land.

There were intermediate patterns for cultural value hotspots, with eight patches covering ~55 km² (8.5%). While fewer in overall number, these clusters tended to be larger relative to biodiversity hotspot areas, suggesting that the cultural values participants mapped were associated with relatively expansive but discrete areas.

Finally, economic and tourism values covered ~113 km² (17.5%), with one particularly large patch reaching 86 km². These hotspots were moderately fragmented, indicating that economic/tourism values were more dispersed than the mapped locations of cultural or biodiversity value, but less spatially expansive than agricultural or aesthetic values.

4.5.2. Overlap with coarse-filter conflict data

When overlaid with the national siting conflict layer (combining both environmental and social datasets into a binary 0/1 raster), categorical hotspots showed uniformly high levels of overlap with conflict-classified land. More than 85% of every category's hotspot area fell inside conflict zones, and for biodiversity, cultural, and economic/tourism categories, overlap exceeded 95%. Only landscape aesthetics displayed a modestly higher proportion outside conflict (~12.8%), reflecting its broader footprint and greater likelihood of intersecting non-conflict areas. Still, these areas were adjacent to large expanses of area/pixels classified as potential for conflict.

The pooled hotspots as a whole showed ~91% overlap with conflict areas, leaving just ~8% in non-conflict zones. While this confirms that the Silves municipality is broadly characterized as high-conflict under the coarse-filter dataset, the category-specific analysis demonstrates how local mapping can help differentiate relative priorities within uniformly flagged regions.

Table 19:Percept overlap between pooled and social value category-specific hotspot areas with conflict and non-conflict zones (as defined by pixels classified as combined environmental and social conflict per national-scale coarse-filter data).

Category	**% Overlap - conflict zones**	**% Overlap - non-conflict zones**
Pooled values	91.4	8.1
Agricultural Value	93.4	6.3
Biodiversity Importance	97.5	0.6
Cultural Value	96.4	2.8
Economic/Tourism Value	98.7	0.9
Landscape/Visual Aesthetics	86.9	12.8

Sensitivity Analyses:

We tested the sensitivity of our points retention threshold and confirmed that the same core clusters persisted across thresholds (65%, 70%, 75%), though total hotspot area increased at higher retention levels (*Table 20*; *Figure 31*). Broadly, this suggests that the approach to hotspot delineation was relatively robust and our spatial patterns were not highly sensitive to cut-off choice for this sample.

We also tested sensitivity of pooled hotspots generated from a range of KDE point-retention thresholds (65%, 70%, 75%). Results indicated that the same core clusters were preserved across all thresholds, though total hotspot area and patch counts increased slightly at higher retention levels. At 65%, one fewer cluster was retained; at 75%, larger and denser clusters dominated. We performed this test as an exploratory check for robustness and to ensure that the pilot results were not an artefact of a particular cutoff, though we recommend retaining 70% as a balanced threshold. The primary methodology we followed for this analysis set their minimum density threshold at 80%, however their study had a relatively larger project area and sample size.

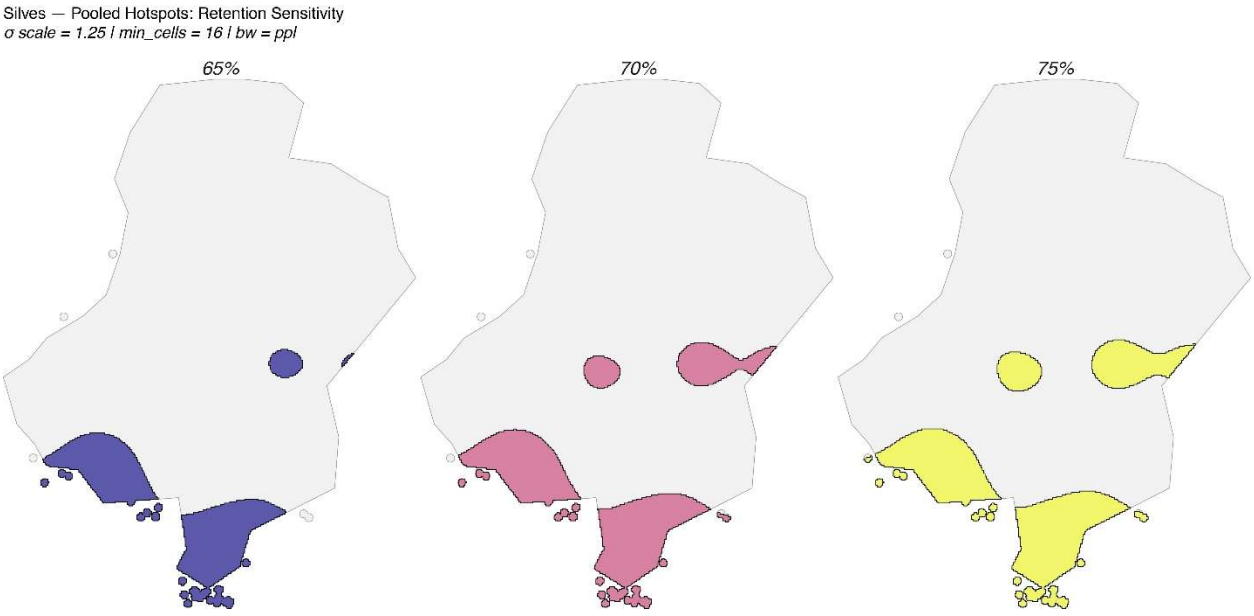

Figure 31: Hotspot sensitivity analysis across 65%-, 70%-, and 75%-point retention thresholds. Faceted plots represent output hotspot polygons from each of these applied thresholds.

Table 20: Summary of hotspot metrics by social value categories in Silves.

Retention Threshold	**# Patches**	**Area (km²)**	**% of Window Area**	**% Points Inside**	**Median Patch Size (km²)**	**Mean Patch Size (km²)**	**IQR Patch Size (km²)**	**Min Patch Size (km²)**	**Max Patch Size (km²)**
65%	10	63.4	9.8	65	0.55	6.34	2.90	0.26	31.8
70%	11	84.5	13.1	70	0.57	7.68	8.84	0.28	35.4
75%	12	93.3	14.5	75	0.55	7.78	9.56	0.17	36.7

5. References

Almeida, J., Godinho, C., Leitão, D., & Lopes, R. J. (2022). Lista Vermelha das Aves de Portugal Continental. SPEA, ICNF, LabOR/UÉ, CIBIO/BIOPOLIS. https://www.listavermelhadasaves.pt/lista-vermelha/

Baddeley, A., Rubak, E., & Turner, R. (2016). *Spatial point patterns: methodology and applications with R* (Vol. 1). Boca Raton: CRC press.

Baudry, J., & Merriam, H. G. (1988). Connectivity and connectedness: functional versus structural patterns in landscapes. *Connectivity in landscape ecology*, *29*, 23-28.

Bolinger, M., & Bolinger, G. (2022). Land Requirements for Utility-Scale PV: An Empirical Update on Power and Energy Density. IEEE Journal of Photovoltaics, 12(2), 589–594. IEEE Journal of Photovoltaics. https://doi.org/10.1109/JPHOTOV.2021.3136805

Breiman, L. (2001). Random Forests. Machine Learning, 45(1), 5–32. https://doi.org/10.1023/A:1010933404324

Brennan, A., Naidoo, R., Greenstreet, L., Mehrabi, Z., Ramankutty, N., & Kremen, C. (2022). Functional connectivity of the world's protected areas. *Science*, *376*(6597), 1101-1104. DOI: 10.1126/science.abl8974

BREUER, W. (2001). Ausgleichs-und Ersatzmaßnahmen für Beeinträchtigungen des Landschaftsbildes. Vorschläge für Maßnahmen bei Errichtung von Windkraftanlagen. *Naturschutz und Landschaftsplanung*, *33*(8), 237-245.

Brown, G., & Raymond, C. (2007). The relationship between place attachment and landscape values: Toward mapping place attachment. *Applied geography*, *27*(2), 89-111. https://doi.org/10.1016/j.apgeog.2006.11.002

Casalegno, S., Inger, R., DeSilvey, C., & Gaston, K. J. (2013). Spatial covariance between aesthetic value & other ecosystem services. *PloS one*, *8*(6), e68437. https://doi.org/10.1371/journal.pone.0068437

Cerveira, A., Pires, E. J. S., & Baptista, J. (2021). Wind Farm Cable Connection Layout Optimization with Several Substations. Energies, 14(12), Article 12. https://doi.org/10.3390/en14123615

Copeland, H. E., Doherty, K. E., Naugle, D. E., Pocewicz, A., & Kiesecker, J. M. (2009). Mapping oil and gas development potential in the US Intermountain West and estimating impacts to species. PloS One, 4(10), e7400. https://doi.org/10.1371/journal.pone.0007400

Copernicus (2018). CORINE Land Cover (CLC2018). Copernicus Land Monitoring Service - European Environment Agency. https://doi.org/10.2909/71c95a07-e296-44fc-b22b-415f42acfdf0

Currie, M., Saafi, M., Tachtatzis, C., & Quail, F. (2015). Structural integrity monitoring of onshore wind turbine concrete foundations. Renewable Energy, 83, 1131–1138. https://doi.org/10.1016/j.renene.2015.05.006

Dai, X., Felsenstein, D., & Grinberger, A. Y. (2023). Viewshed effects and house prices: Identifying the visibility value of the natural landscape. *Landscape and Urban Planning*, *238*, 104818. https://doi.org/10.1016/j.landurbplan.2023.104818

Davidson, A., Dunn, L., Gergely, K., McKerrow, A., Williams, S., & Case, M. (2021). Refining the coarse filter approach: Using habitat-based species models to identify rarity and vulnerabilities in the protection of US biodiversity. *Global Ecology and Conservation*, *28*, e01598. https://doi.org/10.1016/j.gecco.2021.e01598

de Luis-Ruiz, J. M., Salas-Menocal, B. R., Pereda-García, R., Pérez-Álvarez, R., Sedano-Cibrián, J., & Ruiz-Fernández, C. (2024). Optimal Location of Solar Photovoltaic Plants Using Geographic Information Systems and Multi-Criteria Analysis. Sustainability, 16(7), Article 7. https://doi.org/10.3390/su16072895

DGEG (2024). Geoportal for Energy Infrastructure in Portugal. Direção-Geral de Energia e Geologia. https://portalgeo.dgeg.gov.pt/arcgis/apps/webappviewer/index.html?id=de764a4a5ccd446292cb26a7e5c2e725

DGT (2018). Carta de Uso e Ocupação do Solo para 2018 (COS2018). Direção-Geral do Território. https://www.dgterritorio.gov.pt/Carta-de-Uso-e-Ocupacao-do-Solo-para-2018

DGT (2023). Carta Administrativa Oficial de Portugal (CAOP). Direção-Geral do Território. https://www.dgterritorio.gov.pt/cartografia/cartografia-tematica/caop

Dilts, T. (2023). Topography Toolbox for ArcGIS Pro [Computer software]. Great Basin Landscape Ecology Lab, Department of Natural Resources and Environmental Science, University of Nevada Reno. https://www.arcgis.com/home/item.html?id=247fbe56c7ff48229c9b1fe132d1b5e9

Dunkel, A. (2015). Visualizing the perceived environment using crowdsourced photo geodata. *Landscape and urban planning*, *142*, 173-186. https://doi.org/10.1016/j.landurbplan.2015.02.022

E2P – Energy and Environmental Planning Platform (2024). Instituto Nacional de Engenharia, Tecnologia e Inovação (INEGI). https://e2p.inegi.up.pt/

ESRI (2024). ArcGIS Pro (Version 3.6.0) [Computer software]. Esri. https://www.esri.com/en-us/arcgis/products/arcgis-pro/overview

EUROBATS. (2025). National Report: Portugal. https://www.eurobats.org/sites/default/files/2025-07/Portugal.pdf

Evans, J. S. (2025a). spatialEco (Version 2.3) [R]. https://github.com/jeffreyevans/spatialEco

Evans, J. S. (2025b). Jeffreyevans/rfUtilities [R]. https://github.com/jeffreyevans/rfUtilities

Evans, J. S., & Kiesecker, J. M. (2014). Shale gas, wind and water: Assessing the potential cumulative impacts of energy development on ecosystem services within the Marcellus play. PloS One, 9(2), e89210. https://doi.org/10.1371/journal.pone.0089210

Fischer, C., & Roth, M. (2020). Empfindlichkeit des Landschaftsbildes. Bewertung durch großräumige Einsehbarkeitsanalysen. *Naturschutz und Landschaftsplanung*, (6), 280-287.

Fischer, C., & Roth, M. (2021). Assessing visual landscape sensitivity towards wind turbines with a distance decay effect: An exploration of different GIS approaches. *J. Digit. Landsc. Archit*, *6*, 148-162.

Florio, P., Roecker, C., Probst, M. M., & Scartezzini, J. L. (2016, December). Visibility of Building Exposed Surfaces for the Potential Application of Solar Panels: A Photometric Model. In *UDMV* (pp. 45-50).

Fox, N., Chamberlain, B., Lindquist, M., & Van Berkel, D. (2022). Understanding landscape aesthetics using a novel viewshed assessment of social media locations within the Troodos UNESCO Global Geopark, Cyprus. *Frontiers in Environmental Science*, *10*, 884115. https://doi.org/10.3389/fenvs.2022.884115

Gameiro, J., Ribeiro, L., Pacheco, C., L., Guedes, A., Pereira, J., Marques, A.T., Valerio, F., Venâncio, Diamantino, J., Santos, C., Tomás, A., Sampaio, H., Alcazar, R., Elias, G., Arroyo, B., and Silva, J.P., (2023). 1º Censo Nacional da Águia-caçadeira Circus pygargus: Resultados Finais. BIOPOLIS-CIBIO. https://steppebirdsmove.com/wp-content/uploads/2024/01/Gameiro-et-al_2023_1o-Censo-Nacional-Aguia-cacadeira-resultados-finais.pdf

Geselbracht, L., R. Torres, G. Cumming, D. Dorfman, M. Beck. (2005). Marine/Estuarine Site Assessment for Florida: A Framework for Site Prioritization. Final Report for Florida's Wildlife Legacy Initiative, a program of the Florida Fish and Wildlife Conservation Commission. The

Nature Conservancy, Gainesville, Florida. https://myfwc.com/research/habitat/coastal-wetlands/chimmp/workshop/

Global SRTM mTPI (CSP ERGo 1.0). (2024) Google Earth Engine. https://developers.google.com/earth-engine/datasets/catalog/CSP_ERGo_1_0_Global_SRTM_mTPI

Global Wind Atlas. (2024). Global Wind Atlas. World Bank Group & Technical University of Denmark. https://globalwindatlas.info/en/

Gobster, P. H., Nassauer, J. I., Daniel, T. C., & Fry, G. (2007). The shared landscape: what does aesthetics have to do with ecology?. Landscape ecology, 22(7), 959-972. https://doi.org/10.1007/s10980-007-9110-x

Gregório, I., Barros, T., Pando, D., Morante, J., Fonseca, C., & Ferreira, E. (2020). Paths for colonization or exodus? New insights from the brown bear (Ursus arctos) population of the Cantabrian Mountains. *PLoS One*, *15*(1), e0227302. https://doi.org/10.1371/journal.pone.0227302

GREW (2024). Global Renewable Energy Monitoring Platform. Global Renewables Watch. https://www.globalrenewableswatch.org/

Groves, C., Beck, M. W., Higgins, J. V., & Saxon, E. C. (2003). Drafting a conservation blueprint: a practitioner's guide to planning for biodiversity.

GTAER (2024). Resultados e conclusões do GTAER – Grupo de Trabalho para a definição das Áreas de Aceleração de Energias Renováveis. Laboratório Nacional de Energia e Geologia (LNEG). https://repositorio.lneg.pt/entities/publication/001b2bff-9aa0-4813-90de-d529915d3e25

Guilherme JL, Morais B, Alonso H, Andrade J, Almeida A, Barros N & Dias MP (2023). Mapping seabird and marine biodiversity sensitivity to marine wind farm expansion in Portugal | Mapeamento da sensibilidade das aves marinhas à energia eólica no mar em Portugal (Version 1). Sociedade Portuguesa para o Estudo das Aves (SPEA). https://doi.org/10.5281/zenodo.10045918

ICNF. (2024a). Rede Natura 2000 – Protected Areas in Portugal. Instituto da Conservação da Natureza e das Florestas https://www.icnf.pt/conservacao/redenatura2000

ICNF. (2024b). Ramsar Sites – Wetlands of International Importance. Instituto da Conservação da Natureza e das Florestas. https://www.icnf.pt/conservacao/ambitointernacional/ramsar

ICNF. (2024c). Spatial Data Portal for Nature Conservation in Portugal. Instituto da Conservação da Natureza e das Florestas. https://sig.icnf.pt/portal/home/item.html?id=02b7a03f8fbd4dada77f5f3e5f91f186

IEA. (2023, January 12). Average lead times to build new electricity grid assets in Europe and the United States, 2010-2021 – Charts – Data & Statistics. IEA. https://www.iea.org/data-and-statistics/charts/average-lead-times-to-build-new-electricity-grid-assets-in-europe-and-the-united-states-2010-2021

Inglis, N. C., Vukomanovic, J., Costanza, J., & Singh, K. K. (2022). From viewsheds to viewscapes: Trends in landscape visibility and visual quality research. *Landscape and Urban Planning*, *224*, 104424. https://doi.org/10.1016/j.landurbplan.2022.104424

Jiang, B. (2013). Head/tail breaks: A new classification scheme for data with a heavy-tailed distribution. *The Professional Geographer*, *65*(3), 482-494. https://doi.org/10.1080/00330124.2012.700499

JRC. (2025) European Commission Joint Research Centre - Global Human Settlement Layer (GHSL) Data Collection. https://data.jrc.ec.europa.eu/collection/ghsl

Kennedy, C. M., Oakleaf, J. R., Theobald, D. M., Baruch-Mordo, S., & Kiesecker, J. (2019). Managing the middle: A shift in conservation priorities based on the global human modification gradient. *Global change biology*, *25*(3), 811-826. https://doi.org/10.1111/gcb.14549

Kiesecker, J. M., Nagaraju, S. K., Oakleaf, J. R., Ortiz, A., Lavista Ferres, J., Robinson, C., Krishnaswamy, S., Mehta, R., Dodhia, R., Evans, J. S., Heiner, M., Priyadarshini, P., Chandran, P., & Sochi, K. (2023). The Road to India's Renewable Energy Transition Must Pass through Crowded Lands. Land, 12(11), Article 11. https://doi.org/10.3390/land12112049

Kiesecker, J.M., Evans, J.S., Oakleaf, J.R., Dropuljić, K.Z., Vejnović, I., Rosslowe, C., Cremona, E., Bhattacharjee, A.L., Nagaraju, S.K., Ortiz, A., Robinson, C., Ferres, J. L., Zec, M., Sochi, K. (2024). Land use and Europe's renewable energy transition: identifying low-conflict areas for wind and solar development. *Frontiers in Environmental Science*, *12*, p.1355508. https://doi.org/10.3389/fenvs.2024.1355508

Kim, Y., Kim, C. K., Lee, D. K., Lee, H. W., & Andrada, R. I. T. (2019). Quantifying nature-based tourism in protected areas in developing countries by using social big data. *Tourism Management*, *72*, 249-256. https://doi.org/10.1016/j.tourman.2018.12.005

Lehto, C., Hedblom, M., Filyushkina, A., & Ranius, T. (2024). Seeing through their eyes: Revealing recreationists' landscape preferences through viewshed analysis and machine

learning. *Landscape and Urban Planning*, *248*, 105097. https://doi.org/10.1016/j.landurbplan.2024.105097

Lemelin, L. V., & Darveau, M. (2006). Coarse and fine filters, gap analysis, and systematic conservation planning. *The Forestry Chronicle*, *82*(6), 802-805. https://doi.org/10.5558/tfc82802-6

Liaw, A., & Wiener, M. (2002). Classification and regression by randomForest. *R news*, *2*(3), 18-22. https://journal.r-project.org/articles/RN-2002-022/RN-2002-022.pdf

LIFE Aegypius Return. (2024). Vulture Conservation Foundation. https://4vultures.org/life-aegypius-return/project/

LNEG. (2018). Atlas Eólico de Portugal. Laboratório Nacional de Energia e Geologia - LNEG Geoportal. https://geoportal.lneg.pt/mapa/?mapa=AtlasEolico

LNEG. (2025). Laboratório Nacional de Energia e Geologia - Geoportal LNEG – Geossítios Database. https://geoportal.lneg.pt/pt/bds/geossitios/#!/?page=1

Lumbierres, M., Dahal, P.R., Soria, C.D., Di Marco, M., Butchart, S.H.M., Donald, P.F., and Rondinini, C., (2022). Area of Habitat maps for the world's terrestrial birds and mammals. *Sci Data.* 2022 Dec 3;9(1):749. https://pubmed.ncbi.nlm.nih.gov/36463270/

Mathias, M.L. (coord.), Fonseca, C., Rodrigues, L., Grilo, C., Lopes-Fernandes, M., Palmeirim, J.M., Santos-Reis, M., Alves, P.C., Cabral, J.A., Ferreira, M., Mira, A., Eira, C., Negrões, N., Paupério, J., Pita, R., Rainho, A., Rosalino, L.M., Tapisso, J.T., Vingada, J. (eds.), 2023. Livro Vermelho dos Mamíferos de Portugal Continental. FCiências.ID, ICNF, Lisboa https://dspace.uevora.pt/rdpc/handle/10174/35224

META, 2024. Meta AI: High-Resolution Population Density Maps Dataset. https://ai.meta.com/ai-for-good/datasets/high-resolution-population-density-maps/#accessdata

Murphy, M. A., Evans, J. S., & Storfer, A. (2010). Quantifying Bufo boreas connectivity in Yellowstone National Park with landscape genetics. Ecology, 91(1), 252–261. https://doi.org/10.1890/08-0879.1

NASA, SRTM. (2024). Digital Elevation Terrain Model (DEM). NASA Earthdata. https://www.earthdata.nasa.gov/topics/land-surface/digital-elevation-terrain-model-dem

New European Wind Atlas. (2024). New European Wind Atlas. https://map.neweuropeanwindatlas.eu/

Noss, R. F. (1987). From plant communities to landscapes in conservation inventories: a look at The Nature Conservancy (USA). *Biological conservation*, *41*(1), 11-37. https://doi.org/10.1016/0006-3207(87)90045-0

Oakleaf, J., Kennedy, C., Baruch-Mordo, S., Gerber, J., West, P., Johnson, J., & Kiesecker, J. (2019). Mapping global development potential for renewable energy, fossil fuels, mining and agriculture sectors. Scientific Data, 6(1), 101. https://doi.org/10.1038/s41597-019-0084-8

Ong, S., Campbell, C., Denholm, P., Margolis, R., & Heath, G. (2013). Land-Use Requirements for Solar Power Plants in the United States. National Renewable Energy Laboratory.

OrtoSat2023 – Complete Orthophoto Coverage of Portugal (2023). Direção-Geral do Território. https://www.dgterritorio.gov.pt/Disponibilizacao-da-OrtoSat2023-Completa

OSM (2024). Global OpenStreetMap Data Viewer. OpenStreetMap. https://www.openstreetmap.org/#map=6/51.32/10.46

Palliwoda, J., Büermann, A., Fischer, J., Kraemer, R., & Schröter, M. (2021). Zoning of UNESCO biosphere reserves: A comprehensive set of geodata for Europe. *Frontiers in Ecology and Evolution*, *9*, 736358. https://doi.org/10.3389/fevo.2021.736358

Palmer, J. F. (2022). Cumulative viewsheds in wind energy visual impact assessments and how they are interpreted. *Journal of Digital Landscape Architecture*, 7-2022.

Palmer, J. F. (2022a). Deconstructing viewshed analysis makes it possible to construct a useful visual impact map for wind projects. *Landscape and Urban Planning*, *225*, 104423. https://doi.org/10.1016/j.landurbplan.2022.104423

PCIP. (2024). Cultural Heritage Geoportal – ArcGIS Services. Património Cultural, I.P. https://geo.patrimoniocultural.gov.pt/arcgis/rest/services

Pimenta, V., Barroso, I., Álvares, F., Barros, T., Borges, C., Cadete, D., Carneiro, C., Casimiro, J., Ferrão da Costa, G., Ferreira, E., Fonseca, C., García, E.J., Gil, P., Godinho, R., Hipólito, D., Llaneza, L., Marcos Perez, A., Martí-Domken, B., Monzón, A., Nakamura, M., Palacios, V., Paulino, C., Pereira, J., Pereira, A., Petrucci-Fonseca, F., Pinto, S., Rio-Maior, H., Roque, S., Sampaio, M., Santos, J., Serronha, A., Simões, F., Torres, R.T., (2023). Situação populacional do lobo em Portugal: Resultados do censo nacional de 2019/2021. ICNF, Lisboa, 145p. https://censo-2019-2021.loboiberico.pt/

Planet Labs (2024). PlanetScope Monthly Mosaics [Satellite imagery]. Planet Labs PBC. Retrieved in October 2024 from https://www.planet.com/

Poudyal, N. C., Hodges, D. G., Fenderson, J., & Tarkington, W. (2010). Realizing the economic value of a forested landscape in a viewshed. *Southern Journal of Applied Forestry*, *34*(2), 72-78. https://doi.org/10.1093/sjaf/34.2.72

QGIS Development Team. (2024). QGIS Geographic Information System (Version 3.44.6) [Computer software]. QGIS Association. https://qgis.org/en/site/

R Core Team (2021). R: A language and environment for statistical computing. R Foundation for Statistical Computing, Vienna, Austria. URL https://www.R-project.org/ .

Richards, D. R., & Tunçer, B. (2018). Using image recognition to automate assessment of cultural ecosystem services from social media photographs. *Ecosystem services*, *31*, 318-325. https://doi.org/10.1016/j.ecoser.2017.09.004

Riitters, K. H., O'neill, R. V., & Jones, K. B. (1997). Assessing habitat suitability at multiple scales: a landscape-level approach. *Biological Conservation*, *81*(1-2), 191-202. https://doi.org/10.1016/S0006-3207(96)00145-0

Riitters, K., Wickham, J., O'Neill, R., Jones, B., & Smith, E. (2000). Global-scale patterns of forest fragmentation. *Conservation ecology*, *4*(2). https://www.jstor.org/stable/26271763

Ross, G. J., & Jones, T. (2015). Understanding the heavy-tailed dynamics in human behavior. *Physical Review E*, *91*(6), 062809. https://doi.org/10.1103/PhysRevE.91.062809

RSIS. (2024). Global Ramsar Wetlands Database - Ramsar Sites Information Service. Ramsar Convention Secretariat. https://rsis.ramsar.org/

Rubolini, D., Bassi, E., Bogliani, G., Galeotti, P., & Garavaglia, R. (2001). Eagle Owl Bubo bubo and power line interactions in the Italian Alps. *Bird Conservation International*, *11*(4), 319-324. https://doi.org/10.1017/S0959270901000363

Sergio, F., Marchesi, L., Pedrini, P., Ferrer, M., & Penteriani, V. (2004). Electrocution alters the distribution and density of a top predator, the eagle owl Bubo bubo. *Journal of Applied Ecology*, *41*(5), 836-845. https://doi.org/10.1111/j.0021-8901.2004.00946.x

Serratosa, J., & Allinson, T. (2022). AVISTEP: the Avian Sensitivity Tool for Energy Planning. Technical Manual. https://avistep.birdlife.org/AVISTEPTechnicalManual.pdf

Shahriar Haque, A. S. M., Rahman, Md. M., Joy, C. J. I., Hasan, Md. S., Aftabuzzaman, M., & Rahman, Md. S. (2022). Levelized Cost of Energy and Cost-Benefit Analysis of 230 kV Bulk Power Transmission in Bangladesh. 2022 12th International Conference on Electrical and

Computer Engineering (ICECE), 236–239. https://doi.org/10.1109/ICECE57408.2022.10088682

Sochi, K., Oakleaf, J., Bhattacharjee, A., Evans, J. S., Vejnovic, I., Dropuljic, K. Z., Mileunsnic, D., Bevk, T., Bjelic, I. B., Dedinec, A., Doljak, D., Gorin, S., Pavlovic, B., Zec, M., & Kiesecker, J. M. (2023). Mapping a Sustainable Renewable Energy Transition: Handbook for Practitioners (No. Ver 1; p. 25). The Nature Convservancy. https://www.nature.org/content/dam/tnc/nature/en/documents/Europe_Energy_Practitioners_Guide.pdf

Solar Atlas V2: Solar capacity factor – average daily totals (PVOUT). (2024) World Solar Atlas. https://globalsolaratlas.info/map?c=11.609193,8.4375,3

Sonter, L. J., Watson, K. B., Wood, S. A., & Ricketts, T. H. (2016). Spatial and temporal dynamics and value of nature-based recreation, estimated via social media. *PLoS one*, *11*(9), e0162372. https://doi.org/10.1371/journal.pone.0162372

SPEA. (2024). Important Bird Areas (IBAs) in Portugal. Sociedade Portuguesa para o Estudo das Aves. https://spea.pt/categoria-observacao/ibas-areas-importantes/

SPEA. (2025). III Atlas das Aves Nidificantes. Sociedade Portuguesa para o Estudo das Aves. https://spea.pt/censos/iii-atlas-aves-nidificantes/

Strager, M. P., Strager, J. M., Evans, J. S., Dunscomb, J. K., Kreps, B. J., & Maxwell, A. E. (2015). Combining a spatial model and demand forecasts to map future surface coal mining in Appalachia. PLoS ONE, 10(6), e0128813. https://doi.org/10.1371/journal.pone.0128813

Sullivan, R., Abplanalp, J. M., Zvolanek, E., & Brown, J. (2015). *Visual Resource Analysis for Solar Energy Zones in the San Luis Valley* (No. ANL/EVS--16/6). Argonne National Lab.(ANL), Argonne, IL (United States). https://doi.org/10.2172/1327813

Swetnam, R. D., Harrison-Curran, S. K., & Smith, G. R. (2017). Quantifying visual landscape quality in rural Wales: A GIS-enabled method for extensive monitoring of a valued cultural ecosystem service. *Ecosystem Services*, *26*, 451-464. https://doi.org/10.1016/j.ecoser.2016.11.004

Takaku, J., Tadono, T., Doutsu, M., Ohgushi, F., & Kai, H. (2021). Updates of 'AW3D30'ALOS global digital surface model in Antarctica with other open access datasets. *The International Archives of the Photogrammetry, Remote Sensing and Spatial Information Sciences*, *43*, 401-408. https://doi.org/10.5194/isprs-archives-XLIII-B4-2021-401-2021

Theobald, D. M., Harrison-Atlas, D., Monahan, W. B., & Albano, C. M. (2015). Ecologically-Relevant Maps of Landforms and Physiographic Diversity for Climate Adaptation Planning. PLOS ONE, 10(12), e0143619. https://doi.org/10.1371/journal.pone.0143619

Theobald, D. M., Oakleaf, J. R., Moncrieff, G., Voigt, M., Kiesecker, J., & Kennedy, C. M. (2025). Global extent and change in human modification of terrestrial ecosystems from 1990 to 2022. *Scientific Data*, *12*(1), 606. https://doi.org/10.1038/s41597-025-04892-2

Tingley, M. W., Darling, E. S., & Wilcove, D. S. (2014). Fine-and coarse-filter conservation strategies in a time of climate change. *Annals of the New york Academy of Sciences*, *1322*(1), 92-109. https://doi.org/10.1111/nyas.12484

TNC. 2007. *A Biodiversity and Conservation Assessment of the Southern Shortgrass Prairie Ecoregion*. Southern Shortgrass Prairie Ecoregional Planning Team, The Nature Conservancy, San Antonio, TX.

Torre, I., Compaña, A., Ramot, J., Grajera, J., Andino, H., & Bontzorlos, V. (2025). Population structure and mortality of the Eurasian Eagle-Owl (Bubo bubo) in NE Spain. *Journal of Ornithology*, 1-9. https://doi.org/10.1007/s10336-025-02292-2

UNESCO. (2024). World Network of Biosphere Reserves. UNESCO. https://www.unesco.org/en/mab/wnbr/about

Van Berkel, D. B., Tabrizian, P., Dorning, M. A., Smart, L., Newcomb, D., Mehaffey, M., ... & Meentemeyer, R. K. (2018). Quantifying the visual-sensory landscape qualities that contribute to cultural ecosystem services using social media and LiDAR. *Ecosystem services*, *31*, 326-335. https://doi.org/10.1016/j.ecoser.2018.03.022

Wheatley, D. (2022). Cumulative viewshed analysis: a GIS-based method for investigating intervisibility, and its archaeological application. In *Archaeology and geographic information systems* (pp. 171-185). CRC Press.

Wilson, T., Lovelace, R., & Evans, A. J. (2019). A path toward the use of trail users' tweets to assess effectiveness of the environmental stewardship scheme: an exploratory analysis of the Pennine Way National Trail. *Applied spatial analysis and policy*, *12*(1), 71-99. https://doi.org/10.1007/s12061-016-9201-7

Wood, S. A., Guerry, A. D., Silver, J. M., & Lacayo, M. (2013). Using social media to quantify nature-based tourism and recreation. *Scientific reports*, *3*(1), 2976. https://doi.org/10.1038/srep02976

WRI. (2024). Global Power Plant Database. World Resources Institute. https://datasets.wri.org/datasets/global-power-plant-database

Wright, M., Wager, S., & Probst, P. (2024). A Fast Implementation of Random Forests (Version 17) [R]. https://github.com/imbs-hl/ranger

Yang, X., Fox, N., Van Berkel, D., & Lindquist, M. (2024). Viewscape: An R package for the spatial analysis of landscape perception and configurations in viewsheds of landscapes. *SoftwareX*, *26*, 101662. https://doi.org/10.1016/j.softx.2024.101662

Zhang, H., Huang, R., Zhang, Y., & Buhalis, D. (2022). Cultural ecosystem services evaluation using geolocated social media data: A review. *Tourism Geographies*, *24*(4-5), 646-668. https://doi.org/10.1080/14616688.2020.1801828

Supplementary material:

1) Biodiversity values used in the Extent layer from the coarse filter (in Portuguese)

COS2018 Classes	**Biodiversity value**
Tecido edificado contínuo predominantemente vertical	0.0
Tecido edificado contínuo predominantemente horizontal	0.0
Tecido edificado descontínuo	0.0
Tecido edificado descontínuo esparso	0.0
Áreas de estacionamentos e logradouros	0.0
Espaços vazios sem construção	0.0
Indústria	0.0
Comércio	0.0
Instalações Agrícolas	0.0
Infraestruturas de produção de energia renovável	0.0
Infraestruturas de produção de energia não renovável	0.0
Infraestruturas para captação, tratamento e abastecimento de Águas para consumo	0.0
Infraestruturas de tratamento de resíduos e Águas residuais	0.0
Rede viária e espaços associados	0.0
Rede ferroviária e espaços associados	0.0
Terminais portuários de mar e de rio	0.0
Estaleiros navais e docas secas	0.0
Marinas e docas pesca	0.0
Aeroportos	0.0
AerÃ³dromos	0.0
Minas a céu aberto	0.0
Pedreiras	0.0
Aterros	0.0

Lixeiras e Sucatas	0.0
Áreas em construção	0.0
Campos de golfe	0.0
Instalações desportivas	0.0
Parques de campismo	0.0
Equipamentos de lazer	0.0
Equipamentos culturais	0.0
Cemitérios	0.0
Outros equipamentos e Instalações turísticas	0.0
Parques e jardins	0.5
Arrozais	0.5
Vinhas	0.0
Pomares	0.0
Olivais	0.0
Culturas temporárias e/ou pastagens melhoradas associadas a vinha	0.5
Culturas temporárias e/ou pastagens melhoradas associadas a pomar	0.5
Culturas temporárias e/ou pastagens melhoradas associadas a olival	0.5
Mosaicos culturais e parcelares complexos	0.5
Agricultura com espaços naturais e seminaturais	0.5
Agricultura protegida e viveiros	0.0
Pastagens melhoradas	0.5
Pastagens espontâneas	1.0
SAF de sobreiro	1.0
SAF de azinheira	1.0
SAF de outros carvalhos	1.0
SAF de pinheiro manso	1.0
SAF de outras espécies	1.0
SAF de sobreiro com azinheira	1.0

SAF de outras misturas	1.0
Florestas de sobreiro	1.0
Florestas de azinheira	1.0
Florestas de outros carvalhos	1.0
Florestas de castanheiro	1.0
Florestas de eucalipto	0.0
Florestas de espécies invasoras	0.0
Florestas de outras folhosas	1.0
Florestas de pinheiro bravo	0.5
Florestas de pinheiro manso	0.5
Florestas de outras resinosas	0.5
Matos	0.5
Praias, dunas e areais interiores	1.0
Praias, dunas e areais costeiros	1.0
Rocha nua	0.5
Vegetação esparsa	0.0
Pauis	1.0
Sapais	1.0
Zonas entremarés	1.0
Cursos de Água naturais	1.0
Cursos de Água modificados ou artificializados	0.5
Lagos e lagoas interiores artificiais	0.5
Lagos e lagoas interiores naturais	1.0
Albufeiras de barragens	0.5
Albufeiras de represas ou de açudes	0.5
Charcas	0.5
Aquicultura	0.0
Salinas	0.0

Lagoas costeiras	1.0
Desembocaduras fluviais	1.0
Culturas temporárias de sequeiro	0.5
Culturas temporárias de regadio	0.0

1) List of species considered for the fine filter with the IUCN criteria and the numerical value

ID	Rel ID	Group	Species	Common Name	IUCN Bird Atlas/Red Book criteria	IUCN numerical criteria
1	1	Birds	*Accipiter gentilis*	*Açor*	VU	0.6
2	2	Birds	*Actitis hypoleucos*	*Maçarico-das-rochas*	VU	0.6
3	3	Birds	*Aegypius monachus*	*Abutre-preto*	EN	0.8
4	4	Birds	*Alaudala rufescens*	*Calhandrinha-das-marismas*	EN	0.8
5	5	Birds	*Anthus spinoletta*	*Petinha-ribeirinha*	EN	0.8
6	6	Birds	*Apus caffer*	*Andorinhão-cafre*	VU	0.6
7	7	Birds	*Aquila chrysaetos*	*Águia-real*	EN	0.8
8	8	Birds	*Aquila fasciata*	*Águia-perdigueira*	VU	0.6
9	9	Birds	*Ardea purpurea*	*Garça-vermelha*	VU	0.6
10	10	Birds	*Ardeola ralloides*	*Papa-ratos*	EN	0.8
11	11	Birds	*Asio otus*	*Bufo-pequeno*	VU	0.6
12	12	Birds	*Aythya ferina*	*Zarro-comum*	EN	0.8
13	13	Birds	*Bubo bubo*	*Bufo real*	NT	0.4
14	14	Birds	*Bubulcus ibis*	*Carraceiro*	VU	0.6
15	15	Birds	*Burhinus oedicnemus*	*Alcaravão*	VU	0.6
16	16	Birds	*Calonectris borealis*	*Cagarra*	EN	0.8
17	17	Birds	*Cercotrichas galactotes*	*Solitário*	EN	0.8
18	18	Birds	*Charadrius alexandrinus*	*Borrelho-de-coleira-interrompida*	EN	0.8
19	19	Birds	*Chlidonias hybrida*	*Gaivina-dos-pauis*	CR	1.0

20	20	Birds	*Ciconia nigra*	*Cegonha-preta*	EN	0.8
21	21	Birds	*Circus cyaneus*	*Tartaranhão-cinzento*	CR	1.0
22	22	Birds	*Circus pygargus*	*Águia-caçadeira*	EN	0.8
23	23	Birds	*Columba oenas*	*Seixa*	VU	0.6
24	24	Birds	*Coracias garrulus*	*Rolieiro*	CR	1.0
25	25	Birds	*Corvus monedula*	*Gralha-de-nuca-cinzenta*	EN	0.8
26	26	Birds	*Emberiza citrinella*	*Escrevedeira-amarela*	EN	0.8
27	27	Birds	*Emberiza hortulana*	*Sombria*	VU	0.6
28	28	Birds	*Emberiza schoeniclus*	*Escrevedeira-dos-caniços*	EN	0.8
29	29	Birds	*Falco naumanni*	*Francelho*	EN	0.8
30	30	Birds	*Falco peregrinus*	*Falcão-peregrino*	VU	0.6
31	31	Birds	*Falco subbuteo*	*Ógea*	VU	0.6
32	32	Birds	*Falco tinnunculus*	*Peneireiro-comum*	VU	0.6
33	33	Birds	*Gallinago gallinago*	*Narceja-comum*	CR	1.0
34	34	Birds	*Gelochelidon nilotica*	*Tagaz*	VU	0.6
35	35	Birds	*Glareola pratincola*	*Perdiz-do-mar*	VU	0.6
36	36	Birds	*Gulosus aristotelis*	*Gulosus aristotelis*	EN	0.8
37	37	Birds	*Hydrobates castro*	*Roque-de-castro*	VU	0.6
38	38	Birds	*Ixobrychus minutus*	*Garçote*	VU	0.6
39	39	Birds	*Lanius collurio*	*Picanço-de-dorso-ruivo*	VU	0.6
40	40	Birds	*Lanius meridionalis*	*Picanço-real*	VU	0.6
41	41	Birds	*Lanius senator*	*Picanço-barreteiro*	VU	0.6
42	42	Birds	*Larus fuscus*	*Gaivota-d'asa-escura*	VU	0.6

43	43	Birds	*Locustella luscinioides*	*Cigarrinha-ruiva*	VU	0.6
44	44	Birds	*Loxia curvirostra*	*Cruza-bico*	VU	0.6
45	45	Birds	*Milvus milvus*	*Milhafre-real*	CR	1.0
46	46	Birds	*Monticola saxatilis*	*Melro-das-rochas*	EN	0.8
47	47	Birds	*Neophron percnopterus*	*Britango*	EN	0.8
48	48	Birds	*Netta rufina*	*Pato-de-bico-vermelho*	VU	0.6
49	49	Birds	*Oenanthe hispanica*	*Chasco-ruivo*	VU	0.6
50	50	Birds	*Oenanthe leucura*	*Chasco-preto*	CR	1.0
51	51	Birds	*Otis tarda*	*Abetarda*	EN	0.8
52	52	Birds	*Otus scops*	*Mocho-d'orelhas*	VU	0.6
53	53	Birds	*Pandion haliaetus*	*Águia-pesqueira*	CR	1.0
54	54	Birds	*Pterocles orientalis*	*Cortiçol-de-barriga-preta*	EN	0.8
55	55	Birds	*Pyrrhocorax pyrrhocorax*	*Gralha-de-bico-vermelho*	VU	0.6
56	56	Birds	*Saxicola rubetra*	*Cartaxo-nortenho*	EN	0.8
57	57	Birds	*Spatula clypeata*	*Pato-colhereiro*	VU	0.6
58	58	Birds	*Sterna hirundo*	*Garajau-comum*	EN	0.8
59	59	Birds	*Sylvia borin*	*Toutinegra-das-figueiras*	VU	0.6
60	60	Birds	*Tetrax tetrax*	*Sisão*	CR	1.0
61	61	Birds	*Tringa totanus*	*Perna-vermelha-comum*	CR	1.0
62	62	Birds	*Uria aalgae**	*Airo*	CR	1.0
63	1	Bats	*Myotis blythii*	*Morcego-rato-pequeno*	CR	1.0
64	2	Bats	*Myotis emarginatus*	*Morcego-lanudo*	EN	0.8
65	3	Bats	*Myotis escalerai*	*Morcedo-de-franja-do-sul*	VU	0.6

66	4	Bats	*Myotis myotis*	*Morcego-rato-grande*	VU	0.6
67	5	Bats	*Myotis mystacinus*	*Morcedo-de-bigodes*	VU	0.6
68	6	Bats	*Rhinolophus euryale*	*Morcego-de-ferradura-mediterrânico*	EN	0.8
69	7	Bats	*Rhinolophus mehelyi*	*Morcego-de-ferradura-mourisco*	EN	0.8
70	1	Mammals	*Arvicola sapidus*	*Rato-de-água*	VU	0.6
71	2	Mammals	*Canis lupus*	*Lobo*	EN	0.8
72	3	Mammals	*Crocidura suaveolens*	*Musaranho-de-dentes-brancos-pequeno*	EN	0.8
73	4	Mammals	*Felis silvestris*	*Gato-bravo*	EN	0.8
74	5	Mammals	*Galemys pyrenaicus*	*Toupeira-de-água*	EN	0.8
75	6	Mammals	*Lepus granatensis*	*Lebre-ibérica*	VU	0.6
76	7	Mammals	*Lynx pardinus*	*Lince-ibérico*	EN	0.8
77	8	Mammals	*Martes martes*	*Marta*	VU	0.6
78	9	Mammals	*Microtus agrestis (Microtus rozianus)*	*Rato-do-campo-lusitano*	VU	0.6
79	10	Mammals	*Microtus cabrerae*	*Rato-de-cabrera*	VU	0.6
80	11	Mammals	*Mustela putorius*	*Toirão*	EN	0.8
81	12	Mammals	*Neomys anomalus*	*Musaranho-de-água*	VU	0.6
82	13	Mammals	*Oryctolagus cuniculus*	*Coelho-ibérico*	VU	0.6
83	14	Mammals	*Sorex granarius*	*Musaranho-de-dentes-vermelhos*	VU	0.6
84	15	Mammals	*Sorex minutus*	*Musaranho-anão-de-dentes-vermelhos*	EN	0.8
85	16	Mammals	*Ursus arctos*	*Urso-pardo*	CR	1.0

3. Statistical parameters for the Coarse and Fine Filters

Statistics	Coarse Filter (complete)	Coarse Filter (without 3's)	Fine Filter
Minimum	0.00	0.00	0.00
1st Quantile	0.81	0.30	0.29
Median	1.45	0.91	0.39
3rd Quantile	3.00	1.14	0.50
Maximum	3.00	2.00	1.00

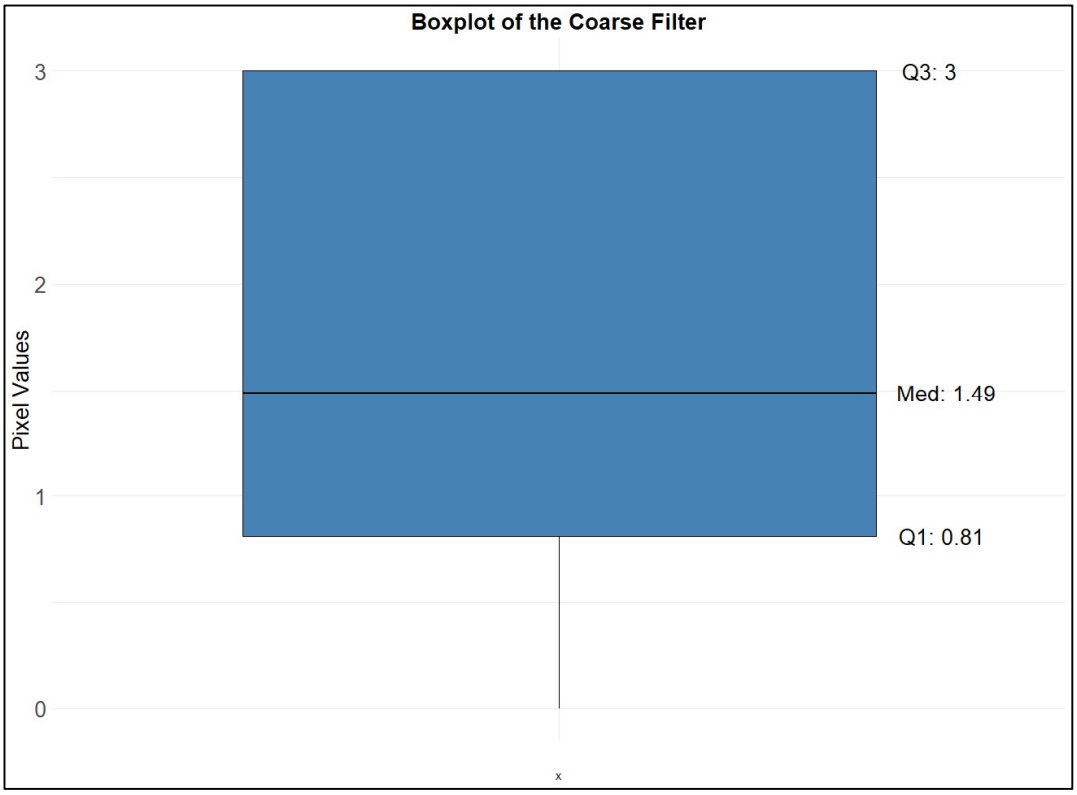

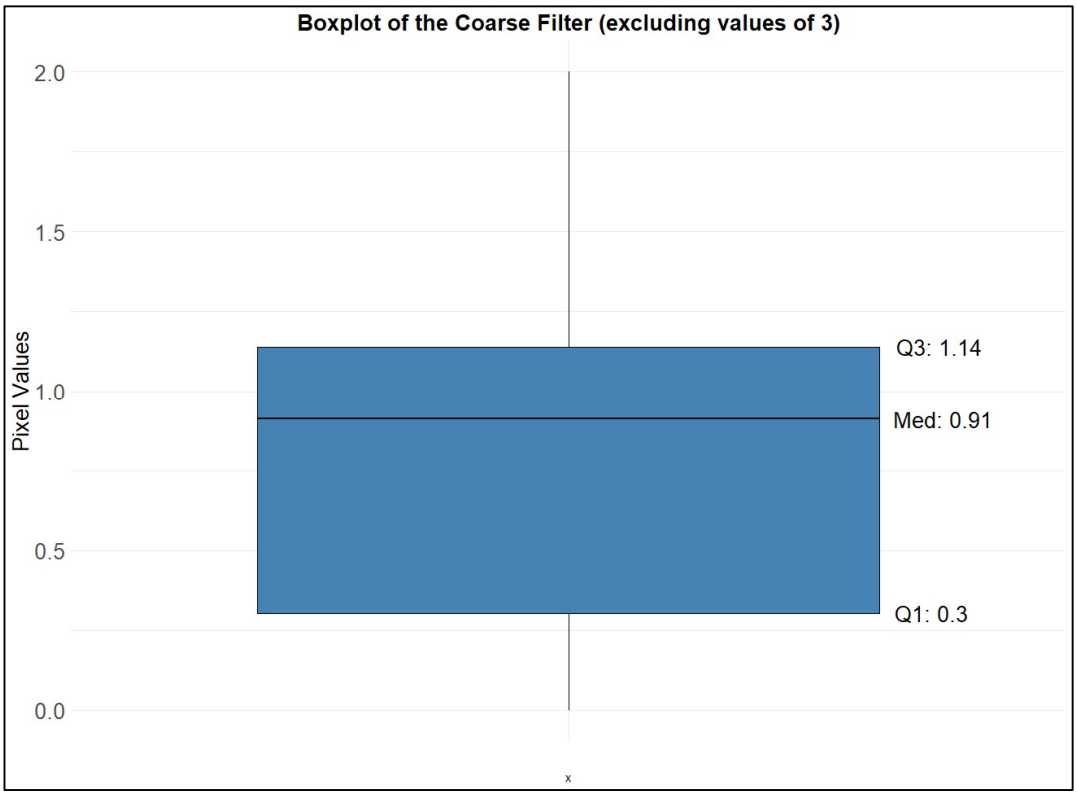
Boxplot of the Coarse Filter (excluding values of 3)
Pixel Values
2.0
1.5
1.0
0.5
0.0
Q3: 1.14
Med: 0.91
Q1: 0.3
x

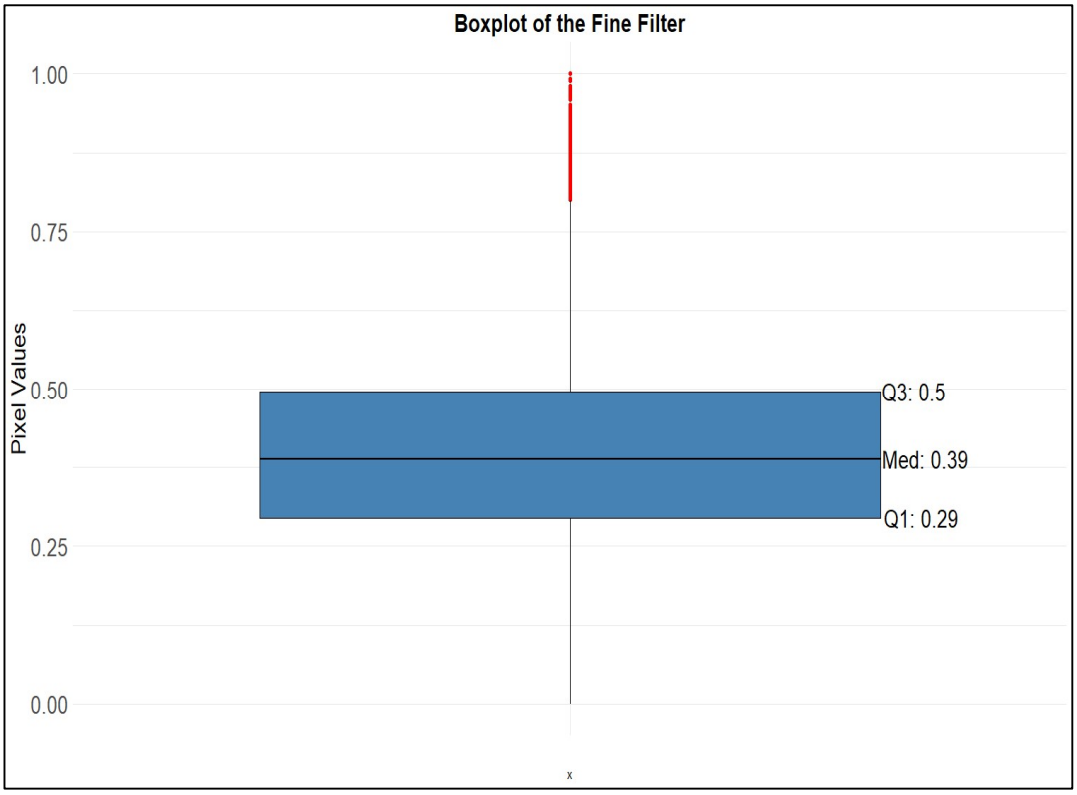
Boxplot of the Fine Filter
Pixel Values
1.00
0.75
0.50
0.25
0.00
Q3: 0.5
Med: 0.39
Q1: 0.29
x

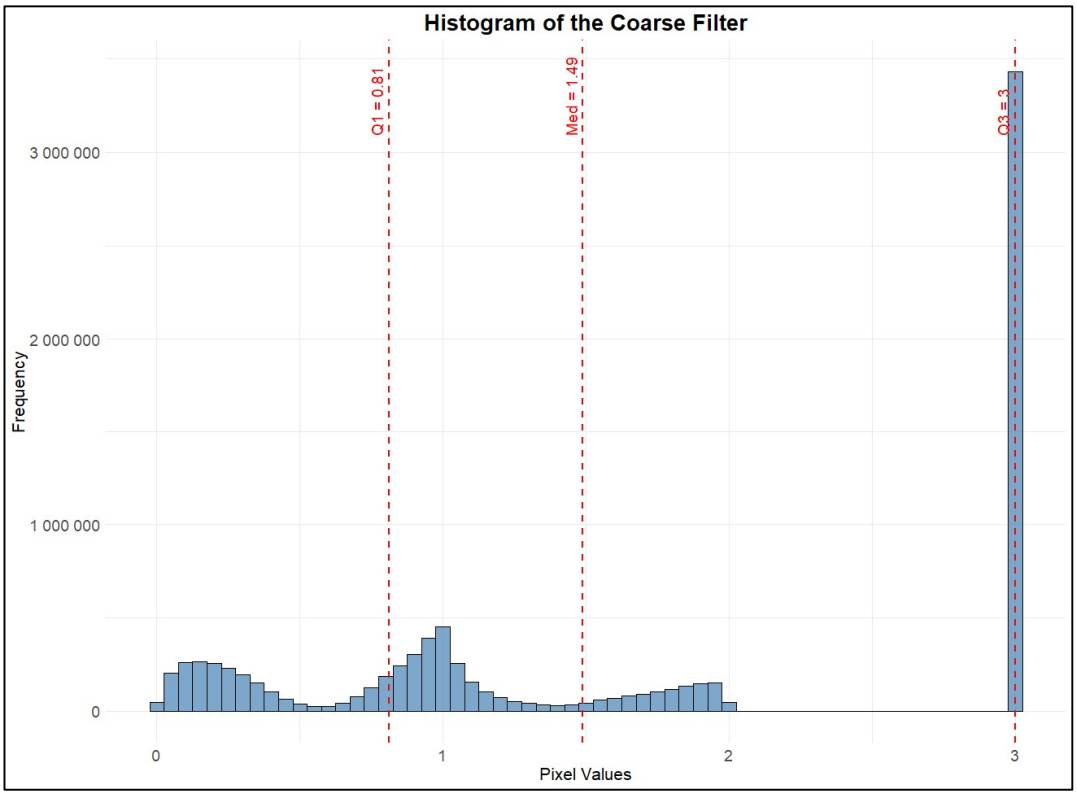
Histogram of the Coarse Filter
Q1 = 0.81
Med = 1.49
Q3 = 3
3 000 000
2 000 000
1 000 000
0
Frequency
0
1
2
3
Pixel Values

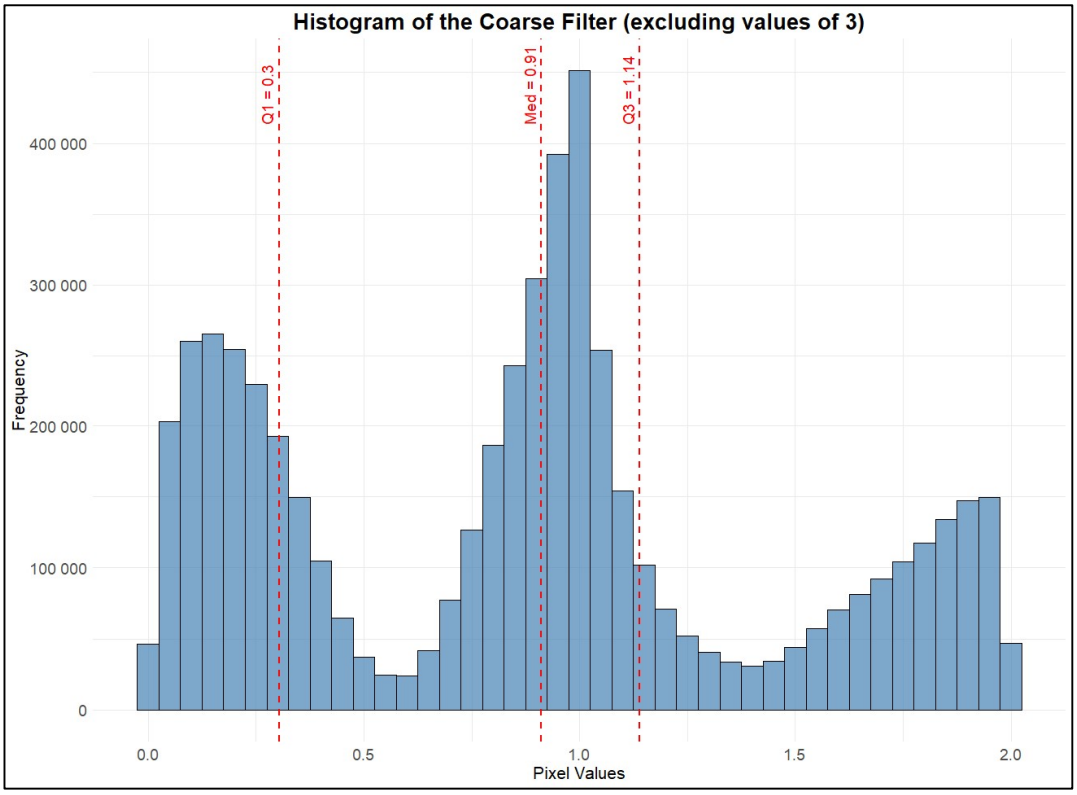
Histogram of the Coarse Filter (excluding values of 3)
Q1 = 0.3
Med = 0.91
Q3 = 1.14
400 000
300 000
200 000
100 000
0
Frequency
0.0
0.5
1.0
1.5
2.0
Pixel Values

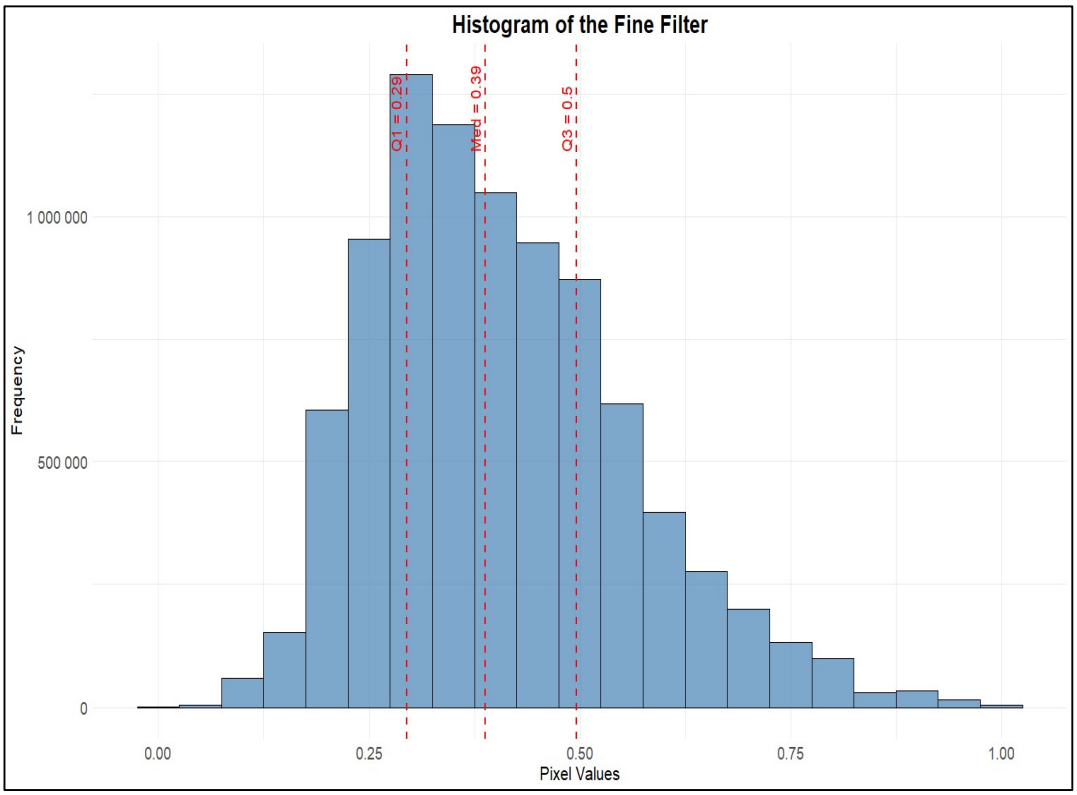
Histogram of the Fine Filter
Q1 = 0.29
Med = 0.39
Q3 = 0.5
1 000 000
500 000
0
Frequency
0.00
0.25
0.50
0.75
1.00
Pixel Values

Supplementary Materials

Table S1: Keywords considered in this analysis for content filtering.

Category	Subcategory	Portuguese	English	Spanish	German	Italian
Generic Landscape Features	General	natureza, paisagem, paisagem cultural, território cultural, colina	nature, landscape, cultural landscape, cultural land, hill	naturaleza, paisaje, paisaje cultural, tierra cultural, colina	Natur, Landschaft, Kulturlandschaft, Kulturlandschaften, Kulturland	natura, paesaggio, paesaggi, paesaggio culturale, paesaggi culturali, territorio culturale
	Terrain	montanha, serra, vale, bacia, planalto, cume, penhasco, pico, desfiladeiro, geleira	mountain, valley, basin, highland, ridge, cliff, peak, gorge, glacier	montaña, valle, cuenca, meseta, cresta, acantilado, pico, desfiladero, glaciar	Hügel, Berg, Berge, Tal, Täler, Hochebene, Kamm, Klippe, Klippen, Gipfel, Schlucht, Kar, Joch, Plateau, Gebirge, Ebene	collina, colline, montagna, montagne, valle, valli, altopiano, altopiani, scogliera, scogliere, vetta, vette, gola, gole, ghiacciaio
	Waterbodies/Coastal Ecosystems	praia, margem, costa, mar, oceano, zona	beach, shore, coast, sea, ocean, wetland,	playa, orilla, costa, mar, océano, humedal, río,	Strand, Strände, Ufer, Küste, Meer, Meere, Ozean, Sumpfgebiet, Fluss, Deich, Bach,	spiaggia, spiagge, riva, rive, costa, coste, mare, mari,

		húmida, rio, dique, riacho, lago, cascata, cachoeira, duna, pântano, lagoa, vala, canal, estuário, ribeira	river, dike, brook, lake, waterfall, dune, swamp, pond, ditch, channel, estuary, creek	dique, arroyo, lago, cascada, duna, pantano, estanque, zanja, canal, estuario	See, Wasserfall, Düne, Sumpf, Teich, Graben, Kanal, Mündung, Gletscher	oceano, oceani, fiume, fiumi, diga, dighe, ruscello, ruscelli, lago, laghi, cascata, duna, dune, palude, stagno, stagni, fossato, fossati, canale, canali, estuario, torrente, torrenti
	Woodlands	floresta, árvore, bosque, copa, arvoredo, sebe, arbusto, matos, Sobreiro, Azinheira	forest, tree, woods, canopy, grove, hedgerow, bush, meadow, grassland, pasture	bosque, árbol, arboleda, seto, arbusto, prado, pradera, pastizal, campo	Wald, Wälder, Forst, Baum, Bäume, Hain, Hecke, Busch, Gebüsch	foresta, foreste, albero, alberi, bosco, boschi, ulivo, ulivi, oliveto, oliveti, siepe, siepi, cespuglio, cespugli
	Agrarian LU/Management	prado, pastagem, pasto, interior, pradaria, milho, trigo, aveia,	prairie, maize, corn, wheat, oats, livestock, cattle, cow, sheep,	pradera, maíz, trigo, avena, ganado, vaca, oveja, huerto, campo, viñedo, cultivos, tierras	Wiese, Weide, Mais, Weizen, Hafer, Vieh, Rind, Kuh, Schaf, Obstplantage, Acker, Weinberg,	prato, prati, prateria, praterie, pascolo, pascoli, campagna, granturco, granoturco, mais,

		pecuária, bovino, vaca, ovelha, pomar, campo, vinha, culturas, terras de cultivo, pastoreio	orchard, field, vineyard, crops, cropland, grazing	de cultivo, pastoreo	Nutzpflanzen, Alm, Sonnenblumen	grano, avena, bestiame, mucca, mucche, pecora, pecore, frutteto, frutteti, campo, campi, terreno, terreni, vigna, vigneto, coltivato, coltivati, raccolto, vendemmia
	Other LULC	urze, charneca, parque, turfa, turfeira, pântano, sapais, pauis, brejo, arbustos, matagal	heather, heath, heathland, park, peat, peatland, peatbog, marsh, moor, shrubs, shrubland	brezo, brezal, parque, turba, turbera, pantano, marismas, páramo, arbustos, matorrales	Heide, Heideland, Park, Moor, Torfmoor, Torf, Niedermoor, Hochmoor, Sumpfland, Strauch, Sträucher	erica, brughiera, brughiere, parco, torba, torbiere, torbiera, paludi, arbusto, arbusti
Ambiguous Cultural Services	-	relaxar, cruzeiro, relaxante, beleza, belo, magnífico, esplendor,	relax, cruising, relaxing, beauty, beautiful, magnificent,	relajarse, crucero, relajante, belleza, hermoso, magnífico,	entspannen, Kreuzfahrt, entspannend, Schönheit, prächtig, Glanz, inspirierend, erhaben,	rilassarsi, crociera, rilassante, bellezza, bello, bella, bellissimo, magnificenza,

		brilho, brilhante, inspirador, sublime, lindo, excelente, encantador, maravilhoso	splendour, brilliance, inspiring, sublime, gorgeous, outstanding, enchanting	esplendor, brillante, inspirador, sublime, sobresaliente, encantador	wunderschön, hervorragend, bezaubernd	magnifico, splendore, brillantezza, ispira, ispirato, sublime, meraviglioso, eccezionale, godendo, magico, mozzafiato
Unambiguous Cultural Services	Recreation	andar, caminhar, caminhada, acampar, campismo, recreação, ciclismo, equitação, pesca, turismo, escalada, trekking, esqui, vela, remo, cruzeiro, alpinismo	walk, hiking, camp, recreation, cycling, horse riding, fishing, tourism, climbing, trekking, skiing, sailing, rowing, cruising	caminar, senderismo, campamento, recreación, ciclismo, montar a caballo, pescar, turismo, escalar, montañismo, esquiar, navegar, remar	wandern, spazieren, campen, Erholung, Radfahren, Reiten, Fischerei, Tourismus, segeln, rudern, Kreuzfahrt, Bergsteigen, Klettern, Trekking, ski fahren	camminata, camminare, trekking, campeggio, ricreazione, ciclismo, equitazione, pescare, mountain bike, corsa, jogging, caccia, turismo, vela, canottaggio, crociera, rilassamento, relax, all'aperto, arrampicata, sci

	Aesthetics	ao ar livre, vista, panorama, cenário, património, valor histórico, magnífico, esplêndido, inspirador, sublime, excepcional	outdoor, vista, panorama, scenic, heritage, historic value, magnificent, splendid, inspiring, sublime, exceptional	al aire libre, vista, panorama, pintoresco, patrimonio, valor histórico, magnífico, espléndido, inspirador, sublime, excepcional	Aussicht, Panorama, landschaftlich, Kulturerbe, historischer Wert, prächtig, großartig, inspirierend, erhaben, außergewöhnlich	vista, panorama, scenico, veduta, bellezza, punto panoramico, patrimonio, valore storico, magnifico, splendido, ispira, sublime, grandioso, eccezionale, godendo, magico, mozzafiato